ORIGIN OF DOLOMITES ENCRYPTED IN THEIR GEOCHEMICAL SIGNATURES

By

©Yong Hou

A thesis submitted to the

School of Graduate Studies

in partial fulfillment of the requirements for the degree of

Master of Science

Department of Earth Sciences

Memorial University of Newfoundland

August, 2015

St. John's, Newfoundland

ABSTRACT

The Esino Limestone of the Western Southern Alps represents a differentiated Ladinian - (?) Lower Carnian carbonate platform comprising of margin, slope and peritidal inner platform facies up to 1000m thick. A major regional subaerial exposure event led to a coverage by another peritidal Lower Carnian carbonate platform (Breno Formation). Multidolomitization events affected the carbonate sediments. Petrographic examinations identified at least three main generations of dolomites (D1, D2, and D3) that occur as both replacement and fracture-filling cements. These phases have crystal-size ranges of 3 to 35μm (dolomicrite D1), 40 to 600μm (eu- to subhedral crystals D2), and 200μm to 5mm (cavity- and fracture-filling anhedral to subhedral saddle dolomite D3), respectively.

The fabric retentive near-micritic grainsize coupled with low mean Sr concentration (76 ± 37 ppm) and estimated $\delta^{18}O$ value (~ -8 to +2.8‰ SMOW) of the parent dolomitizing fluids of D1 suggest formation in shallow burial setting at temperature ~ 45 - 50 ºC with possible contributions from volcanic-related fluids (basinal fluids circulated in volcaniclastics or related to volcanic activity), which is consistent with its abnormal high Fe (4438 ± 4393 ppm) and Mn (1219 ± 1418 ppm) contents. The larger crystal sizes, homogenization temperatures (D2, 108 ± 9 ºC; D3, 111 ± 14 ºC) of primary two-phase fluid inclusions, and calculated salinity estimates (D2, 23 ± 2 eq wt% NaCl; D3, 20 ± 4 eq wt% NaCl) of D2 and D3 suggest that they formed at later stages under mid- to deeper burial settings at higher temperatures from dolomitizing fluids of higher salinity, which is supported by higher estimated $\delta^{18}O$ values of their parent dolomitizing fluids. This is also

consistent with their high Fe (4462 ± 4888 ppm; and 1091 ± 1183 ppm, respectively) and Mn (556 ± 289 ppm and 1091 ± 1183 ppm) contents, and low Sr concentrations (53 ± 31 ppm and 57 ± 24 ppm, respectively).

The similarity in shale-normalized REE patterns and Ce $(Ce/Ce^*)_{SN}$ and La $(Pr/Pr^*)_{SN}$ anomalies of the investigated carbonates support the genetic relationship between the dolomite generations and their calcite precursor. Positive Eu anomalies, coupled with fluid-inclusion gas ratios (N_2/Ar, CO_2/CH_4, Ar/He) and high F/Cl molar ratios suggest an origin from diagenetic fluids associated with the Late Triassic (? Carnian) volcanic activities or circulated through volcanic rocks, which is consistent with the co-occurrence of volcaniclastic lenses in the investigated sequence.

Earlier studies of the St. George Group carbonates in Western Newfoundland have also identified dolomite generations (D1, D2, and D3) with comparable crystal sizes and shapes but different cathodoluminescence characterisitics in D2 and D3 relative to their counterparts of the Esino and Breno formations. However, the comparison of the major and trace elements, O-isotopes, REEs, and fluid-inclusion gases of the dolomites from the Breno and Esino formations (Western South Alps) with their counterparts from the St. George Group carbonates shows clearly the influence of the co-occurrence of volcanic rocks on the dolomites from the Alps region.

Keywords: Carbonate diagenesis; Dolomitization; stable isotopes; Rare Earth Elements; Microthermometry; Fluid-inclusion gases; Triassic; western Southern Alps (Italy).

ACKNOWLEDGEMENTS

The author wishes to express his sincere gratitude to Prof. Karem Azmy for his supervision and critical reading of the thesis. This project was supported by funds (to Karem Azmy) from the Petroleum Exploration Enhancement Program (PEEP).

The author is grateful to Allison Pye (Stable Isotope Lab) and Pam King (Trace Element Lab) for their technical assistance in geochemical analyses, to Gillespie Helen and Babatunde-John Olanipekun for their technical assistance in fluid inclusions analyses, to Dr. Nigel Blamey for his assistance in the analysis of fluid-inclusion gas and constructive comments on the manuscript, to Dr. Sarah Gleeson for her assistance in the analysis of halogens and constructive comments on the manuscript, and to Dr. Fabrizio Berra and Dr. Flavio Jadoul for their assistance in field sampling and constructive comments on the manuscript.

The author appreciates the efforts of the thesis examiners and the assistance of the Department of Earch Sciences. Also, the author expresses the gratitude to his family, especially his wife for her encouragement and cooperation.

TABLE OF CONTENTS

LIST OF FIGURES

LIST OF TABLES

LIST OF APPENDICES

CHAPTER 1

INTRODUCTION

1.1. Scope and purpose of study

Many studies have been focused on the investigation of hydrothermal dolomites that developed mainly from basinal fluids since dolomites constitute a significant part of the global hydrocarbon carbonate reservoirs (e.g., Lonnee and Machel, 2006; Azmy et al., 2008, 2009, 2013; Conliffe et al., 2009, 2010, 2012; Azmy and Conliffe, 2010; Azomina et al., 2013; Haeri-Ardakani et al 2013; Olanipekun et al., 2014). However, little attention has been directed towards the contribution of volcanic activity to dolomitization of carbonates. To investigate the possible causal relationship between volcanic activity and dolomitization, it is important to identify successions where the dolomites occur in carbonate facies having volcanic or volcaniclastic deposits. The presence of these deposits may affect the composition of the fluids responsible for dolomitization and the geochemical fingerprints are expected to be recorded in the dolomites. A favorable scenario for this type of dolomite is presented by the Triassic succession of the Southern Alps of Italy, where dolomitized platform facies are associated with volcaniclastic deposits.

In the Southern Alps, crustal mobility and volcanic activities took place during Middle and Late Triassic (Castellarin et al. 1979; Pisa et al., 1979, Brusca et al., 1981), and volcanogenic sediments (volcaniclastic sandstones, volcanic conglomerate and tuffs) have been extensively preserved within Anisian - Carnian carbonate sequences (Jadoul

and Rossi, 1982; Crisci et al., 1984; Obenholzner, 1991). The carbonate units of the Western Southern Alps (Esino Limestone, Calcare Rosso, Breno Formation and Calcare Metallifero Bergamasco) interbedded with volcaniclastic units are locally dolomitized and host important Pb-Zn mineralizations (Assereto et al., 1979; Brusca et al., 1981). Therefore, the study of petrography and geochemistry of these dolomites is an ideal approach to understand the possible role of volcanic activities (documented in the geographical and stratigraphic neighborhood) in the development of the associated dolomites. The current investigation is the first multiapproach study focused on the evaluation of possible contribution of volcanic activity to dolomitization of carbonates via petrographic and geochemical examinations including microthermometry, fluid-inclusion gas ratios, stable isotopes, major and minor and rare earth elements (REE), and halogens.

The main objectives of this study are to:

1. Investigate the petrographic and geochemical characteristics and diagenetic evolution of the Esino and Breno dolomites, which are associated with volcaniclastic sandstones and volcanic deposits (mostly tuffs), in the Western Southern Alps of Italy.

2. Identify and characterize (petrographically and geochemically) the dolomitization phases and investigate the characteristics and nature of the dolomitizing fluids.

3. Investigate the control of the volcanic activity on the chemical signatures of the dolomitizing fluids and the associated dolomites.

4. Compare the petrographic and geochemical characteristics of the investigated Esino and Breno dolomites in Western Southern Alps (Italy) with those of the St. George Group in Western Newfoundland (Canada) in attempt to shed the light on the identification of the origin of dolomites from their geochemical signatures.

1.2. Chemistry of dolomite (Overview)

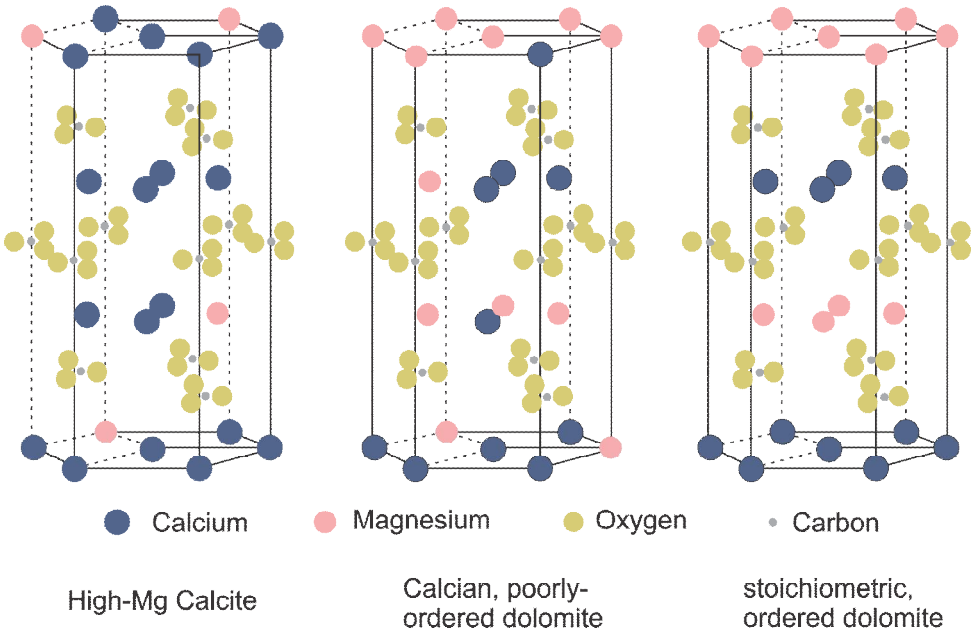

Figure 1.1. Molecular structure of dolomite and high-Mg calcite (from Scholle and Ulmer-Scholle, 2003)

Dolomite is a rhombohedral mineral composed of alternated layers of Ca^{2+} and Mg^{2+}cations with CO_3^{2-} anions (Fig 1.1; Tucker and Wright, 1990; Scholle and Ulmer-Scholle, 2003). Stoichiometric dolomite is highly ordered with equal number of Ca^{+2} and Mg^{+2} ions, i.e. molar ratio of Ca^{2+}/Mg^{2+} is 50:50. However, most of the dolomites in the

nature are not stoichiometric and commonly contain a small quantity of other ions, such as Fe, Mn, Na, and Sr substituting for the Mg and/or Ca cations.

Dolomites can theoretically be formed by direct precipitation from Mg^{2+} saturated aqueous solutions, which can be expressed by following chemical equation (Tucker and Wright, 1990):

$$Ca^{2+} + Mg^{2+} + 2CO_3^{2-} \rightleftharpoons CaMg(CO_3)_2$$

or via dolomitization of the previous marine calcium carbonates, which is a multi-step process involving dissolution of calcite and precipitation of dolomite that can be expressed by following chemical equation (e.g. Land, 1985; Lippmann, 1973):

$$CaCO_3 + Mg^{2+} + CO_3^{2-} \rightleftharpoons CaMg(CO_3)_2$$

or

$$2CaCO_3 + Mg^{2+} \rightleftharpoons CaMg(CO_3)_2 + Ca^{2+}$$

However, direct precipitation or dolomitization of calcium carbonate can hardly occur on the seafloor even though seawater is supersaturated with respect to dolomite (e.g. Bathurst, 1975; Machel and Mountjoy, 1986; Tucker and Wright, 1990) because of the following kinetic inhibitions:

(1) Fast precipitation rates of calcite relative to that of dolomite (Folk and Land, 1975; Tucker and Wright, 1990)

(2) Hydration of Mg^{2+} ion is stronger than that of Ca^{2+}

(3) Dolomite precipitates from CO_3^{2-} rather than HCO_3^- and the activity of CO_3^{2-} is lower than that of HCO_3^- (Lippmann, 1973; Tucker and Wright, 1990)

(4) Dissolved SO_4^{2-} inhibits dolomite precipitation (Baker and Kastner, 1981)

The kinetic inhibitions to dolomite precipitation from seawater can be overcome by raising the temperature or by modifying the seawater including evaporating, diluting, mixing with meteoric waters and lowering the SO_4^{2-} content. Hence, there are three prerequisites to be met for dolomitization: the sources of enough Mg^{2+}, the pumping of the Mg^{2+} containing aqueous solutions through the calcium carbonate sequences and the overcome of kinetic inhibitions (e.g. Machel and Mountjoy, 1986; Tucker and Wright, 1990; Scholle and Ulmer-Scholle, 2003). For early and near-surface dolomitization, seawater is the only abundant source of Mg^{2+} ions but and for dolomitization in the burial environment, the substantial volumes of Mg^{2+} might be derived from mixed marine and meteoric waters, dissolution of Mg-rich salts such as polyhalite or carnallite (Warren 2000), interactions of diagenetic fluids and Mg-rich minerals such as clay mineral or mafic to ultramafic igneous units (Boles and Franks 1979; Warren 2000; Conliffe et al., 2010), or possibly from magmatic fluids of mantle origin (Andersen, 1986; Bogoch et al., 1986).

CHAPTER 2

GEOLOGICAL SETTING

The study area (Southern Alps of Lombardy) is a part of the Western Southern Alps and bordered by the Trento-Dolomites high to the West, the Insubric Line to the North, and the Po plain to the South (Fig. 2.1; e.g., Feist-Burkhardt et al., 2008). The region underwent several subsidence events and sea-level fall cycles during the Triassic (Jadoul and Rossi, 1982; Gaetani et al., 1998; Berra and Carminati, 2010) and intense deformation during the Alpine orogenesis. During Ladinian and Carnian, this part of the Tethyan domain recorded major paleogeographic changes, with the stratigraphic evolution form a high relief platform system with intraplatform deep troughs (Ladinian) to mixed deposits consisting of volcaniclastic fluvio-deltaic systems bordered by lagoon in front of a peridídal carbonate platform (Early Carnian).

The studied dolomites come from two different carbonate platforms (Fig. 2.2) that belong to different evolutionary stages in the Western Southern Alps: a high relief isolated Ladinian system and a Lower Carnian inner platform. The Ladinian sediments are characterized by thick carbonate platforms with steep-slopes (Esino Limestone) and a rapid progradation in its upper part. Inner platform facies in the core of the platform are separated by a narrow reef belt from slope breccias (Jadoul et al., 1992a; Berra et al., 2012). This unit (up to 1000m) is bordered by basinal successions consisting of re-sedimented limestones and volcaniclastic sandstones (e.g., Assereto and Casati, 1965; Jadoul et al., 1992a, Berra and Carminati, 2012). In the Southern Alps, at the end of the

Ladinian, most of the intraplatform seaways were closed due to the intense progradation of the platform (Berra et al., 2011) so that sedimentation was dominated by shallow-water carbonates (Jadoul et al., 1992a; Berra, 2007).

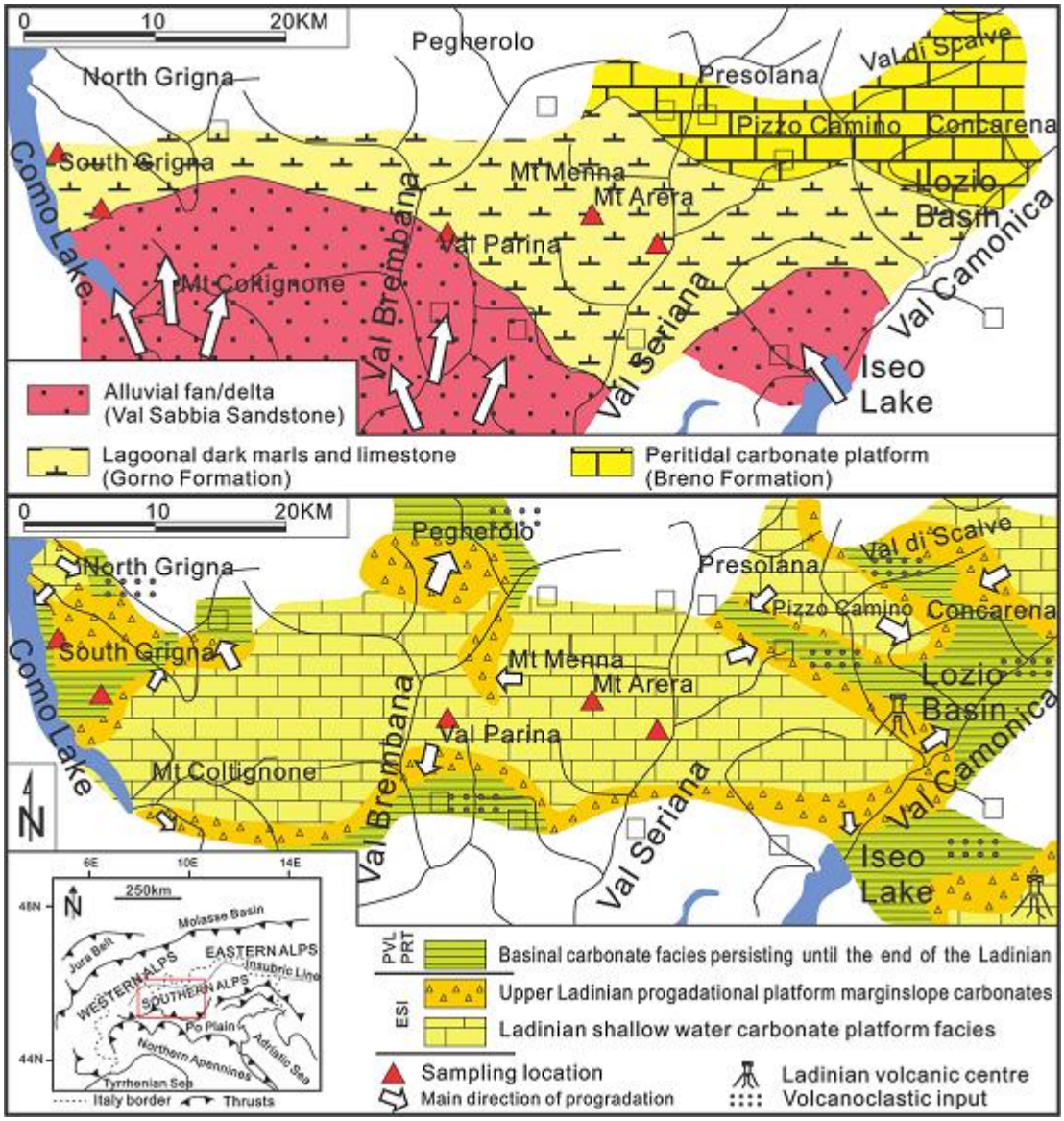

Figure 2.1. Late Ladinian (below, modified after Berra et al., 2011) and early Carnian (above, modified after Brusca et al., 1981) palaeogeography of the Western

Southern Alps with inset of simplified tectonic map of Northern Italy (modified from Ronchi et al. (2011).

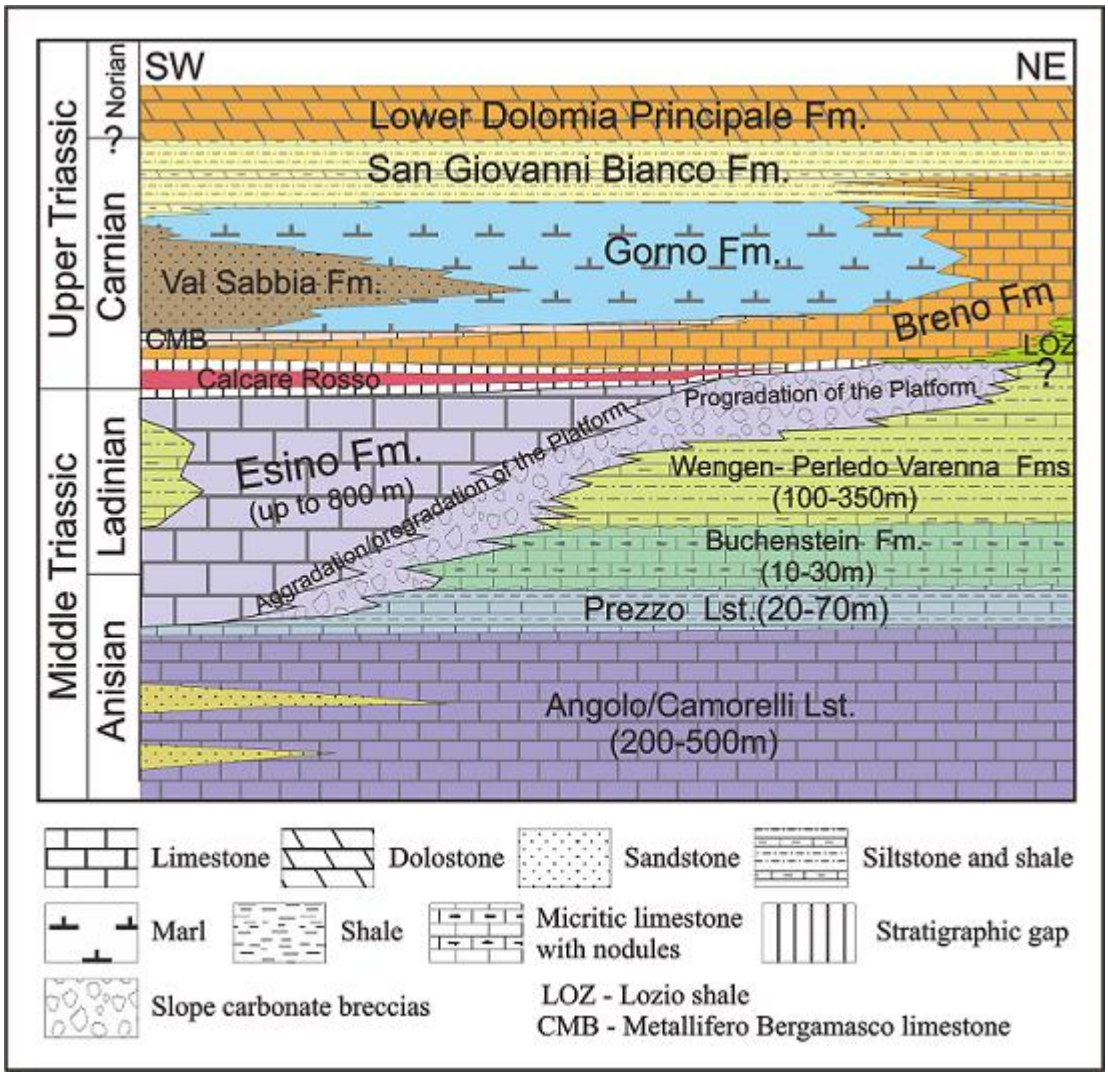

Figure 2.2. Facies and stratigraphic framework of Middle-Upper Triassic sediments of the Western Southern Alps (modified from Assereto and Folk, 1980). Sampling sites (Appendix 1) are placed mostly in the Breno Formation, covered by the progradation of the lagoonal facies of the Gorno Formation and alluvial-coastal Val Sabbia Sandstone from the south.

Close to the Ladinian-Carnian boundary, a major sea-level fall was responsible for the subaerial exposure of the top of the Esino Limestone platform, followed by a general reorganization of the facies distribution. The repeated subaerial exposure of the platform top accounts for the development of palaeokarsts and tepee horizons at the top of Esino Formation (Assereto et al., 1977), which is also indicated by the occurrence of a thin wedge of peritidal limestone, residual breccias and terra-rossa deposits (Calcare Rosso Formation, Assereto and Kendall, 1971, 1977; Mutti, 1994; Jadoul et al., 2002: Berra, 2012, Vola and Jadoul 2014) overlying the Esino Limestone. Tuff and volcanic deposits are also locally present at the top of the Esino Limestone and in the Breno Formation, indicating coeval volcanic activity in the surrounding areas close to the Ladinian-Carnian boundary.

After the subaerial exposure, the depositional system records a major event of paleogeographic re-organization (Assereto and Casati, 1965). In the northern sector, peritidal carbonate platform facies (Breno Formation) covered by lagoonal dark limestone (Calcare Metallifero Bergamasco) were deposited (Gnaccolini and Jadoul 1990; Berra and Jadoul, 2002), recording the drowning of the carbonate platform. Alluvial fan and deltaic volcaniclastic sandstones, prograding northward, prevail toward the south (Val Sabbia Sandstone, Gnaccolini, 1983; Garzanti, 1985). Between these sandstones and the northern carbonate platform (Breno Formation), lagoonal facies were deposited (Gorno Formation; Gnaccolini, 1986; Gnaccolini, 1988; Gnaccolini and Jadoul, 1988). The petrographic composition of the prograding deltaic bodies reveals the erosion of volcanic edifices (Garzanti, 1985) originally developed in the area presently occupied

by the Po Plain. The overlying San Giovanni Bianco Formation (SGB) records the end of this paleogeographically complex scenario, with the development of coastal to sabkha facies (Garzanti et al. 1995) that can be traced for most of the Southern Alps of Italy (San Giovanni Bianco Formation, in the western Southern Alps; Travenanzes Formation, upper Raibl Group in the central and eastern Southern Alps).

During the Ladinian, intense volcanic activity is well-documented in the Southern Alps, where thick lava flows are coeval with the Ladinian carbonate platforms (e.g., Castellarin et al; 1979; Brusca et al., 1981; Berra et al., 2011). In the Western Southern Alps, the evidence of volcanism is provided mostly by deep-water volcaniclastic deposits (Wengen Formation) preserved in the deep intraplatform troughs. An early Carnian volcanic activity is further recorded in the sediments of the Western Southern Alps. This volcanism is documented by tuffs and minor proximal volcanic deposits, which are discontinuously preserved in peritidal facies of the Breno Formation.

CHAPTER 3

METHODS AND THEORY

The analytical protocols of the petrographic and geochemical investigations of the current study are explained below (cf. Azmy et al., 2008, 2009, 2011; Azmy and Conliffe, 2010; Azmy and Blamey, 2013; Blamey and Norman, 2002; Gleeson and Turner, 2007).

3.1. Sampling

Samples were collected from limestones and dolomites at abandoned mines (Resinelli, Pedrozio, Arera and Trevasco) from Esino and Breno formations in the Western Southern Alps of Lombardy (Fig. 2.1 and 2.2; Appendix 1): Resinelli, Pedrozio, Arera and Trevasco. The distribution of the sampling sites defines an east-west oriented belt that follows the outcrops of the Ladinian-Carnian boundary and the top of lower Carnian (Breno Formation) peritidal carbonates. Samples are mostly derived from the peritidal facies of the Breno Formation, the unit that hosts the most important Pb-Zn ore bodies and for the miners represents a morphologic and stratigraphic marker (from a few tens to 150 m thick), called "*Metallifero*". This unit is bracketed between a unit recording multiple episodes of subaerial exposure at the base (Calcare Rosso) and the drowning recorded by subtidal lagoonal facies of the Calcare Metallifero Bergamasco, in turn covered by the lagoonal facies of the Gorno Formation or by the volcaniclastic deposits of the Val Sabbia Sandstone.

3.2. Petrography

Petrographic analyses were carried out by the examination of thin sections under a standard polarizing microscope and cathodoluminoscope (CL). The thin sections were cut and stained with a mixture solution of Alizarin Red-S and potassium ferricyanide (Dickson, 1966). Cathodoluminescence was performed using a Technosyn cold cathodoluminoscope operated at 12kV accelerating voltage and 0.7mA gun current intensity whereas the UV luminescence was by a CRAIC-QDI 202 UV luminescope mounted on a Zeiss imager D1m microscope. A mirror-image slab of each thin section was also polished and cleaned with de-ionized water to be utilized for micro-sampling the different carbonate generations for geochemical analyses.

Cathodoluminescence (CL) is a phenomenon of temporary emission of photons (‘‘particles’’ of light) when a mineral crystal is bombarded by a stream of high-energy electrons in a scanning electron microscope or other suitable instrument (Boggs and Krinsley, 2006). The electron bombardment promotes electrons within a crystal from the lower-energy valence band to the higher-energy conduction band, and as they return to the ground state, they may be trapped momentarily by extrinsic or intrinsic defects within the band gap. When electrons vacate traps and continue their transit to the valence band, energy is released in the form of photons of light. The wavelengths of most photons are within the visible light range and therefore luminescence occurs; however, emissions may also occur in the near ultraviolet and infrared (Boggs and Krinsley, 2006).

Cathodoluminescence is widely used in mineralogical and petrological investigations such as the identification of different mineral constituents and their distribution within rocks, the internal textures, zonal growth and distribution of trace elements within solid phases, the radiation damage in minerals, the processes of mineral formation, alteration and diagenesis, the conditions during crystal growth, defect density, and incorporation of certain trace elements (Gucsik, A., 2009).

Since Mn^{2+} ion is the most important activator and Fe^{2+} ion is a major quencher of extrinsic CL in carbonate minerals, the intensity of CL emissions in carbonates mainly reflects the relative abundance of Fe^{2+} and Mn^{2+} (Marshall, 1988, Machel, 2000; Richter et al., 2003; Boggs and Krinsley, 2006). Generally speaking, the application of CL in the study of carbonate rocks has been focused on:

1. The identification of carbonate grains, textures, and structures
2. The internal features of microfossils and ooids
3. Shapes of dolomite crystals, zoning in dolomite crystals, and other textural features of dolomites
4. The burial history of carbonate sediments
5. The properties of diagenetic fluid including fluid chemistry, temperature, pressure, and possibly redox conditions
6. The environment of dolomitization
7. The neomorphism in carbonates such as recrystallization of dolomite
8. The development of porosity

9. Details of cement textures, characteristics and generations (cement stratigraphy; Boggs and Krinsley, 2006).

3.3. Microthermometry

Fluid-inclusion microthermometric (Appendix 2) measurements were performed on double polished wafers (about 80μm thick) using a Linkam THMSG600 heating-freezing stage at Memorial University of Newfoundland (MUN). Precision of ±0.1 °C at -56.6 °C and ±0.3 °C at 374.1 °C was calculated via calibration using synthetic H_2O and CO_2 fluid inclusion standards. The homogenization temperatures (T_h), initial melting temperatures (T_i), and last ice melting ($T_{m\ (ice)}$) of primary two phases fluid of dolomite and calcite generations were measured according to the procedures of Shepherd et al. (1985). Heating was carried out before freezing to avoid stretching of the inclusions due to freezing (Lawler and Crawford, 1983). The salinity estimates were calculated by applying the measured $T_{m\ (ice)}$ values to the equation of Bodnar (1993), and reported as equivalent weight percent NaCl (eq. wt% NaCl).

3.4. Geochemical analyses

Representative samples from different carbonate generations were microdrilled under a binocular microscope from the polished mirror-image slabs by a low-speed microdrill. The slabs were previously cleaned with deionized water and dried at temperature between 30 °C and 34 °C prior to microsampling.

3.4.1. Elemental geochemistry

About 10mg of each powder sample was weighed into an acid-washed 11ml test tube using an analytical balance and 1 drop of clean 8N Nitric acid is added. Clean 0.2N nitric acid was used to make the final solution to 5g and left for two days at room temperature. Two grams of sample solution was weighed in an acid washed test tube and diluted with 3g of clean 0.2N Nitric acid. The sample solutions were analyzed for Ca, Mg, Sr, Mn and Fe as well as rare earth elements (REE) using a Perkin Elmer Sciex "Elan DRCII" ICP-MS at MUN. The relative uncertainties are less than 5%, and results are normalized to a 100% carbonate basis (e.g. Azmy et al., 2014).

Iron (Fe), Mn, and Sr are the common minor elements utilized in the studies of dolomitization. They are proxies of the nature of the dolomitizing fluids and diagenetic environments. Iron and Mn reflect the redox conditions that dominated during burial and they are generally enriched in the diagenetic carbonates and with progressive burial (Tucker and Wright, 1990). The Sr concentration in dolomites is controlled by the Sr/Ca molar ratio of dolomitizing fluids and the water/rock ratio of certain diagenetic environment (Tucker and Wright, 1990). Thus, it is useful in interpreting the sources of dolomitizing fluids and the diagenetic environment. Early diagenetic dolomites tend to have higher Sr concentrations than later dolomites because Sr is depleted with alteration and progressive burial.

The REE concentrations were normalized relative to the Post-Archean Australian Shale (McLennan, 1989). Anomalies of Europium $(Eu/Eu^*)_{SN} = Eu_{SN}/ (0.67Sm_{SN} +$

$0.33Tb_{SN}$), Cerium $(Ce/Ce^*)_{SN} = Ce_{SN}/(0.5La_{SN} + 0.5Pr_{SN})$, and Lanthanum $(Pr/Pr^*)_{SN} = Pr_{SN}/(0.5Ce_{SN} + 0.5Nd_{SN})$ were calculated according to the formulae of Bau and Dulski (1996). The relative uncertainties are less than 5%, and results are normalized to a 100% carbonate basis (e.g. Azmy et al., 2014).

The rare earth elements (REE) have been increasingly used as proxies to understand the controls on carbonate diagenesis and identify the origin of diagenetic fluids (e.g., Azmy et al., 2011; Azomani et al., 2013; Haeri-Ardakani et al., 2013). The suite of REE consists of 15 lanthanides (Alibo and Nozaki, 1999), which are classified into light (LREE; La to Nd), medium (MREE: Sm to Dy) and heavy rare earth elements (HREE; Ho to Lu). They are all trivalent except for Ce^{4+} and Eu^{2+} (in some environments) and have similar ionic radii but their chemical characteristics change systematically along the series (Sholkovitz and Shen, 1995). They are incorporated into carbonates within a narrow range of partition coefficient values (Zhong and Mucci, 1995) and their series variation therefore reflects the oceanic and/or the diagenetic fluid compositions. Ce is sensitive to redox conditions (Sholkovitz et al., 1994) and Eu is known to be more enriched in volcanic rocks relative to sedimentary carbonates (Elderfield and Greaves, 1982). Some recent studies suggested that diagenesis, particularly by meteoric and mixed waters, has no significant effect on the pattern, composition and/or distribution of REEs in carbonates (limestones and dolomites) except in systems with extremely large water-rock ratios (e.g., Banner et al., 1988; Barton et al., 2006; Webb and Kamber, 2000; Kamber and Webb, 2001; Nothdurft et al., 2004; Webb et al., 2009).

3.4.2. Stable Isotopes

A subset of sample powder, each ~ 0.2mg, was reacted in an inert atmosphere (He) with ultra-pure concentrated orthophosphoric acid at 50 °C. The produced CO_2 was automatically flushed through a chromatographic column to the source of a Thermo Finnigan DELTA V plus isotope ratio mass spectrometer in a helium stream to be ionized and measured for isotope ratios. Uncertainties of better than 0.1‰ (2σ) for the analyses were determined by repeated measurements of NBS-19 ($\delta^{18}O$ = -2.20‰ and $\delta^{13}C$ = +1.95‰ vs. VPDB) and L-SVECS ($\delta^{18}O$ = -26.64‰ and $\delta^{13}C$ = -46.48‰ vs. VPDB) as well as internal standards during each run of samples.

Stable isotopes data have been increasingly used in the study of the origin of dolomites. Oxygen has 3 isotopes (^{16}O, ^{17}O and ^{18}O) and the δ value is generally expressed as

$$\delta^{18}O\ ‰ = \frac{(^{18}O/^{16}O)_{sample} - (^{18}O/^{16}O)_{standard}}{(^{18}O/^{16}O)_{standard}} \times 1000$$

by the standard of VPDB (Vienna Pee Dee Belemnites) for carbonates and VSMOW (Vienna Standard Mean Ocean Water) for water. The oxygen isotopic composition of precipitated carbonates depends on several factors:

1. The oxygen isotopic composition of seawater and diagenetic fluids,
2. The temperature and salinity of diagenetic fluids,

3. The water-rock interaction ratio between precipitated $CaCO_3$ and diagenetic fluids,

The oxygen isotopic composition of dolomite is controlled by the temperature of dolomitization, the isotopic composition of the dolomitizing fluids, and the water-rock interaction between dolomitizing fluids and precursor calcites (Turker and Wright, 1990; Land, 1992). According to Land (1983), the $\delta^{18}O$ values of the dolomitizing fluid can be calculated if the temperature of dolomitization and the $\delta^{18}O$ values of dolomites are provided. Earlier studies (e.g., Azmy et al., 2008, 2009; Azomani et al., 2013; Olanipekun et al., 2014) used the homogenization temperatures of primary 2-phase fluid inclusions and the $\delta^{18}O$ composition of dolomites to calculate estimates for the $\delta^{18}O$ values of the dolomitizing fluids and better understand their origin.

Carbon has 2 stable isotopes (^{12}C and ^{13}C) and the δ value is generally expressed as

$$\delta^{13}C\ ‰ = \frac{(^{13}C/^{12}C)_{sample} - (^{13}C/^{12}C)_{standard}}{(^{13}C/^{12}C)_{standard}} \times 1000$$

by the standard of VPDB (Vienna Pee Dee Belemnite).

The factors that control the carbon isotopic composition in marine carbonates include:

1. The isotope fractionation between CO_2 gas and $CaCO_3$,
2. Isotope fractionation among the aqueous carbonate species ($Co_{2(aq)}$, H_2CO_3, HCO_3^-, and CO_3^{2-})

3. The mineral composition of the precipitated $CaCO_3$ (Calcite or aragonite),
4. Subsequent alteration of carbonate sediment during diagenesis,
5. Deposition of late phases of $CaCO_3$ (Faure and Mensing, 2004).

Unlike the oxygen isotopes, the carbon isotopic composition of dolomite is generally buffered by the composition of its precursor calcite (Turker and Wright, 1990) since the dolomitizing fluids rarely contain that much dissolved CO_2 to reset the $\delta^{13}C$ of dolomite. Therefore, the carbon isotopic composition of dolomite mainly reflects the composition of the precursor carbonate and/or influence of organic matter.

3.5. Fluid-inclusion gas analyses

Fluid-inclusion gas analysis was performed by the crush-fast scan (CFS) method (Norman and Moore, 1997; Norman and Blamey, 2001; Parry and Blamey, 2010; Blamey, 2012; Azmy and Blamey, 2013; Blamey et al., accepted) at the New Mexico Institute of Mining and Technology (NMT) Fluid Inclusion Gas laboratory. Samples were gently crushed by hand and sieved in 30-mesh sieve, where the smaller fraction was discarded. The 30-mesh size fraction was cleaned with 20% KOH, rinsed several times with deionized water, and dried below 100°C. Approximately 200mg of each sample was incrementally crushed under a vacuum of approximate 10^{-8} Torr, producing up to 10 crushes analyzed by two Pfeiffer-Vacuum Prisma quadrupole mass spectrometers. The measured volatiles include H_2, He, CH_4, H_2O, N_2, O_2, H_2S, Ar, and CO_2. The system calibration was performed using commercial gas mixtures and three in-house fluid inclusion gas standards following the technique described by Norman and Blamey (2001)

and Blamey et al. (accepted). H_2 is reliably detected at 50 ppm, He at <0.5 ppm. Precision for the major gas species CO_2, CH_4, N_2, and Ar is better than 5%, whereas it is ~10% for the minor species.

The trapped gases in fluid inclusions (Table 4.5) provide valuable clues of the origin of diagenetic fluids and the oxidation state of diagenetic environments (e.g., Giggenbach, 1986; Norman and Moore, 1999; Blamey and Norman, 2002; Azmy and Blamey, 2013). Giggenbach (1986) introduced the N_2-Ar-He ratios to identify the sources of volatiles in geothermal fluids and attributed high N_2/Ar to magmatic sources. However, Norman and Moore (1999) pointed out that organic nitrogen may also contribute N_2 to increase the N_2/Ar ratio, and thus introduced a CO_2/CH_4 ratio as a proxy since CH_4 reflects the crustal components in thermal fluids and is easy to be analyzed. Norman and Moore (1999) also established the correlation of CO_2/CH_4 with N_2/Ar ratios to identify fluids bearing significant organic nitrogen, which could lead to errors in interpretation. This correlation allows the classification of source fluids into magmatic, meteoric and crustal fluids. Meteoric fluids are those near-surface recharge waters whereas crustal fluids can be sourced from meteoric fluids, and subsequently interacted with crustal rocks and may have species derived from the wall rock. The CO_2/CH_4 ratios reflect the redox state and their N_2/Ar counterparts are proxies of fluid source(s).

Blamey and Norman (2002) introduced the Ar/He vs. N_2/Ar diagram as a better method to remedy the weakness of the CO_2/CH_4 vs. N_2/Ar diagram, which assumed that most methane is sedimentary in origin but neglected the fact that methane may be produced by inorganic processes.

3.6. Halogens analyses

The halogens analyses were performed by the bulk fluid crush-leach method (Banks and Yardley, 1992; Gleeson and Turner, 2007; Bernal et al., 2014) at the Department of Earth and Atmospheric Sciences, University of Alberta. The samples were crushed and sieved to obtain ~ 2g with a grainsize of 1-2mm. Each mineral separate was washed, dried, ground to fine powder, and mixed in a vial with 5ml of de-ionized water. The samples were shaken, and filtered through 0.45µm PTFE filters. The leachate was run in on a Dionex DX600 ion chromatograph (IC) with an AS14A anion column (Cl, Br, F, and sulfate). A 7 anion standard solution, pure water blanks and an internal quality control standard were run after every 10 unknowns. The data were reproducible to 5%. The detection limits were 0.03mg/L for Cl^-, Br^-, and 0.01mg/L for F^-.

The factors that determine the concentration of halogens in diagenetic fluids include subaerial evaporation, meteoric water dilution, chloride (eg. halite) precipitation or dissolution, input of fluids derived from magmatic effects or other sources. Thus, halogens are useful in interpreting the origin of dolomitizing fluids and the environment of diagenesis (Banks et al., 2002; Gleeson and Turner, 2007; Conliffe et al., 2010). The study of Orberger et al. (1990) shows that, compare to seawater, ultramafic and mafic rocks have much higher F/Cl molar ratios. Banks et al. (2000) has identified much higher Cl/Br molar ratio in magmatic fluids than that in seawater. Therefore, halogen concentrations and molar ratios (F/Cl and Cl/Br) are, theoretically, helpful in identifying the carbonates have magmatic origination or not. However, halites precipitation and dissolution have strong effect on the variation of Cl concentration, and furthermore the

F/Cl and Cl/Br rations (Hanor, 1994). Thus, using halogen data in the interpretation of diagenesis must consider all the possibilities.

CHAPTER 4

RESULTS

4.1. Petrography

The Esino and Breno formations in Western Southern Alps consist of limestone and dolostone lithofacies. The limestone lithofacies include mudstone, wackstone, packstone, and fine to coarse crystalline carbonate (e.g., Gnaccolini and Jadoul, 1990; Bertotti et al., 1993; Jadoul and Weissert, 1989; Berra et al. 2011; Berra and Carminati; 2012). The dolostone lithofacies vary from fine (dolomicrites) to coarse grained dolomites (saddle dolomite). The dolomite generations occur as both replacement and cements (Fig. 4.1).

Petrographic examination indicates that each of the calcites and dolomites has multiple generations. The calcite generations (Fig. 4.1), from the earliest to the latest, are micrite (microbial mud) and fibrous cement (C1, Fig. 4.1a, b), pore-filling equant calcite (C2, 25 - 400μm, Fig. 4.1b), and coarse fracture filling calcite (C3, 200μm - 15mm, Fig. 4.1e, g). Under cold cathodoluminoscope, C1 and C2 exhibit dull to non-CL (Fig. 4.1b) but calcite C3 exhibits bright orange CL (Fig. 4.1f, h). The dolomite generations (Fig. 4.1), also from the earliest to the latest, are dolomicrites (D1, Fig. 4.1d, e), equant replacive dolomite (D2, Fig. 4.1d, g), and large fracture-filling saddle dolomites (D3, Fig. 4.1e, i). Calcite C3 and dolomite D3 fill the fractures that crosscut of the other calcite and dolomite generations. The paragenetic sequence of events, based on petrographic relationships observed in the Esino and Breno carbonates, is summarized in Figure 4.2.

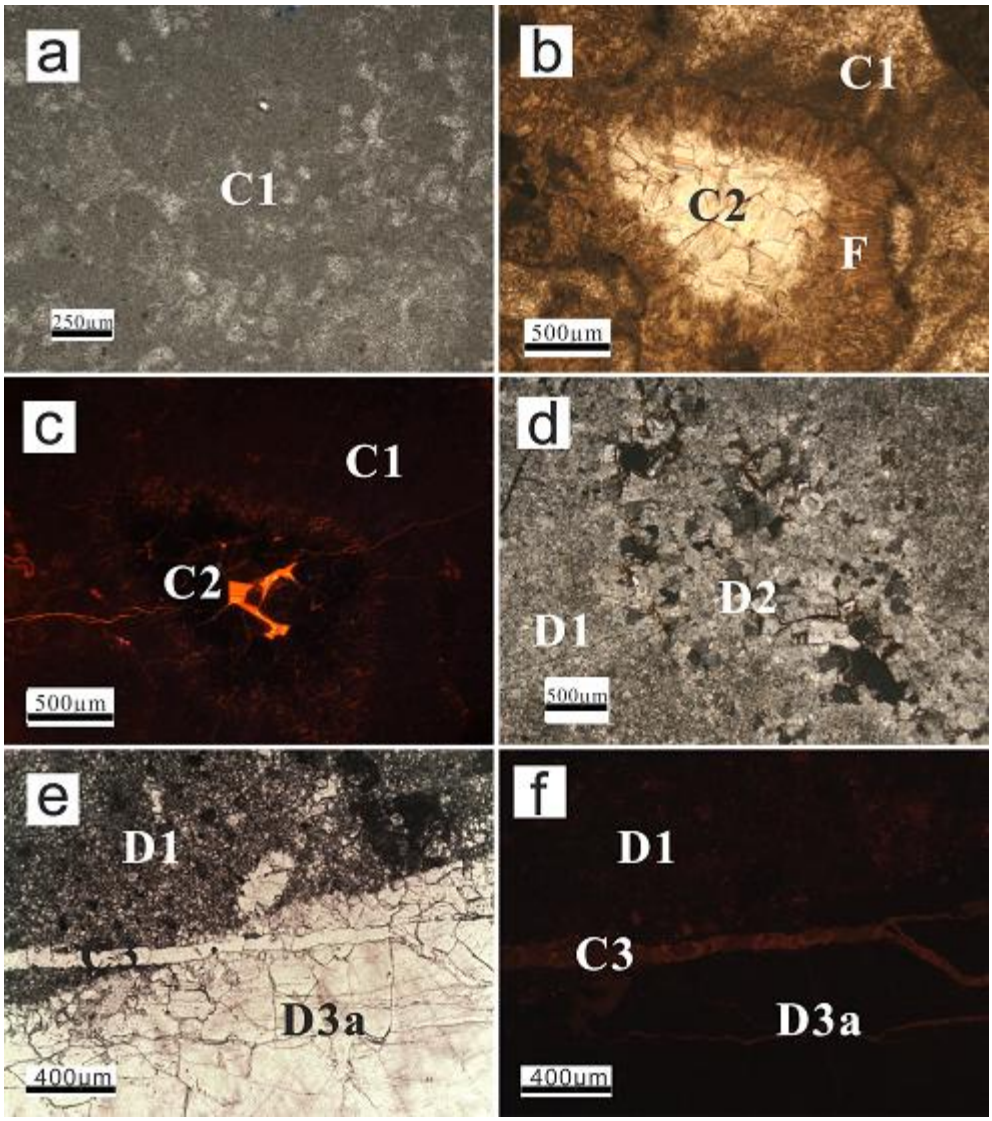

Figure 4.1. Photomicrographs of petrographic features of Esino and Breno carbonates. (a) Calcite C1 (plane polarized; Sample PE1), (b) Calcite C2 and fibrous cement F (crossed polars; Sample PE7), (c) Cathodoluminescence image of (b) showing dull CL of C1 and C2, (d) Dolomite D1 and D2 (crossed polars; Sample ES), (e) Dolomite D1, D3a and calcite C3 (plane polarized; Sample PE8), (f) Cathodoluminescence image of (e) showing dull CL in D1 and D3a.

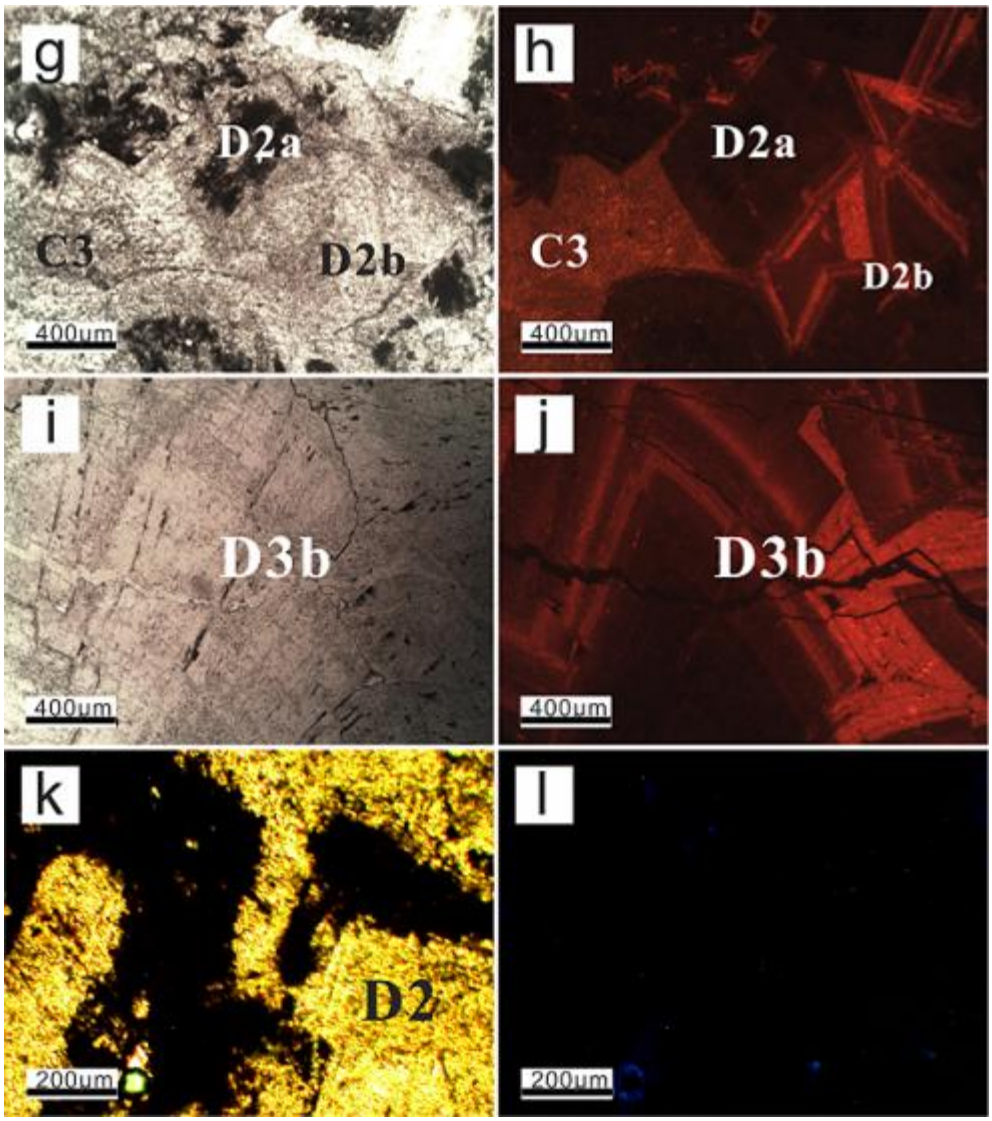

Figure 4.1. Photomicrographs of petrographic features of Esino and Breno carbonates. (g) Dolomite D2a, D2b and calcite C3 showing organic matter along zones in D2a crystals (plane polarized; Sample BR), (h) Cathodoluminescence image of (g) showing dull CL of D2a, zonation CL of D2 and bright orange CL of C3, (i) Saddle dolomite D3b with undulose extinction (crossed polars; Sample BR3), (j) Cathodoluminescence image of (i) showing zonation CL of D3b, (k) D2 with organic material around the crystal rim

(crossed polars; Sample BR), and (l) Ultraviolet image of (k) showing no florescence of the organic matter.

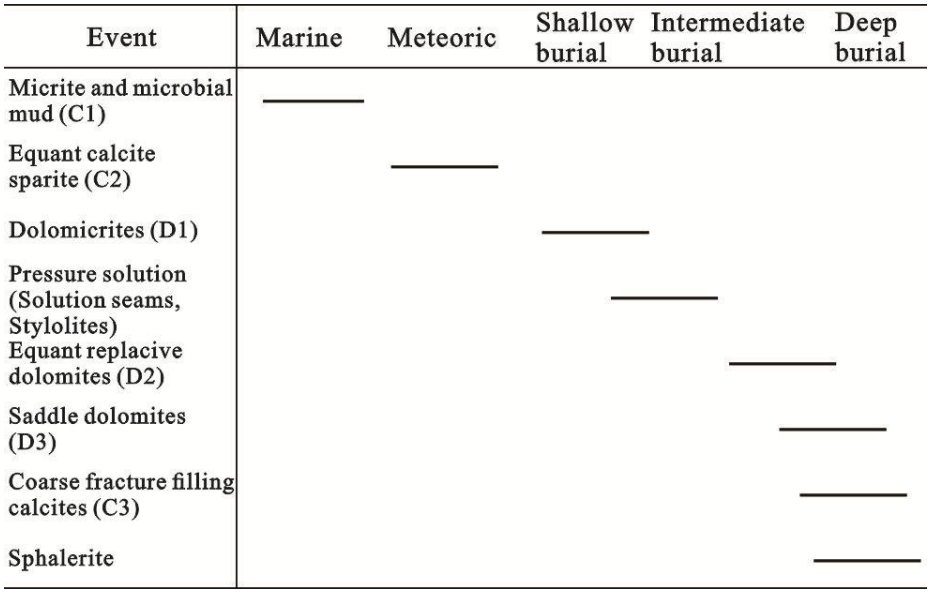

Figure 4.2. Paragenetic sequence of the main diagenetic events that influenced the Esino and Breno carbonates based on petrographic relationships.

The early dolomite (D1) consists of replacive fabric retentive near-micritic to non-planar mosaic crystals (Fig. 4.1d, e) ranging from 3 to 35μm with irregular intercrystalline boundaries. D1 is nonporous with dull to non-CL image (Fig. 3f) and crosscut occasionally by microstylolites (Fig. 4.1f). D2 is a replacive fabric destructive dolomite and consists of eu- to subhedral crystals ranging from 30 to 600μm where crystals may have cloudy cores with clear rims (Fig. 4.1d, g). D2 exhibit dull (D2a, Fig. 4.1h) to, at times, concentric zoning CL (D2b, Fig. 4.1h). Like D1, D2 is crosscut by the late fractures, which are filled with the latest D3 and C3. Organic material is visible around the crystal rims of D2 and also marks their growth zones inside the crystals but

shows no fluorescence under UV (Fig. 4.1k, l). The D3 is fracture-filling, coarse (250μm - 5mm) an- to subhedral crystals of saddle dolomite with typical undulose extinction (Fig. 4.1e, i) and dull CL (D3a, Fig. 4.1f) to occasionally concentric zoning (D3b, Fig. 4.1j) like D2. All the dolomite and calcite generations are nonporous.

4.2. Fluid inclusions

The primary two-phase (liquid + vapour) fluid inclusion (Goldstein and Reynolds, 1994) were measured in D2 and D3, as well as C3, which have larger crystals (Appendix 2) but no measurements were obtained from D1 (dolomicrite) because of the small crystal sizes. The measured inclusions have relatively consistent liquid: vapour ratios (~ 0.95) and narrow range (less than 15 °C) of homogenization temperatures (Goldstein and Reynolds, 1994, Bodnar, 2003). The homogenization temperatures (T_h), initial melting temperatures (T_i), final melting temperatures of ice ($T_{m\,(ice)}$), and calculated salinities as well as their statistics are presented in Appendix 2 and summarized in Table 4.1 and Figure 4.3a-d.

The mean values of T_h of D2, D3 and C3 (Table 4.1) did not vary dramatically (108 ± 9 °C， n = 58, 111 ± 14 °C, n = 108, and 112 ± 9 °C, n = 80, respectively) and similarly their mean values of $T_{m\,(ice)}$ (-21 ± 3 °C, n = 44, -18 ± 6 °C, n = 104, and -20 ± 6 °C, n = 63) and their salinity estimates too (23 ± 2 eq wt% NaCl, n = 44, 20 ± 4 eq wt% NaCl, n = 104, and 22 ± 5 eq wt% NaCl, n = 63, respectively).

Table 4.1

Statistics of microthermometric measurements of the investigated carbonates.

Host mineral		T_i (°C)	$T_{m\,(ice)}$ (°C)	Eq. wt% NaCl	T_h (°C)
D2	*n*	1	44	44	58
(2 - 20µm)	Mean	-43	-21	23	108
	S.D.		3	1.7	9
	Max	-43	-15	27	128
	Min	-43	-27	19	94
D3	*n*	77	104	104	108
(2 - 30µm)	Mean	-32	-18	20	111
	S.D.	8	6	4	14
	Max	-18	-8	30	144
	Min	-51	-32	12	86
C3	*n*	66	63	63	80
(3 - 50µm)	Mean	-41	-20	22	112
	S.D.	7	6	5	9
	Max	-21	-8	29	140
	Min	-52	-31	12	91

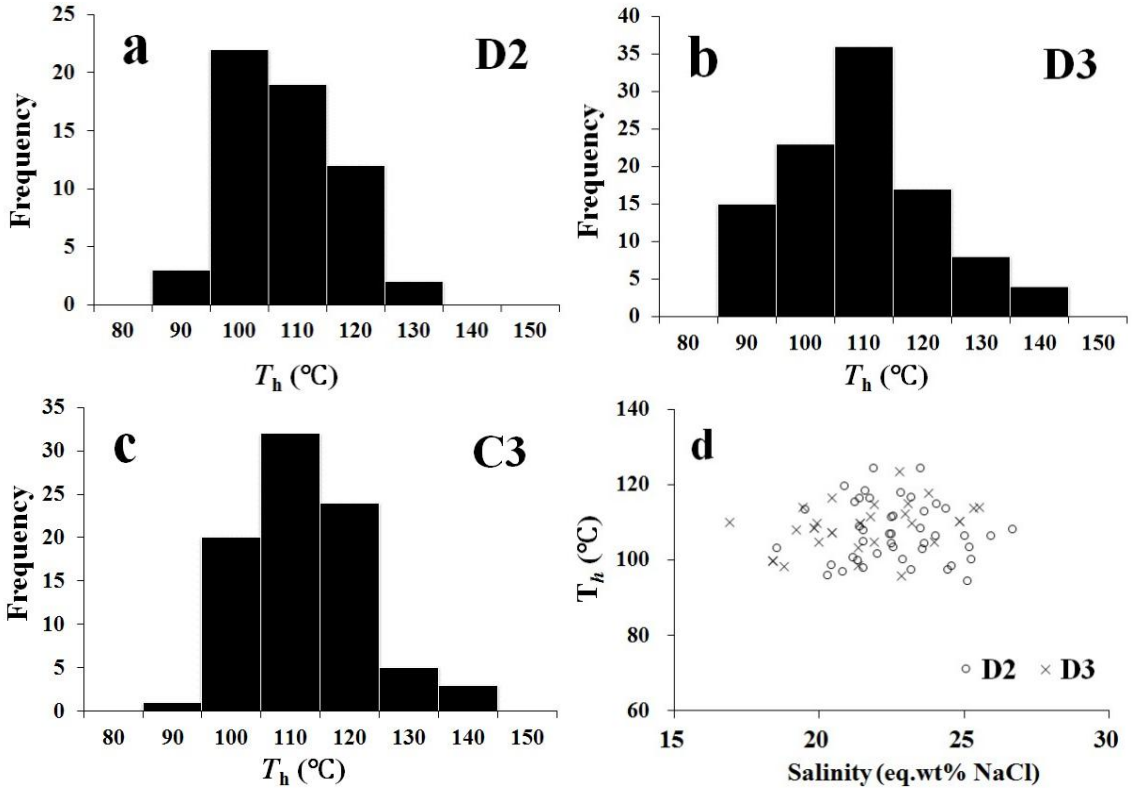

Figure 4.3. Plots of the microthermometric data of primary two-phase fluid inclusions trapped in D2, D3 and C3, showing histograms of homogenization temperature of (a) D2, (b) D3, and (c) C3, and a scatter diagram (d) of estimated salinity (Bodnar, 2003) vs. homogenization temperatures of D2 and D3.

4.3. Major and minor elements

The results of major and minor elements of Esino and Breno carbonates are presented in Appendix 1 and summarized in Table 4.2. They indicate that the investigated dolomites are near stoichiometric and have around the same Mg concentrations ($MgCO_3$%, D1, 43.6 ± 3.9%, n = 33; D2, 45.4 ± 6.0%, n = 17; D3, 44.7 ± 5.4%, n = 49).

Table 4.2

$CaCO_3$, $MgCO_3$, Mn, Sr, Fe, $\delta^{18}O$ and $\delta^{13}C$ statistics of the investigated Esino and Breno carbonates in the Western Southern Alps.

Phase		$CaCO_3$%	$MgCO_3$%	Fe (ppm)	Mn (ppm)	Sr (ppm)	$\delta^{13}C$‰ (VPDB)	$\delta^{18}O$‰ (VPDB)
C1	*n*	36	36	36	36	36	18	18
	Mean	98.2	1.8	217	203	237	1.0	-7.9
	S.D.	1.5	1.5	153	131	123	0.9	1.8
	Max	99.4	7.1	703	565	606	1.8	-5.2
	Min	92.9	0.6	56	56	146	-1.1	-13.2
C3	*n*	18	18	18	18	18	9	9
	Mean	97.6	2.4	805	1328	178	0.7	-9.3
	S.D.	1.8	1.8	1111	1192	192	0.6	2.7
	Max	99.4	5.6	3788	3655	649	1.6	-5.2
	Min	94.4	0.6	74	102	47	0.0	-13.0
D1	*n*	33	33	40	40	40	20	20
	Mean	56.4	43.6	4438	1219	76	1.7	-5.9
	S.D.	3.9	3.9	4393	1418	37	0.6	3.3
	Max	64.6	51.3	16735	4863	155	2.6	-0.8
	Min	48.7	35.4	289	122	27	0.7	-10.2
D2	*n*	17	17	22	22	22	8	8
	Mean	54.6	45.4	1460	556	53	1.8	-8.4

	S.D.	6.0	6.0	900	289	31	0.3	1.2
	Max	62.9	55.3	3162	1078	125	2.3	-6.6
	Min	44.7	37.1	276	156	18	1.3	-9.8
D3	*n*	49	49	53	53	53	25	25
	Mean	55.3	44.7	4462	1091	57	1.9	-9.0
	S.D.	5.4	5.4	4888	1183	24	0.5	1.0
	Max	64.9	54.9	24955	6049	151	2.9	-6.1
	Min	45.1	35.1	714	266	31	0.9	-10.4

D2 has the lowest mean Fe (1460 ± 900, *n* = 22) and Mn (556 ± 289 ppm, *n* = 22) concentrations relative to those of D1 (Fe = 4438 ± 4393 ppm, *n* = 40 and Mn = 1219 ± 1418 ppm, *n* = 40, respectively) and D3 (Fe = 4462 ± 4888 ppm, *n* = 53 and Mn = 1091 ± 1183 ppm, *n* = 53, respectively). D2 and D3 have similar Sr concentrations (53 ± 31 ppm, *n* = 22 and 57 ± 24 ppm, *n* = 53, respectively), which are lower than those of D1 (76 ± 37 ppm, *n* = 40). Calcites have lower mean Fe concentrations (C1 = 217± 153 ppm, *n* = 36 and C3 = 805 ± 111 ppm, *n* = 18) but higher Sr contents (C1 = 237 ± 123 ppm, *n* = 36 = C3, 178 ± 193 ppm, *n* = 18) than their calcite counterparts (Table 4.2). Among all the calcite and dolomite generations, calcite C1 has the lowest mean Fe and Mn concentrations (217 ± 153 ppm, *n* = 36 and 203 ± 131 ppm, *n* = 36, respectively) and highest Sr contents (237 ± 123 ppm, *n* = 36), whereas calcite C3 has the highest mean Mn concentrations (1328 ± 1192 ppm, *n* = 18). C2 was impossible to microsample because it is rare and always mixed with C1.

4.4. Carbon and oxygen isotopes

The results of carbon and oxygen isotopes of Esino and Breno carbonates are presented in Appendix 1 and summarized in Table 4.2. The mean $\delta^{13}C$ and $\delta^{18}O$ values of C3 are more depleted than those of C1 (+0.7 ± 0.6‰ VPDB,*n* = 9 and -9.3 ± 2.7‰ VPDB, *n* = 9 vs. +1.0 ± 0.9‰ VPDB, *n* = 18 and -7.9 ± 1.8‰ VPDB, *n* = 18, respectively). The mean $\delta^{13}C$ values increases slightly from D1 (1.7 ± 0.6‰ VPDB, *n* = 20) to D2 (1.8 ± 0.3‰ VPDB, *n* = 8) and the latest D3 (1.9 ± 0.5‰ VPDB, *n* = 25), but the mean $\delta^{18}O$ values follows the opposite direction although the change is also insignificant between D2 and D3 (D1 = -5.9 ± 3.3‰ VPDB, *n* = 20; D2 = -8.4 ± 1.2‰ VPDB, *n* = 8; and D3 = -9.0 ± 1.0‰ VPDB, *n* = 25, respectively). C3 has the most depleted mean $\delta^{13}C$ and $\delta^{18}O$ values among all the investigated calcites and dolomites (Table 4.2).

4.5. Rare earth elements (REE)

The results of Rare earth elements (REE) of Esino and Breno carbonates are presented in Appendix 1 and summarized in Table 4.3, and Figure 4.4 shows the corresponding shale normalized profiles. Calcite C3 has the highest mean∑REE value (17 ± 12 ppm, *n* = 9) among all the investigated calcites and dolomites, and D1 has the highest mean value (∑REE = 10 ± 9 ppm, *n* = 19) among all the dolomites but D2 has the lowest (∑REE = 3 ± 1 ppm, *n* = 11).

Table 4.3

Summary of rare earth element concentrations in the investigated Esino and Breno carbonates in the Western Southern Alps.

Phase		La (ppb)	Ce (ppb)	Pr (ppb)	Nd (ppb)	Sm (ppb)	Eu (ppb)	Gd (ppb)	Tb (ppb)	Dy (ppb)	Ho (ppb)	Er (ppb)	Tm (ppb)	Yb (ppb)	Lu (ppb)	ΣREE (ppm)
D1	n	19	19	19	19	19	19	19	19	19	19	19	19	19	19	19
	average	1956	4146	523	2107	402	91	398	57	294	56	157	20	127	17	10
	stdev	1830	3710	443	1758	322	76	296	39	172	31	84	10	65	9	9
	max	7937	16176	1770	6765	1217	295	1182	148	613	113	311	38	250	35	37
	min	316	478	74	308	57	11	64	10	52	12	34	4	35	5	2
D2	n	11	11	11	11	11	11	11	11	11	11	11	11	11	11	11
	average	702	1105	138	528	107	22	135	23	137	30	88	12	69	10	3
	stdev	267	490	47	171	39	7	48	9	55	12	33	5	31	5	1
	max	1298	2297	231	815	174	37	219	40	234	53	146	19	115	17	6
	min	353	481	74	290	52	14	69	10	59	13	34	3	18	2	2

D3	n	26	26	26	26	26	25	26	26	26	26	26	26	26	25	26
	average	1564	2994	359	1350	240	56	258	34	164	30	81	9	53	7	7
	stdev	1868	4109	495	1876	325	70	342	45	211	36	95	11	65	8	9
	max	6943	18095	2267	8658	1569	298	1610	221	1060	182	486	55	337	40	42
	min	186	284	37	138	27	6	27	2	25	4	11	0	11	1	1
C1	n	18	18	18	18	18	18	18	18	18	17	18	18	18	15	18
	average	1064	2013	249	968	174	39	171	23	119	24	72	10	64	11	5
	stdev	1335	2772	357	1407	250	57	233	32	183	41	122	18	113	20	7
	max	5640	11964	1518	5910	1000	193	838	119	757	172	531	79	494	79	28
	min	185	313	34	124	15	4	31	0	15	2	9	0	8	0	1
C3	n	9	9	9	9	9	9	9	9	9	9	9	9	9	9	9
	average	3159	6672	802	3095	603	163	633	99	516	106	316	46	311	48	17
	stdev	1943	4924	489	1954	473	144	523	93	527	119	359	53	377	62	12
	max	7370	18336	1663	6607	1524	484	1546	263	1494	344	1086	157	1127	186	41
	min	1238	2793	311	1173	219	42	242	26	86	10	34	7	21	2	7

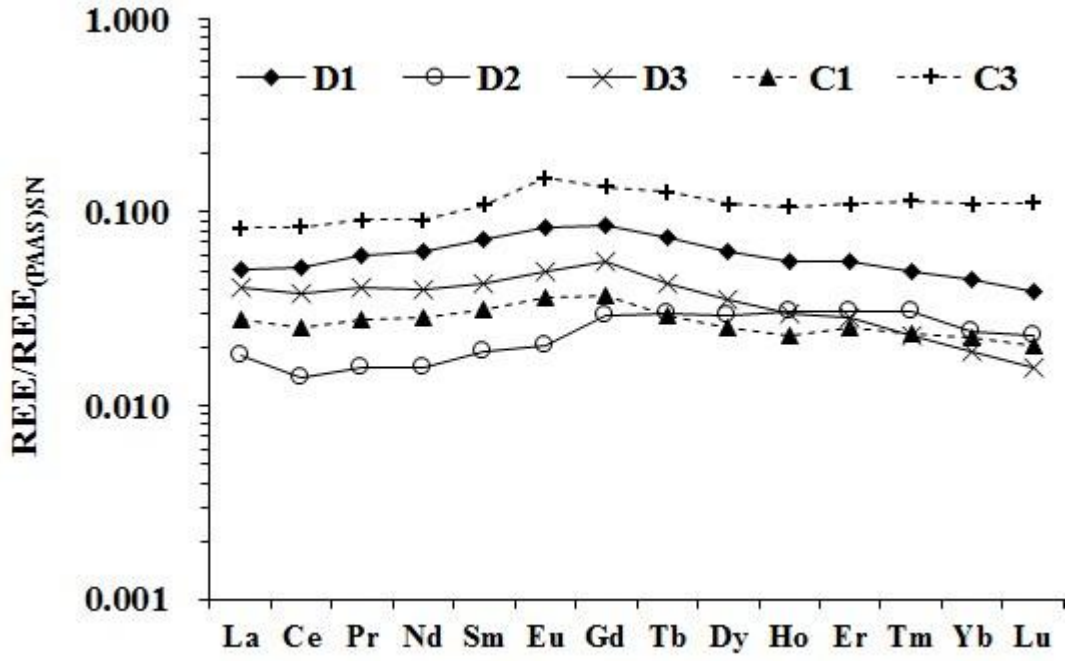

Figure 4.4. Patterns of mean shale-normalized REE concentrations of the investigated calcite and dolomite generations.

A narrow range of mean Ce anomaly values is displayed in both calcites and dolomites (Table 4.4). However, the calcites have slightly higher mean Ce anomaly values (C1 = 0.90 ± 0.07, *n* = 18 and C3 = 0.94 ± 0.15, *n* = 9) than those of dolomites (D1 = 0.93 ± 0.10, *n* = 19, D2 = 0.80 ± 0.07, *n* = 11, and D3 = 0.87 ± 0.13, *n* = 26). Similarly, the mean Eu anomaly values (Table 4.4) are higher in calcites (C1 = 1.30 ± 0.51,*n* = 18 and C3 = 1.34 ± 0.51, *n* = 9) than in dolomites (D1 = 1.13 ± 0.23, *n* = 19, D2 = 0.93 ± 0.20, *n* = 11, and D3 = 1.17 ± 0.30, *n* = 26). However, C3 has the highest value, whereas D2 has the lowest of both Ce and Eu anomalies. There are no distinctions in the La anomaly values of both calcite and dolomite generations (Table 4.4). Except for D2 that

has Eu anomaly slightly below unity (0.93±0.2, n = 11), the other carbonate generations that are slightly above unity (Table 4.4).

Table 4.4

Summary of statistics of Ce $(Ce/Ce^*)_{SN}$, Eu $(Eu/Eu^*)_{SN}$ and La $(Pr/Pr^*)_{SN}$ anomalies based on the equations of Bau and Dulski (1996).

Phase		Ce^*_{SN} anomaly	Eu^*_{SN} anomaly	La^*_{SN} anomaly
D1	*n*	19	19	19
	average	0.93	1.13	1.04
	stdev	0.10	0.23	0.05
	max	1.06	1.58	1.11
	min	0.69	0.45	0.94
D2	*n*	11	11	11
	average	0.80	0.93	1.07
	stdev	0.07	0.20	0.05
	max	0.96	1.12	1.16
	min	0.68	0.52	0.99
D3	*n*	26	25	26
	average	0.87	1.17	1.07
	stdev	0.13	0.30	0.08

	max	1.30	1.88	1.29
	min	0.50	0.56	0.93
C1	*n*	18	18	18
	average	0.90	1.30	1.04
	stdev	0.07	0.51	0.06
	max	1.05	2.40	1.15
	min	0.79	0.50	0.89
C3	*n*	9	9	9
	average	0.94	1.34	1.06
	stdev	0.15	0.51	0.09
	max	1.23	2.56	1.16
	min	0.73	0.95	0.88

4.6. Fluid-inclusion gas

Results of Fluid-inclusion gas analysis of investigated carbonates are presented in Appendix 3. The statistics of CO_2/CH_4, N_2/Ar and Ar/He ratios of weighted mean values of fluid-inclusion gas are shown in Table 4.5. The ratio of CO_2/CH_4 varied from 4.25 to 122.21 in C1, from 7.41 to 43.20 in D1, from 1.90 to 6.23 in D2, and from 8.31 to 74.90 in D3. The ratio of Ar/He varied from 4.86 to 123.57 in C1, from 1.35 to 7.73 in D1, from 1.21 to 10.14 in D2, and from 0.51 to 15.82 in D3. The ratio of N_2/Ar varied from

68.41 to 118.80 in C1, from 50.13 to 109.72 in D1, from 61.61 to 80.41 in D2, and from 79.29 to 136.32 in D3.

Table 4.5

CO_2/CH_4, N_2/Ar and Ar/He ratios of weighted mean values offluid-inclusion gas of investigated carbonates.

Sample	CO_2	CH_4	Ar	He	N_2	CO_2/CH_4	Ar/ He	N_2/Ar
AR5-C1	12.645	2.110	0.031	0.005	2.141	5.99	6.66	68.41
AR5-C1	11.686	2.752	0.018	0.004	1.433	4.25	4.86	79.59
PE4-C1	4.300	0.035	0.024	0.000	2.209	122.21	123.57	92.15
PE5-C1	0.764	0.059	0.001	0.000	0.061	12.89	13.12	118.80
PE5-C1	0.728	0.071	0.002	0.000	0.149	10.32	17.00	87.76
Ar5-D1	15.220	2.054	0.025	0.003	1.259	7.41	7.73	50.13
AR7-D1	10.277	0.950	0.014	0.002	0.855	10.82	7.34	59.22
ES1-D1	11.718	0.271	0.004	0.003	0.411	43.20	1.35	109.72
BR-D2	1.478	0.622	0.002	0.002	0.142	2.38	1.21	61.61
BR2-D2	2.128	1.118	0.004	0.003	0.339	1.90	1.38	80.41
BR3-D2	2.733	0.438	0.021	0.002	1.376	6.23	10.14	66.23
ES1-D3	2.539	0.052	0.002	0.002	0.173	49.12	0.78	96.22
ES1-D3	10.286	0.137	0.005	0.007	0.530	74.90	0.72	109.76
PE1-D3	2.096	0.088	0.017	0.001	1.918	23.95	15.82	110.09
PE14-D3	6.047	0.607	0.010	0.007	0.964	9.95	1.39	99.09
PE3-D3	3.993	0.116	0.001	0.000	0.093	34.31	9.00	103.00

PE3-D3	1.465	0.176	0.003	0.002	0.261	8.31	1.10	101.04
PE4-D3	1.316	0.075	0.003	0.001	0.226	17.54	3.43	79.29
PE5-D3	1.939	0.138	0.002	0.001	0.172	14.07	2.09	100.88
PE5-D3	1.270	0.074	0.004	0.001	0.399	17.14	4.59	96.70
PE13-D3	1.408	0.099	0.001	0.001	0.113	14.26	1.06	95.70
PE15-D3	1.752	0.163	0.001	0.001	0.085	10.73	0.51	136.32

4.7. Halogens

Table 4.6 shows the results of the halogen contents and F/Cl, Cl/Br and Br/Cl molar ratios of the investigated Esino and Breno carbonates. All of the dolomite generations have close F/Cl molar ratios (D1, 0.009 to 0.042; D2, 0.010 to 0.023; D3, 0.006 to 0.060). The F/Cl molar ratios are slightly higher in C1 and C3 (0.017 to 0.052 and 0.014 to 0.068, respectively) than those of dolomites and C3 has the highest value of F/Cl molar ratio. D2 has the narrowest range of Cl/Br ratios (1547 to 2794) and D1 has the highest Cl/Br molar ratios, which are slightly higher than those of D3. C3 has high Cl/Br molar ratios (398 to > 4432) close to those of D1 but C1 has lowest ratios (72 ~ 257), which are much lower than those of C3 and dolomites.

Table 4.6

Results of the halogen contents and F/Cl and Cl/Br molar ratios of the investigated Esino and Breno carbonates.

Analyte Symbol	F	Cl	Br	F/Cl	Cl/Br
Unit Symbol	mg/L	mg/L	mg/L	(Molar)	(Molar)
Detection Limit	0.01	0.03	0.03		
AR5D1	0.49	60.9	< 0.03	0.015	> 4575
AR7D1	0.29	58.5	0.1	0.009	1318
ES1D1	0.28	17.6	< 0.03	0.030	> 1322
PE8D1	0.20	8.8	0.05	0.042	398
ESD2	0.64	124.0	0.1	0.010	2794
BR3D2	0.25	20.6	< 0.03	0.023	> 1547
AR4D3	0.23	44.7	< 0.03	0.010	> 3358
ES1D3	0.98	48.6	0.23	0.038	476
PE5D3	0.92	79.0	0.23	0.022	774
PE8D3	0.20	19.9	< 0.03	0.019	> 1495
PE9D3	0.77	24.1	0.33	0.060	164
PE15D3	0.10	33.6	0.31	0.006	244
PE9C1	0.09	10.0	0.31	0.017	72
PE14C1	0.18	13.7	0.12	0.025	257
PE15C1	0.39	14.1	0.15	0.052	211
AR4C3	0.24	31.8	0.18	0.014	398
PG1C3	2.16	59.0	< 0.03	0.068	> 4432

CHAPTER 5

DISCUSSION

5.1. Dolomite petrography

The near micritic grainsize (3 - 35μm), fabric-retention and dull to non-CL exhibited by D1 imply early dolomitization of limemud in shallow burial settings at near-surface conditions, which is consistent with the crosscutting microstylolites. This is also supported by the limited recrystallization in C1, which suggests that the limemud was not exposed to extensive meteoric alteration before dolomitization. Also, the lack of evaporites reflects dolomitization by diagenetic fluids that were possibly a mixture of meteoric and marine waters (e.g., Azmy et al., 2008, 2009; Olanipekun, 2014) rather than by evaporated brines. On the other hand, the larger crystal sizes (30 - 600μm) of D2, relative to that of D1, and fabric destructive textures as well as the high mean T_h value (108 ± 9 °C, n = 58) suggest formation at a later stage of replacement in relatively deeper burial environment at higher temperature. Some of D2 crystals show cloudy core with clear rims indicating replacement of a precursor carbonate (cloudy core) followed by later cementation as a clear rim (e.g., Olanipekum et al., 2014). Earlier studies suggested that similar types of dolomite (D2) could be formed from direct replacement of C1 and C2 or recrystallization of D1 (e.g., Azmy et al., 2008, 2009; Conliffe et al., 2009; Azomani et al., 2013; Olanipekun et al., 2014). No visual porosity has been found in association with D2 in the Esino and Breno carbonates.

The latest saddle dolomite D3 generation is limited to filling vugs and late fractures that cut through all earlier dolomite phases, which implies formation at the deepest diagenetic settings during progressive burial and this is also consistent with the high mean T_h value (111 ± 14 °C， n = 108). The undulose extinction in D3 is the evidence of distorted crystal lattice caused by crystal growth at high temperatures (e.g., Warren, 2000; Rameil, 2008). The zoned CL images of D2 and D3 reflect variations of the chemical composition of diagenetic fluids during the course of precipitation (Warren, 2000; Boggs and Krinsley, 2006; Lonnee and Machel, 2006; Heira-Ardakan et al., 2013; Olanipekun et al., 2014).

5.2. Major and minor elements

The relative abundance of Mg and Ca concentrations in D1 (Mg/Ca = 43.6/56.4, Table 4.2) and low Sr concentrations (76 ± 37 ppm) support an early dolomitization under shallow burial environment (Sr < 550 ppm; Tucker and Wright, 1990). The low Sr concentrations of D1 argue against the sabkha origin (Sr > 550 ppm, Tucker and Wright, 1990; Azmy et al., 2013) but suggest that the parent dolimitizing fluid was diluted with meteoric water (e.g., Sperber et al., 1984; Azmy et al., 2008; 2009, Azomani et al., 2013; Olanipekun et al., 2014), which is consistent with the absence of evaporite layers in the investigated rocks. The Sr concentration is depleted with progressive diagenesis (Veizer et al., 1983) and the investigated dolomites have generally lower Sr contents than their precursor carbonate (C1), which reflects the influence of diagenetic alteration (Table 4.2). On the other hand, the Sr concentrations are generally lower in volcanic rocks than in marine carbonates (cf, Veizer, 1983; Faure, 2001). Therefore, the contribution from the

interaction of dolomitizing fluids with the co-occurring volcaniclastic lenses, or from fluids associated with volcanic activity, would unlikely overprint the Sr signature of the dolomites or their precursor limestones, particularly when Sr is depleted with diagenesis (progressive burial).

Iron (Fe) and Mn concentrations reflect the redox conditions in the diagenetic environment (e.g., Veizer, 1983; Tucker and Wright, 1990). Therefore, dolomicrites tend to have low Fe and Mn contents within few hundred ppm due to formation at near-surface/shallow burial conditions (e.g., Azmy et al., 2008, 2009; Azomani et al., 2013; Olanipekun et al., 2014), but carbonates of deep burial diagenesis tend to be enriched in Fe and Mn (Veizer, 1983). However, D1 (dolomicrite) has significantly higher concentrations of Fe (4438 ± 4394 ppm) and Mn (1219 ± 1418 ppm) relative to those of their precursor C1 and even the later dolomite generation D2 (Table 4.2). Taking into account the lack of Fe-rich sediments in the succession and the visual estimates of abundance of bacterial microrhombic pyrite in D1 being < 1%, this suggests that there was an intense water-rock interaction of the parent dolomitizing fluid with the volcaniclastic lenses before the dolomitization of calcites so that the fluids became dramatically enriched with Fe and Mn and/or the dolomitizing basinal fluids of D1 had possibly some contributions from fluids associated with the volcanic activities in the surrounding area. Moreover, D1 is unlikely the precursor of D2 due to the dramatic lower Fe and Mn concentrations in D2 (Table 4.2; 1460 ± 900 ppm and 556 ± 289 ppm, respectively) than those in D1. However, the increase in Fe and Mn from D2 to D3 (1091 ± 1183 ppm and 4463 ± 4888 ppm, respectively) is consistent with the concept of

increasing diagenesis with progressive burial (e.g., Veizer et al., 1983; Azmy et al., 2001), and similarly the trend from C1 to C3 (Table 4.2) although the influence of volcaniclastic lenses on the deposition of the hydrothermal D3 and C3 cannot be entirely eliminated since they precipitated likely from basinal fluids that were circulated, through those volcaniclastic and other sediments of the basin, and heated with progressive burial.

5.3. Carbon and oxygen isotopes

Despite the diagenetic alteration, both dolomites and calcites have $\delta^{13}C$ values within the range of the documented signatures of the best preserved Triassic carbonates (Fig. 5.1; Korte et al., 2005), which is also supported by the poor correlation ($R^2 \leq 0.3$) between Mn/Sr and $\delta^{13}C$ values (Fig. 5.2). This suggests that the $\delta^{13}C$ of diagenetic fluids was likely buffered by that of the surrounding carbonates and that the bituminous material around the growth zones of D2 (Fig. 4.1) was introduced to the basin of deposition after or at a very late stage of D2 precipitation and before D3. The close $\delta^{13}C$ values of C1, D1 and D2 (Table 4.2) suggest that C1 was likely the precursor of dolomite D1 and D2, which is supported by the petrographic evidence. On the other hand, the $\delta^{18}O$ values of both dolomites and calcites are more depleted than those of well-preserved Triassic carbonates (Veizer et al., 1999; Korte et al., 2005), thus reflecting the influence of water/rock interaction, $\delta^{18}O$ of the dolomitizing fluids and temperature control of the burial environments (Fig. 5.1).

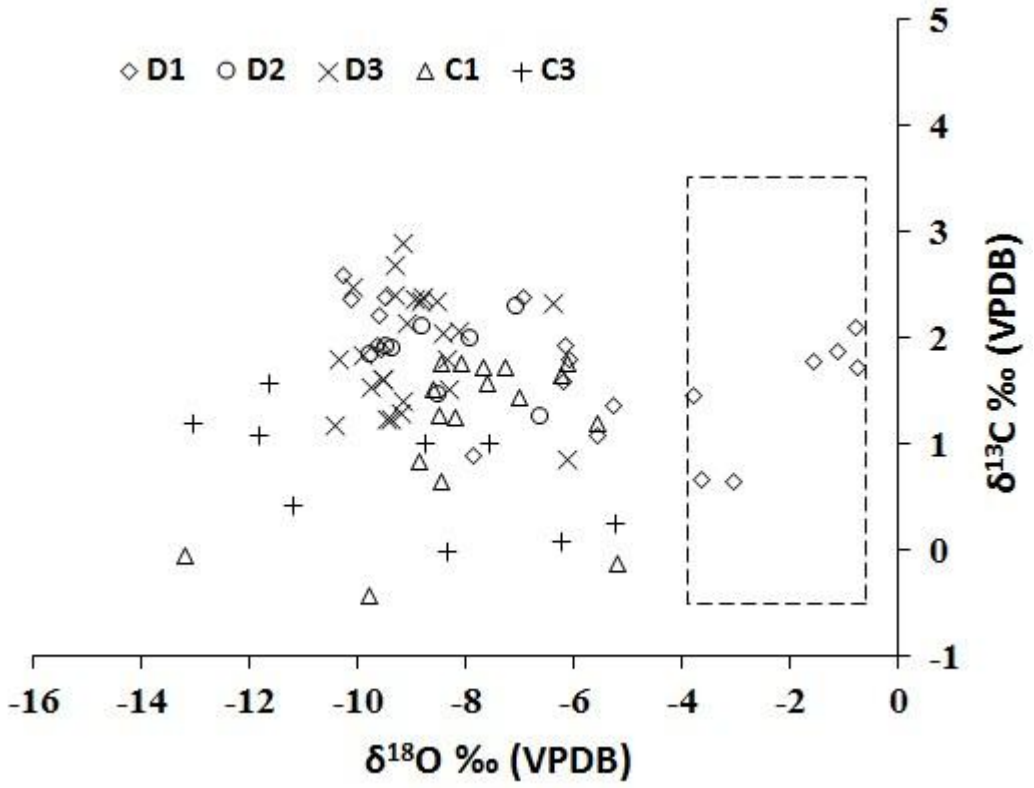

Figure 5.1. Scatter diagram of $\delta^{18}O$ vs. $\delta^{13}C$ of the investigated carbonates. The square marks the $\delta^{18}O$ and $\delta^{13}C$ ranges of composition of the well-preserved Triassic carbonates (Korte et al., 2005)

Dolomitization requires large amounts of Mg-rich fluids and the $\delta^{18}O$ composition of the produced dolomites are therefore dominantly influenced by that of the parent fluid and the temperature of dolomitization. Thus, estimates of $\delta^{18}O$ values of the dolomitizing fluid (Land, 1983) can be calculated by using the T_h values (estimates of minimum entrapment temperature) of primary two-phase fluid inclusions (Goldstein and Reynolds, 1994) and nature of rock fabric, such as grainsize (e.g., Azomani et al., 2013; Olanipekun et al., 2014).

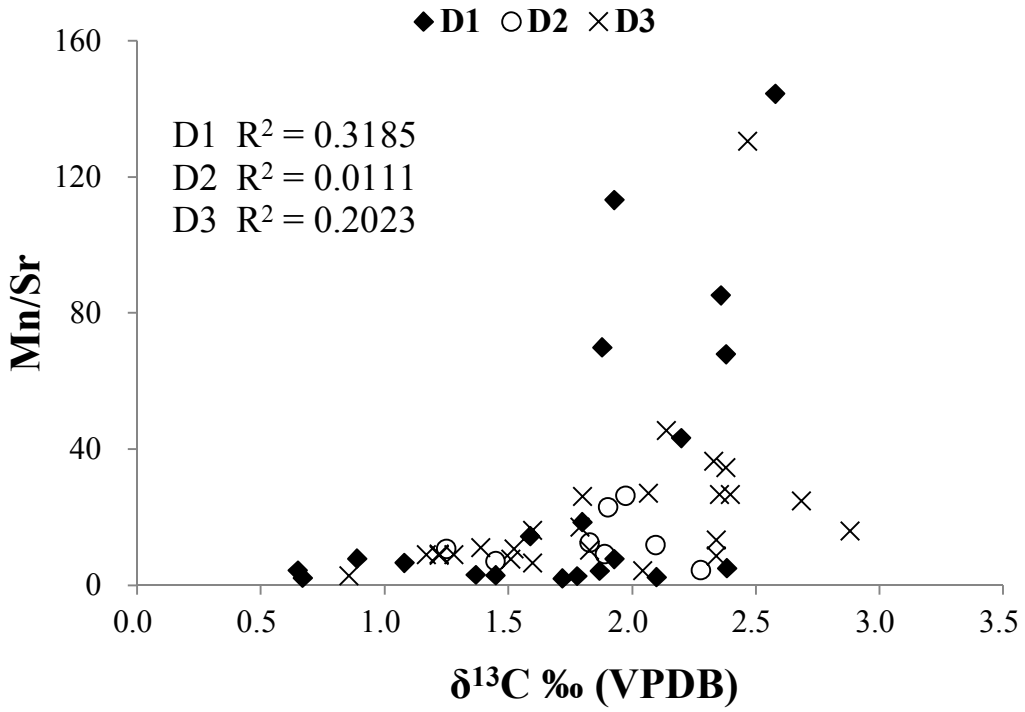

Figure 5.2. Scatter diagrams of $\delta^{13}C$ vs. Mn/Sr of the investigated dolomites.

The fabric retention and near-micritic grain size of D1 suggest that dolomitization occurred at shallow burial settings of near-surface conditions (T < 50ºC, Goldstein and Reynolds, 1994). Thus, the $\delta^{18}O$ (VPDB) values of D1 (-10.2 to -0.8‰ VPDB; Table 4.2) imply a parent dolomitizing fluid with $\delta^{18}O$ values approximately between -12.4 and +2.8‰ SMOW (Fig. 5.3). The estimated $\delta^{18}O$ value of Triassic seawater was between -1 and -4‰ SMOW (Veizer et al., 1999; Korte et al., 2005). The investigated sediments reflect precipitation under tropical conditions. Assuming that the difference in $\delta^{18}O$ compositions between the Triassic meteoric and seawaters was similar to that of our modern environment, which is ~ 4‰ SMOW (Clark and Fritz, 1997), and that the temperature of dolomitization was between 25 to 30 ºC, the calculated $\delta^{18}O$ value of the

Middle Triassic meteoric water is as low as ~ -8‰ SMOW, which is more enriched than the calculated lower end-member value of the D1 parent fluid (~ -12.4‰ SMOW; Fig. 5.3), which is implausible. This suggests dolomitization at slightly warmer near-surface temperature (45 - 50 °C; Fig. 5.3) possibly in a mixing zone or due to contributions from warm volcanic-associated fluids enriched in ^{18}O. Alternatively, the precursor calcite was significantly altered before dolomitization, but the fabric retention and near-micritic grainsize would argue against repeated meteoric alteration. On the other hand, if dolomitization occurred at 45 - 50 °C, the$\delta^{18}O$ of the parent fluid would be between ~ -8 to +2.8 SMOW, which is more plausible. Thus, the O-isotope composition of D1 also supports the scenario of shallow burial settings and also possible minor contributions from fluids related to volcanic activity in the basin, particularly when those fluids are enriched in ^{18}O which may explain the slight enrichment in the estimated$\delta^{18}O$ of the parent fluids (high end member slightly > 0; Fig. 5.3) relative to that of the Middle Triassic sweater (Veizer et al., 1999; Korte et al., 2005).

The calculated $\delta^{18}O$ composition of the parental dolomitizing fluids of D2 and D3 (about 0.4 to 7.1 and -1.5 to 9.4‰ SMOW, respectively) is higher than that of the parental dolomitizing fluid of D1 (Fig. 5.3), which is expected for diagenetic fluids at higher temperatures of deeper burial settings since deep basinal brines are more saline and enriched in ^{18}O regardless the age of rocks or location of basins (Goldstein and Reynolds 1994; Azmy et al., 2001; Lonnee and Machel, 2006; Azomani et al., 2013; Haeri-Ardakani et al., 2013; Olanipekun et al., 2014). The high T_h and salinity values of D2 and D3 (Table 4.1), along with the$\delta^{18}O$ estimates of their parent fluids (Fig. 5.3),

support a hydrothermal origin. Also, the overlap in the $\delta^{18}O$ of D2 and D3 fluids (Fig. 5.3) suggests that those dolomites developed from fluids of similar isotopic compositions that possibly evolved through basinal circulation. Similar overlap has been documented in earlier studies of dolomites in other basins (e.g., Azmy et al., 2009; Azomani et al., 2013; Olanipekun et al., 2014).

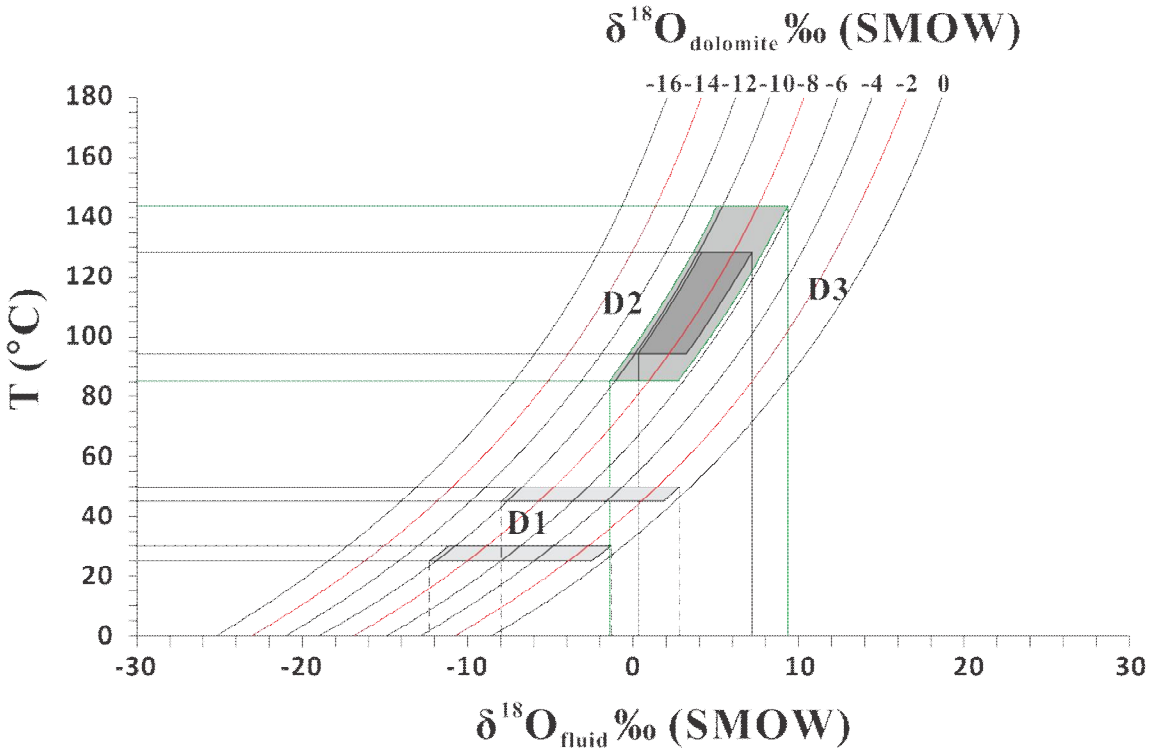

Figure 5.3. Temperature (T) vs. $\delta^{18}O_{\text{dagenetic fluid}}$. $\delta^{18}O_{\text{dolomite}}$ values reconstructed following the equation of Land, 1983 ($10^3 \ln\alpha = 3.2\times10^6 T^{-2} - 3.3$). The shaded areas indicate the ranges of $\delta^{18}O_{\text{fluid}}$ based on the $\delta^{18}O_{\text{dolomite}}$ values and homogenization temperatures (T_h) of each dolomite generation.

5.4. Rare earth elements (REE)

The shale normalized REE patterns of the investigated dolomites (Fig. 4.4) and the similarity of Ce and La anomalies of dolomites to those of C1 (Fig. 5.4) show that they may still retain, to some extent, a remnant of the negative Ce anomaly that characterizes the modern brachiopods and also the well-preserved shallow water marine carbonates of the Paleozoic (Azmy et al., 2011). The REE normalized patterns of seawater and shallow-water marine carbonates do not exhibit Eu anomaly (e.g., Elderfield and Greaves, 1982; Hongo and Nozaki, 2001; Bau et al., 2010). However, the investigated dolomites and calcites exhibit some slight positive (>1) Eu anomaly (Fig. 4.4 and Table 4.4). Positive Eu anomaly has been documented by earlier studies in fluids from hydrothermal vents at the seafloor and from associated bivalve shells living in the close habitat (Bau et al., 2010). This is consistent with the unusual high Fe contents in D1 and the suggested intense reaction of the dolomitizing fluid with the associated volcaniclastic lenses prior to dolomitization. Also, the slight occurrence of positive Eu anomaly (Fig. 4.4 and Table 4.4) in C1 suggests that despite the insignificant the early meteoric diagenesis of the lime mudstone, it still shows the influence by the volcanic activity in the region, which is expected due to the high sensitivity of REE to diagenesis even when minor (Azmy et al., 2011, 2013). The same effect in D3 and C3 also implies that they were formed from the same earlier basinal fluids that were circulated in the basinal deposits with progressive burial. This also agrees with the parallel shale-normalized trends of all of the investigated carbonates (Fig. 4.4), thus suggesting that the REE composition of the diagenetic dolomites is, to some extent, controlled by that of the precursor carbonate (e.g., Azomani

et al., 2013). However, some of the D2 samples exhibit Eu anomaly <1 (Table 4.4; Fig. 4.4), which suggests that the REE composition of its parent diagenetic fluid might have had insignificant influence by the volcanic lenses possibly due to possible temporary restricted fluid circulations caused by changes in tectonic settings in the basin (e.g., Sibson, 1977; Horbury and Robinson, 1993) around the time of formation of D2.

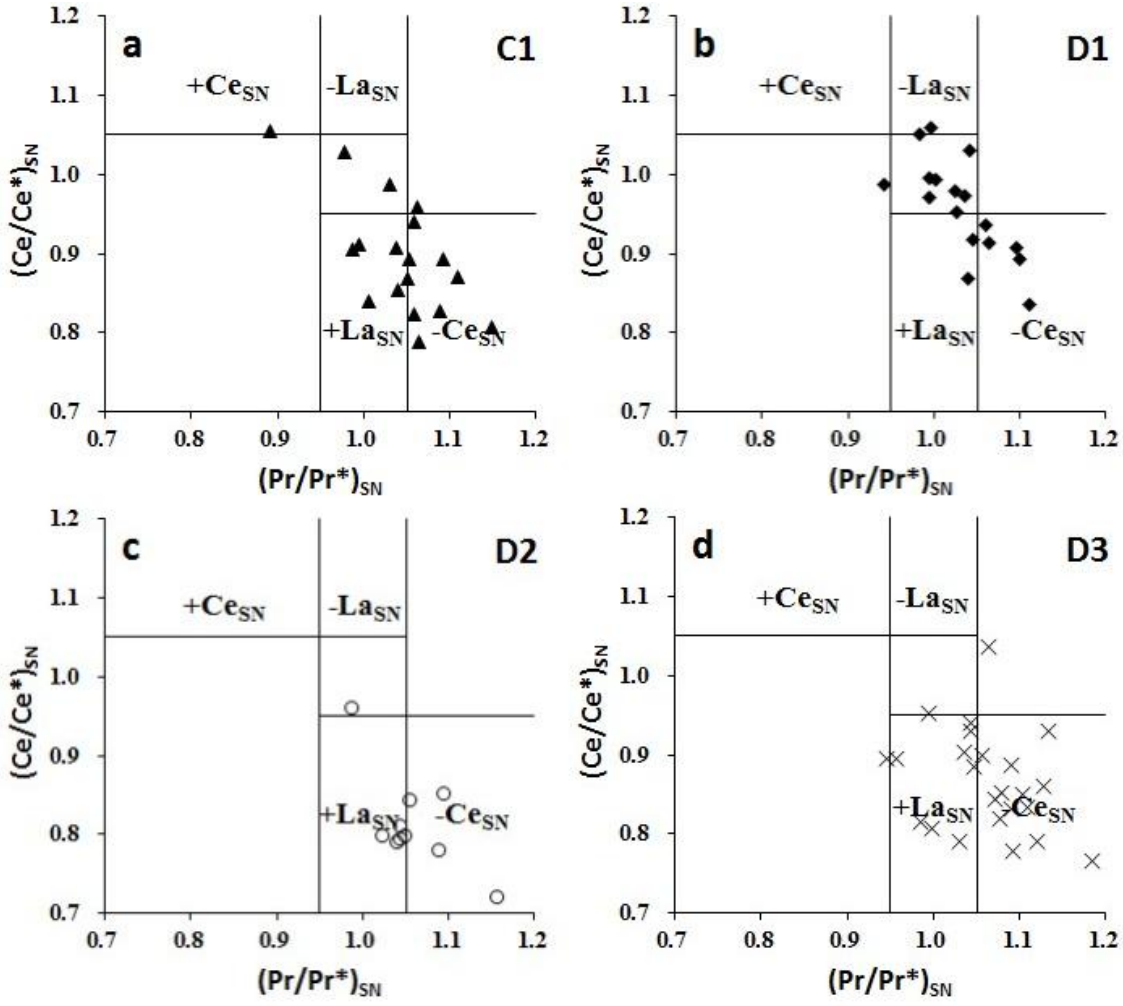

Figure 5.4. Scatter diagrams of $(Ce/Ce^*)_{SN}$ vs $(Pr/Pr^*)_{SN}$ for the precursor lime mudstone (C1) and the investigated dolomites (after Bau and Dulski, 1996).

5.5. Fluid-inclusion gas

Figure 5.5a shows that a considerable number of the data points from each investigated carbonate generation (calcites and dolomites) plots within the magmatic zone and along the boundary of the magmatic zone with other zones. However, D2 plots within the evolved crust zone although very close to the boundary of the magmatic zone. This is consistent with the suggested scenario of possible contributions of fluids from volcanic activities to the parent diagenetic fluids of dolomites and calcites, particularly those of D1 that has distinctly higher Fe contents and also slightly ^{18}O-enriched parental fluids. The occurrence of points along or close to the boundary of the magmatic zones suggests that contribution from the volcanic fluids was likely restricted and that the diagenetic fluid composition was possibly buffered at times by that of the basinal fluids and evolved through circulation with progressive burial.

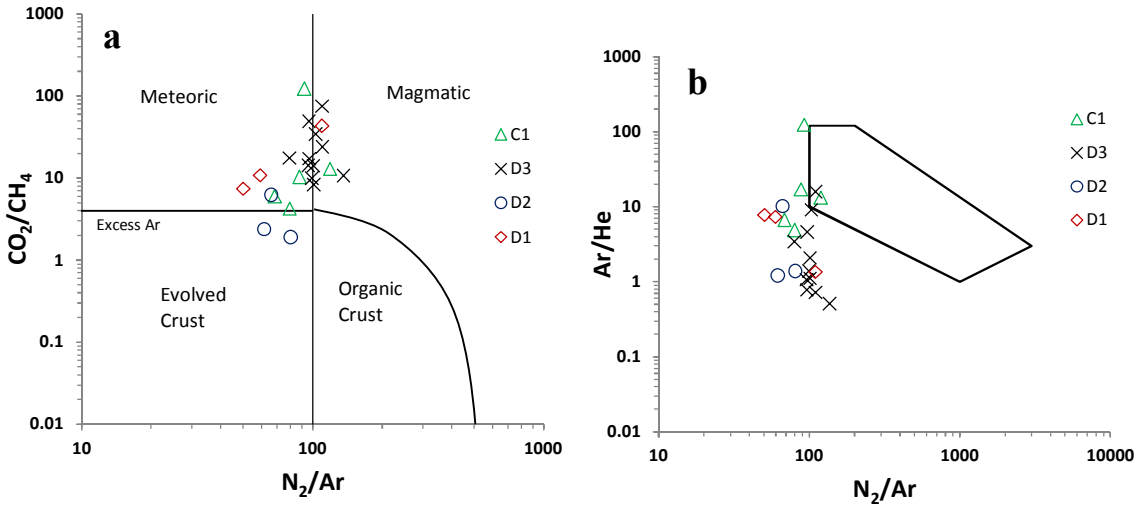

Figure 5.5. Scatter diagrams of (a) N_2/Ar vs. CO_2/CH_4 and (b) N_2/Ar vs. Ar/He for C1 and dolomites (D1, D2, and D3) of the Esino and Breno formations (after Norman and

Moore, 1999; Blamey and Norman, 2002; Blamey, 2012) based on the weighted mean values (Appendix 3).

Figure 5.5b shows similarly points located along or close to the boundary of the magmatic zone and few within the magmatic zone, which is consistent with the suggested scenario of buffering diagenetic fluids with progressive burial. Also, the investigated dolomites are not expected to plot entirely within the calc-alkaline magmatic since they are not magmatic rocks but were formed by diagenetic fluids that had some contributions possibly from fluids associated with volcanic activities.

5.6. Halogens

The halogens contents of fluid inclusions (Table 4.6) are useful in providing information about the diagenetic environment and the sources of dolomitizing fluids (Banks et al., 2002; Gleeson and Turner, 2007; Conliffe et al., 2010). The F/Cl molar ratios of the fluid inclusions of calcites and dolomites of the Esino and Breno formations are within the range of that of ultramafic and mafic rocks (< 0.016 ~ 0.044, Orberger et al., 1990) but much greater than that of seawater (0.1×10^{-3}, Wilson, 1975). Based on Hanor's (1994) classification of the subsurface saline waters in sedimentary basins and the salinities of diagenetic fluids of D2, D3 and C3 (23 ± 2 eq wt% NaCl,*n* = 44, 20 ± 4 eq wt% NaCl, *n* = 104, and 22 ± 5 eq wt% NaCl, *n* = 63, respectively) indicate that they are Cl^--dominated and halite-undersaturated saline waters. Therefore, the high F/Cl molar ratios in the fluid inclusions of calcites and dolomites are likely caused by the increase of F^- rather than the decrease of Cl^-. Regional Pb-Zn mineralization (Mississippi Valley

Type) and fluorite that preserved within the Esino and Breno carbonate sequences are considered to be associated with the volcanic activity (e.g., Castellarin et al; 1979; Brusca et al., 1981; Garzanti, 1985; Jadoul et al., 1992b; Berra et al., 2011). Thus, the high F^- concentrations and high F/Cl molar ratios were likely derived from the contribution of volcanic-associated fluids and/or from the water-rock interaction of the diagenetic fluids with the volcanic rocks.

The fluid inclusions in dolomite generations and C3 show higher Cl/Br molar ratios than that of seawater (648, Wilson, 1975; 653, Jambon et al., 1995) and MORB (969, Jambon et al., 1995) and most Cl/Br molar ratios of dolomite generations and C3 (D1, 398 ~ > 4575; D2, 1547 ~ 2794; D3, 164 ~ > 3358; C3, 398 ~ > 4432) fall within the ranges of seawater (648, Wilson, 1975), ultramafic and mafic rocks (188 ~ 1428, Orberger et al.,1990) and magmatic fluids (1492 ~ 8333, Banks et al., 2000). Therefore, Cl/Br molar ratios of the investigated carbonates are probably overprinted by halite-dissolution, which is supported by the high salinities of diagenetic fluids of D2, D3 and C3 (23 ± 2 eq wt% NaCl, n = 44, 20 ± 4 eq wt% NaCl, n = 104, and 22 ± 5 eq wt% NaCl, n = 63, respectively). Low Cl/Br (72 ~ 257) molar ratio of C1 (and a few other D samples) might be the result of subaerial evaporation and restricted halite precipitation at the boundary of Ladnian - Carnian (i.e. the boundary of Esino and Breno formations; Assereto et al., 1977) since the relatively low Sr concentrations in the investigated carbonates do not support a major evaporation event.

The multitechnique approach has proven an efficient tool in understanding the origin of dolomites. The geochemical signatures retained by dolomites of the Esino and

Breno formations, including petrography, microthermometry, fluid-inclusion gas ratios, stable isotopes, minor and REE, and halogens are consistent and reflect the impact of the associated volcanic activity. They also allow better understanding the origin and nature of the parental dolomitizing fluids in the basin.

5.7. Comparison between Esino and Breno dolomites in Western Southern Alps (Italy) and St. George counterparts in Western Newfoundland (Canada)

It has been well established by earlier studies (Azmy et al., 2008, 2009, 2011, 2013; Azmy and Conliffe, 2010; Azomani et al., 2013; Conliffe et al., 2009, 2010, 2012, Olanipekun et al., 2014), from the detailed petrographic (including cathodoluminescence and microthermometric measurements) and geochemical (stable isotopes, and major, minor, and REE) analyses, that the Lower Ordovician St. George Group dolomites in western Newfoundland formed from typical basinal fluids that were not influenced by volcanic activity. This makes those dolomites ideal candidates for the comparison with their counterparts of the Middle Triassic Esino and Breno dolomites in Western Southern Alps that have geochemical signatures suggesting influence of volcanic activity. The St. George Group dolomites have at least three generations (D1, D2 and D3; Azmy et al., 2008, 2009, 2011, 2013; Conliffe et al., 2009, 2010, 2012; Azmy and Conliffe, 2010; Azomani et al., 2013) similar to those of Esino and Breno formations. However, unlike the non-porous Esino and Breno dolomites, the D2 of the St. George Group has larger crystal size (70μm - 1mm, Table 5.1) with estimated intercrystalline porosity up to 12%. Although undulose extinction is the characteristic feature of D3 in both basins, some D2 of the St. George Group may still exhibit the same feature. On the other hand, D2 of the

Esino and Breno formations show mixed zoned and dull CL images although their St. George counterparts are always CL zoned (Azmy et al., 2008, 2009, 2011, 2013; Azmy and Conliffe, 2010; Azmy and Blamey, 2013; Azomani et al., 2013; Conliffe et al., 2009, 2010, 2012). These petrological differences are suggested to have been caused by the differences in the diagenetic environments and fluid characteristics in both basins.

The D2 in both basins has almost same mean T_h values but slightly higher salinity (23 eq wt% NaCl) values in the Esino and Breno formations relative to their counterparts in St. George Group (21 eq wt% NaCl). The similarity in the mean T_h and minor differences in salinity suggest that the depths of burial were insignificantly different and the geothermal gradients of both basins were likely close, which is consistent with earlier studies of thermal history of those basins (cf. Cooper et al., 2001; Ronchi et al., 2010, 2011). On the other hand, the D3 of St. George Group has slightly higher mean T_h (129 °C vs. 111 °C, Table 5.1), but almost similar mean salinity (19 eq wt% NaCl vs. 20 eq wt% NaCl; Azmy et al., 2008, 2009, 2011, 2013; Azmy and Conliffe, 2010; Azmy and Blamey, 2013; Azomani et al., 2013; Conliffe et al., 2009, 2010, 2012), relative to that of D3 of Esino and Breno formations in the Western Southern Alps. The higher mean T_h value of D3 of St. George Group suggests formation under relatively deeper burial settings. The similarity in salinity would argue for the suggested close geothermal gradients in both basins particularly because the basin of Esino and Breno formations constitute a part of the Central Alps, which have a tectonic history as violent as that of western Newfoundland if not more. This is consistent with studies (e.g., Ronchi et al., 2011) of deep burial hydrothermal dolomites from central Alps (Jurassic-Lower

Cretaceous, Italy) that documented a temperature of dolomitization of up to 105 ºC, which is within the range of temperatures documented for those of the St. George Group counterparts regardless the age of rocks (Azmy et al., 2008, 2009, 2011, 2013; Azmy and Conliffe, 2010; Azmy and Blamey, 2013; Azomani et al., 2013; Conliffe et al., 2009, 2010, 2012), thus arguing for most likely comparable geothermal gradients for both basins.

The dolomites of both basins are non-stoichiometric (Table 5.2) and the Mg contents of Esino and Breno dolomites (43.6%, 45.4%, 44.7%, respectively) are slightly higher than their counterparts of St. George Group dolomites (39.5%, 43.5%, 42.0%, respectively) in western Newfoundland (Table 5.2, Azmy et al., 2008, 2009, 2013; Azmy and Conliffe, 2010; Azomani et al., 2013; Conliffe et al., 2009, 2012; Olanipekun et al 2014), which suggest that the dolomitizing fluids of Esino and Breno dolomites were slightly more enriched in Mg^{2+} compared with their St. George Group counterparts. The D1 of the Esino and Breno formations has dramatically higher Fe and Mn (4438ppm and 1219ppm) but lower Sr (76ppm) contents relative to its counterpart of St. George Group (2847ppm, 204ppm, 98ppm, respectively; Table 5.2), which is consistent with the suggested influence of the co-occurrence of volcanic lenses with the Esino and Breno dolomites on the geochemical composition of the dolomitizing fluids due to the high water/rock interaction of the fluids with the volcanic lenses, a phenomenon that the St. George Group dolomites do not have.

Table 5.1. Summary of the petrographic characteristics and mean values of microthermometric measurements of Breno and Esino dolomites of Western Southern Alps and St. George Group dolomites of Western Newfoundland (The data of the St. George Group dolomites are reproduced from Azmy et al., 2008, 2009, 2013; Azmy and Conliffe, 2010; Azomani et al., 2013; Conliff et al., 2009, 2012; Olanipekun et al 2014).

	Western Southern Alps (Italy)			Western Newfoundland (Canada)		
	D1	D2	D3	D1	D2	D3
Crystal size	3-35µm	30-600µm	250µm-5mm	4-55µm	30µm-1mm	0.1-1cm
Undulose extinction		No	Yes		Yes (occasionally)	Yes
CL	Dull	Dull and zoned	Dull and zoned	Dull	Zoned	Dull and zoned
T_h (°C)		108	111		107	129
T_m (°C)		-21	-18		-19	-17
Salinity		23	20		21	19

Table 5.2. $CaCO_3$, $MgCO_3$, Mn, Sr, Fe, $\delta^{18}O$ and $\delta^{13}C$ statistics of Breno and Esino dolomites of Western Southern Alps and St. George Group dolomites of Western Newfoundland (The data of the St. George Group dolomites are reproduced from Azmy et al., 2008, 2009; Azmy and Conliffe, 2010; Azomani et al., 2013; Conliff et al., 2009, 2012; Olanipekun et al 2014).

		Western Southern Alps							Western Newfoundland						
Phase		$CaCO_3$%	$MgCO_3$%	Sr (ppm)	Mn (ppm)	Fe (ppm)	$\delta^{13}C$‰ (VPDB)	$\delta^{18}O$‰ (VPDB)	$CaCO_3$%	$MgCO_3$%	Sr (ppm)	Mn (ppm)	Fe (ppm)	$\delta^{13}C$‰ (VPDB)	$\delta^{18}O$‰ (VPDB)
C1	n	36	36	36	36	36	18	18	60	60	60	60	60	74	74
	Mean	98.2	1.8	237	203	217	1.0	-7.9	97.8	2.2	245	137	1116	-1.8	-7.7
	S.D.	1.5	1.5	123	131	153	0.9	1.8	3.4	3.4	147	148	1058	1.1	0.9
	Max	99.4	7.1	606	565	703	1.8	-5.2	99.7	24.4	653	598	5238	0.0	-5.7
	Min	92.9	0.6	146	56	56	-1.1	-13.2	75.6	0.3	21	13	73	-4.4	-9.7
C3	n	18	18	18	18	18	9	9	29	29	29	29	28	43	43
	Mean	97.6	2.4	178	1328	805	0.7	-9.3	97.9	2.1	143	585	765	-3.3	-9.5
	S.D.	1.8	1.8	192	1192	1111	0.6	2.7	2.9	2.9	117	735	512	1.7	2.1
	Max	99.4	5.6	649	3655	3788	1.6	-5.2	99.8	13.6	485	2534	1890	0.4	-2.3
	Min	94.4	0.6	47	102	74	0.0	-13.0	86.4	0.2	17	11	91	-7.5	-13.0

D1	n	33	33	40	40	40	20	20	71	71	71	71	71	97	97
	Mean	56.4	43.6	76	1219	4438	1.7	-5.9	60.5	39.5	98	204	2847	-1.6	-6.4
	S.D.	3.9	3.9	37	1418	4393	0.6	3.3	8.5	8.5	57	161	2252	0.8	2.1
	Max	64.6	51.3	155	4863	16735	2.6	-0.8	79.3	50.6	269	836	11943	0.1	-2.9
	Min	48.7	35.4	27	122	289	0.7	-10.2	49.4	20.7	26	47	509	-3.3	-10.4
D2	n	17	17	22	22	22	8	8	103	103	103	103	103	157	157
	Mean	54.6	45.4	53	556	1460	1.8	-8.4	56.5	43.5	64	167	1816	-1.1	-8.4
	S.D.	6.0	6.0	31	289	900	0.3	1.2	5.9	5.9	47	152	1216	0.6	1.5
	Max	62.9	55.3	125	1078	3162	2.3	-6.6	76.7	55.3	299	1031	7941	0.0	-5.0
	Min	44.7	37.1	18	156	276	1.3	-9.8	44.7	23.3	26	32	490	-3.0	-11.6
D3	n	49	49	53	53	53	25	25	28	28	28	28	28	32	32
	Mean	55.3	44.7	57	1091	4462	1.9	-9.0	58.0	42.0	73	390	4473	-1.9	-8.5
	S.D.	5.4	5.4	24	1183	4888	0.5	1.0	6.8	6.8	56	524	6012	1.0	2.7
	Max	64.9	54.9	151	6049	24955	2.9	-6.1	77.4	49.6	264	1945	29279	-0.6	-3.3
	Min	45.1	35.1	31	266	714	0.9	-10.4	50.4	22.6	26	61	65	-4.4	-13.2

The Breno and Esino dolomites have more enriched $\delta^{13}C$ values than their St. George Group counterparts (Table 5.2; Fig 5.6). However, both of them are within the ranges of the $\delta^{13}C$ values of best preserved marine carbonate of their corresponding ages (Korte et al., 2005; Veizer et al., 1999). The relative depletion in the $\delta^{13}C$ values of St. George Group dolomite is most likely related to those of the precursor carbonate (Lower Ordovician ~ -1 ‰ vs. Middle Triassic ~+2 ‰; Veizer et al., 1999) and the possible influence of organic matter (documented oil seeps , Baker and Knight 1993; Cooper et al., 2001).

The differences between the calculated estimates of $\delta^{18}O$ of the hydrothermal dolomitizing fluids of Western Southern Alps (D1, -8 ~ 2.9‰, D2, 0.4 ~ 7.2‰, D3, -1.5 ~ 9.4‰, respectively; Fig 5.3) and those of Western Newfoundland (D1, -11.2 ~ -10‰, 2.1 ~ 8.1‰, 5.8 ~ 8.1‰, respectively; Azomani et al., 2013) are due to the variations in the $\delta^{18}O$ of the marine and meteoric waters (main components of the dolomitizing fluids) through the Phanerozoic (Lower Ordovician vs. Middle Triassic, Clark and Fritz, 1997; Veizer et al., 1999) and temperatures of dolomitization as well as the water/rock interaction ratio during fluid circulation in the basinal sediments. Also, this is influenced by the amounts of meteoric waters that were mixed with the marine waters to form the dolomitizing fluids and with effect of evaporation (if any) that influenced the marine waters before dilution (Conliffe et al., 2012).

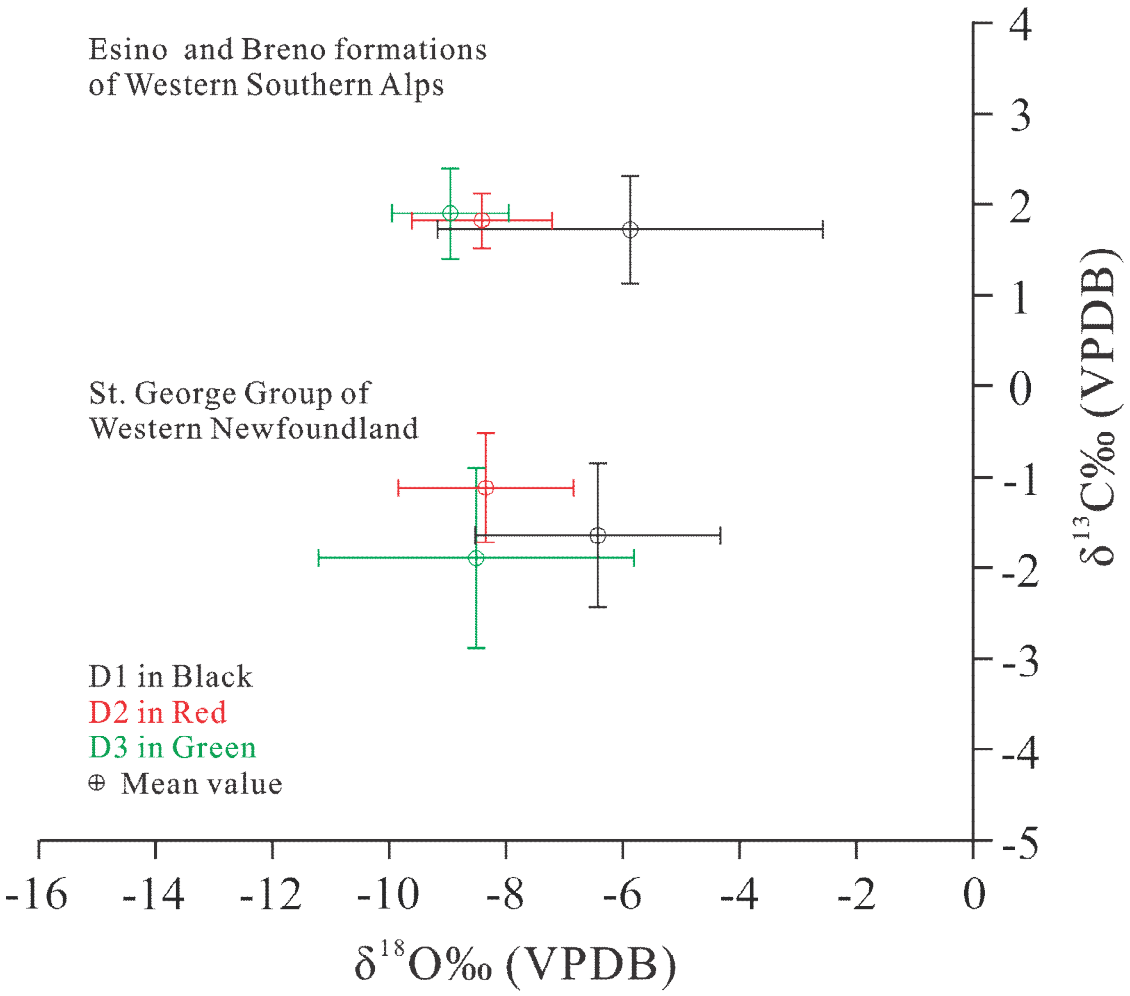

Figure 5.6. Mean $\delta^{18}O$ and $\delta^{13}C$ (with ±1 σ) values of the Middle Triassic Breno and Esino dolomites of Western Southern Alps and Lower Ordovician St. George Group dolomites of Western Newfoundland (The data of the St. George Group dolomites are reproduced from Azmy et al., 2008, 2009; Azmy and Conliffe, 2010; Azomani et al., 2013; Conliff et al., 2009, 2012; Olanipekun et al 2014).

The mean ∑REE values of dolomites in both of the compared basins may vary (Table 5.3) due to the variations in the chemistry of the diagenetic fluids and the nature of basinal deposits through which they were circulated. Dolomites of both basins have

almost similar Ce anomalies, but the Esino and Breno dolomites have higher values of Eu anomalies (Table 5.3) than those of St. George Group dolomites, which reflects the influence of co-occurrence of volcanic lenses since mafic rocks are characteristic of positive Eu anomaly values (Elderfield and Greaves, 1982)

Fluid-inclusion gases have been found to be potential proxies of the nature of the diagenetic fluids (Azomani et al., 2013; Azmy and Blamey, 2013). Unlike the St. Geroge Group dolomites, some of the Esino and Breno dolomites have N_2/Ar, CO_2/CH_4, and Ar/He ratios (Figs. 5.7a-b; Table5.4) plot within the field of magmatic origin (Azomani et al., 2013; Azmy and Blamey, 2013), thus suggesting a possible contribution from the volcanic fluids to the basinal dolomitizing solutions and/or from intense circulation of the dolomitizing fluids through the volcanic lenses. This is consistent with the higher values of Eu anomaly relative to those of the St. George dolomites that had no evidence of volcanic activities involved with the process of dolomitization. The application of fluid-inclusion gas ratios to volcanic-associated dolomites is a new approach that has proven solid reliability of the tool for revealing the origin of dolomites.

Table 5.3. Statistics of ∑REE(ppm), and Ce*SN and Eu*SN anomalies of Breno and Esino dolomites of Western Southern Alps and St. George Group dolomites of Western Newfoundland (The data of the St. George Group dolomites are from Azomani et al., 2013).

		Western Southern Alps			Western Newfoundland		
		∑REE(ppm)	Ce^*_{SN} anomaly	Eu^*_{SN} anomaly	∑REE(ppm)	Ce*SN anomaly	Eu^*_{SN} anomaly
D1	*n*	19	19	19	15	15	15
	Mean	10	0.93	1.13	12	0.85	0.67
	Stdev	9	0.10	0.23	5	0.05	0.05
	Max	37	1.06	1.58	22	0.94	0.79
	Min	2	0.69	0.45	7	0.77	0.59
D2	*n*	11	11	11	35	35	35
	Mean	3	0.80	0.93	11	0.81	0.65
	Stdev	1	0.07	0.20	4	0.06	0.05
	Max	6	0.96	1.12	20	0.91	0.75
	Min	2	0.68	0.52	6	0.70	0.56

D3	*n*	26	26	25	12	12	11
	Mean	7	0.87	1.17	21	0.88	0.7
	Stdev	9	0.13	0.30	16	0.06	0.11
	Max	42	1.30	1.88	60	0.96	0.88
	Min	1	0.50	0.56	6	0.76	0.50
C1	*n*	18	18	18	8	8	8
	Mean	5	0.90	1.30	5	0.68	0.67
	Stdev	7	0.07	0.51	1	0.06	0.08
	Max	28	1.05	2.40	7	0.76	0.76
	Min	1	0.79	0.50	4	0.60	0.52
C3	*n*	9	9	9	1		
	Mean	17	0.94	1.34	26		
	Stdev	12	0.15	0.51			
	Max	41	1.23	2.56			
	Min	7	0.73	0.95			

Table 5.4. Ranges of CO_2/CH_4, N2/Ar, and Ar/He ratios of weighted mean values of Breno and Esino dolomites of Western Southern Alps and St. George Group dolomites of Western Newfoundland (The data of the St. George Group dolomites are reproduced from Azomani et al., 2013 and Azmy and Blamey, 2013).

	Western Southern Alps (Italy)			Western Newfoundland		
	D1	D2	D3	D1	D2	D3
CO_2/CH_4	7.41 - 43.20	1.90 - 6.23	8.31 - 74.90	0.10 - 2.90	0.07 - 1.33	0.58 - 1.36
N_2/Ar	50.13 - 109.72	61.61 - 80.41	79.29 - 136.32	42.32 - 104	22.27 - 105.5	54.4 - 90.67
Ar/He	1.35 - 7.73	1.21 - 10.14	0.51 - 15.82	0.98 - 7.83	0.71 - 4.31	1.06 - 2.57

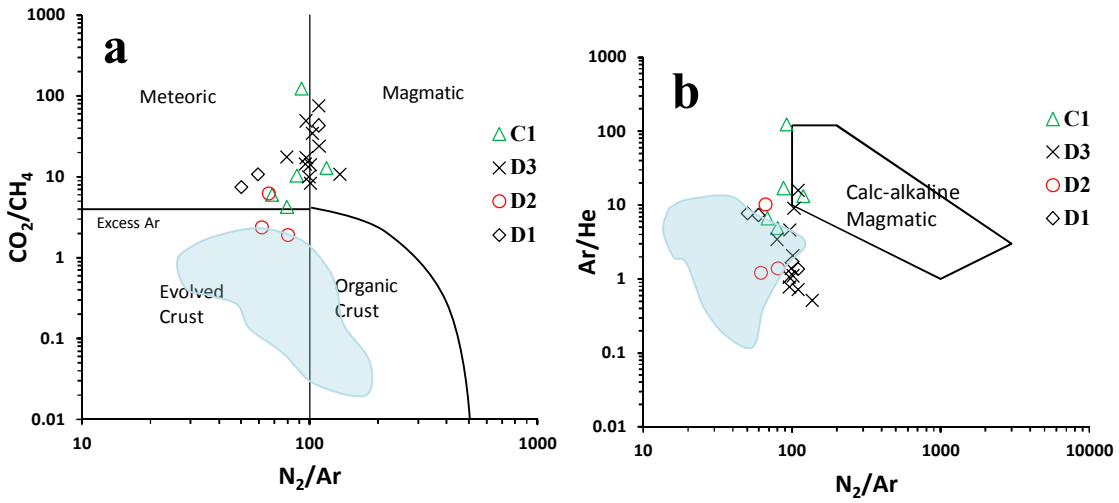

Figure 5.7. Comparison of correlations of (a) N_2/Ar vs. CO_2/CH_4 and (b) N_2/Ar vs. Ar/He between Esino and Breno dolomites in Western Southern Alps and St. George Group dolomites in Western Newfoundland. Shaded areas mark the field of values of St. George Group dolomites (Data of St. George Group dolomites from Azmy and Blamey, 2013 and Azomani et al., 2013).

The halogen contents of fluid inclusions are useful in providing information about the diagenetic environment and the sources of dolomitizing fluids (Banks et al., 2002; Gleeson and Turner, 2007; Conliffe et al., 2010). The high F/Cl molar ratios in the fluid inclusions of dolomites of Esino and Breno dolomite in Western Southern Alps relative to their counterparts in St. George Group dolomites are suggested to be likely caused by the increase of F^- rather than the decrease of Cl^- due to the contribution of volcanic-associated fluids and/or the water-rock interaction of the diagenetic fluids with the volcanic lenses or rocks associated with mineralization during dolomitization. The Cl/Br molar ratios of the Esino and Breno dolomites are higher than those of their St. George

counterparts (Table 5.5; Conliffe et al., 2010). However, Cl/Br molar ratios of Esino and Breno dolomites were caused by halite-dissolution, which is consistent with their slightly high salinities of diagenetic fluids. Thus, although the high Cl/Br ratio of Esino and Breno dolomite in Western Southern Alps do not reflect the influence of volcanic activities, the high F/Cl ratios do.

Table 5.5. F/Cl and Cl/Br molar ratio ranges of Breno and Esino dolomites of Western Southern Alps and St. George Group dolomites of Western Newfoundland (The data of the St. George Group dolomites are reproduced from Conliffe et al., 2010).

	Western Southern Alps (Italy)			Western Newfoundland		
	D1	D2	D3	D1	D2	D3
F/Cl (molar)	0.009 - 0.042	0.010 - 0.023	0.006 - 0.060		$<3.4\times10^{-5} \sim 0.015$	$<1.2\times10^{-4} \sim 1.7\times10^{-4}$
Cl/Br (molar)	398.5 - 4575.2	1547.6 - 2794.7	164.6 - 3358.2		167 ~ 935	306 ~ 494

The comparison of the dolomites of the Esino and Breno formations (influenced by co-occurring volcanic lenses) and those of St. George Group (no volcanic or magmatic influence) shows that

a. The petrographic features of both suites of dolomites are comparable,
b. The microthermometric features are also comparable likely due to close geothermal gradients,
c. The fluid-inclusion gas ratios of the Esino and Breno dolomites suggest contributions from volcanic fluids to the parent dolomitizing basinal fluids,
d. The carbon isotope composition of the Esino and Breno dolomites is more enriched due to the variations in the $\delta^{13}C$ of marine carbonate during the Phanerozoic (Middle Triassic carbonates are more enriched, Veiser et al., 199). However, the difference in the $\delta^{18}O$ are mainly influenced by not only the variations in the oxygen isotope compositions of the marine and meteoric waters during the Phanerozoic but also temperature of dolomitization,
e. The ΣREE values are comparable but the Esino and Breno dolomites have slightly higher Eu anomaly values due to the influence of volcanic activities in the basin, and
f. The Esino and Breno dolomites have significantly higher F/Cl molar ratios due to possible contributions from volcanic-associated fluids or the water-rock interaction of the diagenetic fluids with the volcanic rocks.

CHAPTER 6

CONCLUSIONS

Petrographic examination of carbonates of the Esino and Breno formations in the Western Southern Alps reveals three main non-porous generations of dolomites: an early replacive dolomicrite (D1), later larger replacive eu- to subhedral dolomite (D2) and latest coarse sub- to anhedral fracture-filling saddle dolomite (D3).

Petrographic characteristics of dolomite D1 suggest an early dolomitization event under relatively shallow burial environment at near-surface conditions. The high Fe and Mn contents and ^{18}O enriched estimates of the parental dolomitizing fluids suggest that D1 originated at early stage of diagenesis of shallow burial setting at near-surface conditions (40 - 50 °C).

Microthermometric analyses of fluid inclusions trapped within D2 and D3 mineral crystals and elemental geochemistry suggest that D2 and D3 were formed during later stages of diagenesis under deeper burial settings from hydrothermal fluids with high salinities, which is supported by the estimated $\delta^{18}O$ composition of their parent dolomitizing fluids.

The REE compositions and similarity of shale-normalized patterns of investigated dolomites suggest that they likely developed from similar basinal diagenetic fluids that their composition evolved during progressive burial. The positive Eu anomaly of the investigated dolomites and calcites shows the influence of the reaction of dolomitizing

fluids with the associated volcaniclastic lenses prior to dolomitization or possible minor contributions from volcanic-related fluids.

Fluid-inclusion gas analyses also support some contributions, possibly limited, of fluids related to volcanic activities to the parent diagenetic fluids of all dolomites and calcites. Furthermore, the high F contents and high F/Cl molar ratios in the fluid inclusions of the investigated dolomites suggest the contribution of volcanic-associated fluids or the water-rock interaction of the diagenetic fluids with the volcanic rocks, which is consistent with their geochemistry and fluid inclusion gas data.

Unlike the St. George Group dolomites of western Newfoundland that had no co-occurrence of volcanic rocks or associated volcanic activities, the dolomites of the Esino and Breno formations of Southern Western Alps exhibit positive Eu anomalies, some fluid-inclusion gas ratios consistent with magmatic origin, and high F/Cl reflecting the influence of contributions of volcanic-related fluids to the dolomitizing basinal parent fluids. Thus, the origin of dolomites can be inferred from their geochemical signatures particularly when combined with petrographic studies.

REFERENCES

Alibo, D.S., Nozaki, Y., 1999. Rare earth elements in seawater: particle association, shale normalization and Ce oxidation. Geochimica et Cosmochimica Acta 63, 363 - 372.

Andersen, T., 1986. Magmatic fluids in the Fen carbonatite complex, SE Norway. Contributions to Mineralogy and Petrology 93(4), 491-503.

Assereto, R., Brigo, L., Jadoul, F., Omenetto, P., Perna, G., Rodeghiero, F., Vailati, G., 1979. Recent studies on Pb-Zn-Fluorite and Barite deposits in the Mid- and Upper-Triassic series of the Lombardy Prealps: Verhandlungen der Geologischen Bundesanstalt 1978, 197-204.

Assereto, R., Casati, P., 1965. Revisione della stratigrafia permo-triassica della Val Camonica meridionale (Lombardia). Rivista ltaliana di Paleontologia e Stratigrafia 71, 999 - 1097, Milano.

Assereto, R., Folk, R.L., 1980. Diagenetic fabrics of aragonite, calcite and dolomite in ancient peritidal-spelean environment: Triassic Calcare Rosso, Lombardia, Italy. Journal of Sedimentary Petrology 50, 371 - 394.

Assereto, R., Jadoul, F., Omenetto P., 1977. Stratigrafia e metallo genesi del settore occidentale del distretto a Pb, Zn, fluorite e barite di Gorno (Alpi Bergamasche). Riv. It. Paleont. Strat. 83, 395-532, Milano.

Assereto, R., Kendall, C. G. S. C., 1971. Megapolygons in Ladinian limestones of Triassic of Southern Alps: evidence of deformation by penecontemporaneous desiccation and cementation. Journal of Sedimentary Research, 41(3).

Assereto, R., Kendall, C.G.S.C., 1977. Nature, origin and classification of peritidal tepee structures and relative breccias. Sedimentology 24, 153- 210, Oxford.

Azmy, K., Blamey, N. J. F., 2013. Origin of diagenetic fluids inferred from fluid inclusion gas ratios. Ghemical Geology 347, 246-254.

Azmy, K., Brand, U., Sylvester, P., Gleeson, S., Logan, A., Bitner, M.A., 2011. Biogenic low–Mg calcite (brachiopods): proxy of seawater–REE composition, natural processes and diagenetic alteration. Chemical Geology 280, 180-190.

Azmy, K., Conliffe, J., 2010. Dolomitization of the lower St. George Group on the Northern Peninsula in western Newfoundland: implications for lateral distribution of porosity. Bulletin of Canadian Petroleum Geology 58(4), 1-14.

Azmy, K., Knight, I., Lavoie, D. and Chi, G., 2009. Origin of the Boat Harbour dolomites of St. George Group in western Newfoundland, Canada: implications for porosity controls. Bulletin of Canadian Petroleum Geology 57, 81–104.

Azmy, K., Lavoie, D., Knight, I. and Chi, G., 2008. Dolomitization of the Aguathuna Formation carbonates of Port au Port Peninsula in western Newfoundland, Canada: implications for a hydrocarbon reservoir. Canadian Journal of Earth Sciences 45, 795–813.

Azmy, K., Lavoie, D., Wang, Z., Brand, U., Al-Aasm, I., Jackson, S., Girard, I., 2013. Magnesium-isotope and REE compositions of Lower Ordovician carbonates from eastern Laurentia: implications for the origin of dolomites and limestones. Chemical Geology 356, 64-75.

Azmy, K., Stouge, S., Brand, U., Bagnoli, G., & Ripperdan, R., 2014. High-resolution chemostratigraphy of the Cambrian–Ordovician GSSP: Enhanced global correlation tool. Palaeogeography, Palaeoclimatology, Palaeoecology 409, 135-144.

Azmy, K., Veizer, J., Misi, A., de Oliveira, T. F., Sanches, A. L., Dardenne, M. A., 2001. Dolomitization and isotope stratigraphy of the Vazante Formation, São Francisco Basin, Brazil. Precambrian Research 112(3), 303-329.

Azomani, E., Azmy, K., Blamey, N., Brand, U., Al-Aasm, I., 2013. Origin of Lower Ordovician dolomites in eastern Laurentia: controls on porosity and implications from geochemistry. Marine and Petroleum Geology 40, 99-114.

Baker, P.A., Kastner, M., 1981. Constraints on the formation of sedimentary dolomites. Science 213, 214-216.

Banks D. A., Boyce A. J., Samson I. M., 2002. Constraints on the origins offluids forming Irish Zn-Pb-Ba deposits: evidence from the composition offluid inclusions. Economic Geology 97, 471-480.

Banks, D. A., Green, R., Cliff, R. A., Yardley, B. W. D., 2000. Chlorine isotopes in fluid inclusions: determination of the origins of salinity in magmatic fluids. Geochimica et Cosmochimica Acta 64, 1785-1789.

Banks, D. A., Yardley, B. W. D., 1992. Crush-leach analysis of fluid inclusions in small natural and synthetic samples. Geochimica et Cosmochimica Acta 56, 245-248.

Banner, J.L., Hanson, G.N., Meyers, W.J., 1988. Rare earth element and Nd isotopic variations in regionally extensive dolomites from the Burlington–Keokuk Formation (Mississippian): implications for REE mobility during carbonate diagenesis. Journal of Sedimentary Petrology 58, 415–432.

Barton, E.D., Bau, M., Alexander, B., 2006. Preservation of primary REE patterns without Ce anomaly during dolomitization of Mid-Paleoproterozoic limestone and the potential re-establishment of marine anoxia immediately after the 'Great Oxidation Event'. South African Journal of Geology 109, 81–86.

Bathurst, R.G.C. (1975) Carbonate sediments and their diagenesis, pp. 658. Elsevier, Amsterdam.

Bau, M., Balan, S., Schmidt, K., Koschinsky, A., 2010. Rare earth elements in mussel shells of the Mytilidae family as tracers for hidden and fossil high-temperature hydrothermal systems. Earth and Planetary Science Letters 299(3), 310-316.

Bau, M., Dulski, P., 1996. Distribution of yttrium and rare-earth elements in the Penge and Kuruman iron-formations, Transvaal Supergroup, South Africa. Precambrian Research 79, 37-55.

Bernal, N. F., Gleeson, S. A., Dean, A. S., Liu, X. M., Hoskin, P., 2014. The source of halogens in geothermal fluids from the Taupo Volcanic Zone, North Island, New Zealand. Geochimica et Cosmochimica Acta 126, 265-283.

Berra, F., 2007. Sedimentation in shallow to deep water carbonate environments across a sequence boundary: effects of a fall in sea-level on the evolution of a carbonate system (Ladinian - Carnian, eastern Lombardy, Italy). Sedimentology 54, 721 – 735.

Berra, F., 2012. Sea-level fall, carbonate production, rainy days: How do they relate? Insight from Triassic carbonate platforms (Western Tethys, Southern Alps, Italy). Geology 40, 271–274.

Berra F., Balini M., Levera M., Nicora A. and Salamati R., 2012. Anatomy of carbonate mounds from the Middle Anisian of Nakhlak (Central Iran): architecture and age of a subtidal microbial-bioclastic carbonate factory. Facies 58, 685-705.

Berra, F., Carminati, E., 2010. Subsidence history from a backstripping analysis of the Permo-Mesozoic succession of the Central Southern Alps (Northern Italy). Basin Research 22, 952–975

Berra, F., Carminati, E., 2012. Differential compaction and early rock fracturing in high-relief carbonate platforms: numericalmodelling of a Triassic case study (Esino Limestone, Central Southern Alps, Italy). Basin Research 24, 598 – 614

Berra, F., Jadoul, F., 2002. Sedimentological and paleontological evidences of a “Mid Carnian” transgression in the Western Southern Alps (S. Giovanni Bianco Fm., Lombardy, Italy): stratigraphic and paleogeographic implications. Riv. It. Paleont. Strat. 108, 119-131.

Berra, F., Jadoul, F., Binda, M., Lanfranchi, A., 2011. Large-scale progradation, demise and rebirth of a high relief, flat-topped carbonate factory (Late Anisian-Early Carnian, Lombardy Southern Alps, Italy). Sed. Geol. 23, 48 – 63.

Bertotti, G., Picotti, V., Bernoulli, D., Castellarin, A., 1993. From rifting to drifting: tectonic evolution of the South-Alpine upper crust from the Triassic to the Early Cretaceous. Sedimentary Geology 86, 53-76.

Blamey, N.J.F., 2012. Composition and evolution of crustal, geothermal and hydrothermal fluids interpreted using quantitative fluid inclusion gas analysis. Journal of Geochemical Exploration 116, 17-27.

Blamey, N.J.F., Norman, D. I., 2002. New Interpretations of Geothermal Fluid Inclusion Volatiles: Ar/He and N2/Ar ratios-A Better Indicator of Magmatic Volatiles, and Equilibrium Gas Geothermometry. In Proceedings: Twenty-seventh Workshop on Geothermal Reservoir Engineering, Stanford University, Stanford, California.

Blamey, N.J.F., Parnell, J., McMahon, S., Mark, D., Tomkinson, T., Lee, M., Shivak, J., Izawa, M., Banerjee, M., Flemming, R., "Methane in Martian meteorites implies a subsurface habitat on Mars". Nature Communications (accepted).

Bodnar, R.J., 1993. Revised equation and table for determining the freezing point depression of H2O-NaCl solutions. Geochimica et Cosmochimica Acta 57, 683-684.

Bodnar, R.J., 2003. Interpretation of data from aqueous-electrolyte fluid inclusions. In: Samson, I., Anderson, A., Marshal, D. (Eds.), Fluid Inclusions: Analyses and

Interpretation. Short Course Series, vol. 32, Mineralogical Association of Canada, 81 - 100.

Boggs, S., Krinsley, D., 2006. Application of cathodoluminescence imaging to the tudy of sedimentary rocks, New York, Cambridge University Press, 165p.

Bogoch, R., Magaritz, M., & Michard, A., 1986. Dolomite of possible mantle origin, southeast Sinai. Chemical geology 56(3), 281-288.

Boles J. R., Franks S. G., 1979. Clay diagenesis in Wilcox Sandstones of southwest Texas: implications of smectite diagenesis on sandstone cementation. Journal of Sedimentary Research 49, 55–70.

Brusca, C., Gaetani, M., Jadoul, F., Viel, G., 1981. Paleogeografia e metallogenesi del Sudalpino. Mem. Soc. Geol. It. 22, 65-82, Roma.

Castellarin A; Lucchini F; Rossi P L; Simboli G; Bosellini A; Sommavilla E, 1979. Middle Triassic magmatism in Southern Alps. II: a geodynamic model, Rivista italiana di paleontologia e stratigrafia 85, 1111-1124.

Clark, I.D., Fritz, P., 1997. Environmental Isotopes in Hydrogeology. Lewis Publisher, Boca Raton, FL, 328 pp.

Coleman, M.L., Walsh, J.N. and Benmore, R.A., 1989. Determination of both chemical and stable isotope composition in milligram-size carbonate samples. In: B.W. Sellwood (Editor), Zoned Carbonate Cements: Techniques, Applications and Implications. Sedimentary geology 65, 233-238.

Conliffe, J., Azmy, K., Gleeson, S.A., Lavoie, D., 2010. Fluids associated with hydrothermal dolomitization in St. George Group, western Newfoundland, Canada. Geofluids 10, 422-437.

Conliffe, J., Azmy, K., Greene, M., 2012. Hydrothermal dolomites in the Lower Ordovician Catoche Formation. Marine and Petroleum Geology 30, 161-173.

Conliffe, J., Azmy, K., Knight, I., Lavoie, D., 2009. Dolomitization of the Lower Ordovician Watts Bight Formation of the St. George Group, western Newfoundland; evidence of hydrothermal fluid alteration. Canadian Journal of Earth Sciences 46, 247-261.

Crisci, C. M., Ferrara, G., Mazzuoli, R., Rossi, P. M., 1984. Geochemical and geochronological data on Triassic volcanism of the Southern Alps of Lombardy (Italy): genetic implications. Geologische Rundschau, 73, 279-292.

Dickson, J. A. D., 1966. Carbonate identification and genesis as revealed by staining, Journal of Sedimentary Research, 36(2).

Elderfield, H. and Greaves, M.J., 1982. The rare earth elements in seawater. Nature 296, 214 - 219.

Faure, G., Mensing, T. M., 2004. Isotopes: principles and applications. John Wiley & Sons Inc.

Faure, G., 2001. Origin of Igneous Rocks: The Isotopic Evidence. Springer, Verlag, Berlin, Heildelberg. 496p.

Feist-Burkhardt, S., Götz, A.E., Szulc, J., Borkhataria, R., Geluk, M., Haas, J., Hornung, J., Jordan, P., Kempf, O., Michalík, J., Nawrocki, J., Reinhardt, L., Ricken, W., Röhling, H-G., Rüffer, T., Török, Á., Zühlke, R., 2008. Triassic. In: McCann, T. (Ed.), The Geology of Central Europe, Mesozoic and Cenozoic. Geological Society of London 2, 749–822.

Folk, R.L., Land, L.S., 1975. Mg/Ca ratio and salinity, two controls over crystallization of dolomite. Bull. Am. Ass. Petrol. Geol. 59, 60-68.

Gaetani, M., Gnaccolini, M., Jadoul, F., Garzanti, E., 1998. Multiorder sequence stratigraphy in the Triassic system of the Western Southern Alps. In: de Graciansky, P.C., Hardenbol, J., Jacquin, T., Vail, P.R. (Eds.), Mesozoic and Cenozoic Sequence Stratigraphy of European Basins. SEPM Society for Sedimentary Geology Special Publication. vol. 60, pp. 701–717.

Garzanti, 1985. The sandstone memory of the evolution of a Triassic volcanic arc in the Southern Alps, Italy. Sedimentology 32, 423-433.

Garzanti, E., Gnaccolini, M., Jadoul, F., 1995. Anatomy of a semiarid coastal system: the Upper Carnian of Lombardy (Italy). Riv. It. Paleont. Strat 101(1), 17-36.

Giggenbach, W. F., 1986. "The use of gas chemistry in delineating the origin of fluids discharges over the Taupo Volcanic Zone: A review," International Volcanological Congress, Hamilton, New Zealand. Proceedings Symposium 5, 47-50.

Gleeson S. A. and Turner W. A., 2007. Fluid inclusion constraints on the origin of the brines responsible for Pb-Zn mineralization at Pine Point and coarse non-saddle and saddle dolomite formation in southern Northwest Territories. Geofluids 7, 51–68.

Gnaccolini, M., 1983. Un apparato deltizio Triassico nelle Prealpi Bergamasche. Rivista ltaliana di Paleontologia e Stratigrafia 88, 599-612.

Gnaccolini, M., 1986. La Formazione di Gorno nei dintorni di Dossena e di Gorno (Prealpi Bergamasche): analisi di una la- guna triassica. Riv. Ital. Paleont. Strat. 92, 3-32.

Gnaccolini, M., 1988. Arenaria di Val Sabbia e Formazione di Gorno: Un sistema deposizionale delta - laguna nel Trias superiore delle Prealpi Bergamasche. Riv. Ital. Paleont. Strat. 93, 329-336.

Gnaccolini, M., Jadoul, F., 1988. Un sistema deposizionale delta-laguna-piattaforma carbonatica: un esempio del Trias superiore lombardo (Alpi Meridionali). Riv. Ital. Paleont. Strat. 93, 10-32.

Gnaccolini, M., Jadoul, F., 1990. Carbonate platform, lagoon and delta "high-frequency" cycles from the Carnian of Lombardy (Southern Alps, Italy). Sedimentary Geology 67, 143-159.

Goldstein, R.H., Reynolds, T.J., 1994. Systematics of Fluid Inclusions in Diagenetic Minerals. Society for Sedimentary Geology (SEPM) Short Course, Tulsa, Okla.

Gucsik, A., 2009, Cathodoluminescence and its application in the planetary sciences, Springer Verlag, Berlin

Haeri-Ardakani, O., Al-Aasm, I., Coniglio, M., Samson, I., 2013. Diagenetic evolution and associated mineralization in Middle Devonian carbonates, southwestern Ontario, Canada. Bulletin of Canadian Petroleum Geology 61, 41-58.

Hanor, J. S., 1994. Origin of saline fluids in sedimentary basins. Geological Society, London, Special Publications 78, 151-174.

Hongo, Y., Nozaki, Y., 2001. Rare earth element geochemistry of hydrothermal deposits and Calyptogena shell from the Iheya Ridge vent field, Okinawa Trough. Geochemical Journal-Japan 35(5), 347-354.

Horbury, A.D., Robinson, A.G., 1993. Diagenesis and basin development. AAPG: Studies in Geology, 274p.

Jadoul, F., Gervasutti, M. and Fantini Sestini, N., 1992a. The Middle Triassic of the Brembana Valley: preliminary study of the Esino platform (Bergamasc Alps), Rivista ltaliana di Paleontologia e Stratigrafia 98, 299-324.

Jadoul F., Bailo F., Pezzotta F., 1992b. Le manifestazioni a fluorite, barite e celestina nelle successioni del Norico Superiore delle Prealpi Bergamasche. Bollettino della Società Geologica Italiana 112, 219-233, Roma.

Jadoul, F., Nicora, A., Ortenze, A., Pohar, C., 2002. Ladinian stratigraphy and paleogeography of the Southern Val Canale (Pontebbano-Tarvisiano, Julian Alps, Italy). Memorie della Società Geologica Italiana 57, 29-43.

Jadoul, F., Rossi, P.M., 1982. Evoluzione paleogeografico-strutturale e vulcanismo triassico nella Lombardia centro-occidentale, In: Guida alla geologia del Sudalpino centrooccidentale, Guide Geologiche Regionali della Società Geologica Italiana 143-155, Bologna

Jadoul, F., Weissert, H., 1989. Evinosponges in the Triassic Esino Limestone (Southern Alps): documentation of early lithification and late diagenetic overprint. Sedimentology, 36, 685-699.

Jambon, A., Déruelle, B., Dreibus, G., Pineau, F., 1995. Chlorine and bromine abundance in MORB: the contrasting behaviour of the Mid-Atlantic Ridge and East Pacific Rise and implications for chlorine geodynamic cycle. Chemical Geology 126, 101-117.

Kamber, B.S., Webb, G.E., 2001. The geochemistry of late Archean microbial carbonate: implications for ocean chemistry and continental erosion history. Geochimica et Cosmochimica Acta 65, 2509-2525.

Kesler S. E., Appold M. S., Martini A. M., Walter L. M., Huston TJ, Kyle J. R., 1995. Na–Cl–Br systematics of mineralizing brines in Mississippi Valley-type deposits. Geology, 23, 641–644.

Korte, C., Kozur, H. W., Veizer, J., 2005. $\delta^{13}C$ and $\delta^{18}O$ values of Triassic brachiopods and carbonate rocks as proxies for coeval seawater and palaeotemperature. Palaeogeography, Palaeoclimatology, Palaeoecology 226, 287-306.

Land, L.S. 1983. The application of stable isotopes to studies of the origin of dolomite and to problems of diagenesis of clastic sediments. In Society for Sedimentary Geology (SEPM) Short Course Notes 10. Edited by M.A. Arthur, T.F. Anderson, I.R. Kaplan, J. Veizer, and L.S. Land. pp. 4.1–4.22.

Land, L. S., 1985. The origin of massive dolomite. Journal of Geological Education, 33(2), 112-125.

Land, L.S., 1992. The dolomite problem: stable and radiogenic isotope clues. In: Clauer, N., Chaudhuri, S. (Eds.), Isotopic Signature of Sedimentary Records. Lecture Notes in Earth Science 43, 49–68.

Lawler, J.P., Crawford, M.L., 1983. Stretching of fluid inclusions resulting from a low temperature microthermometric technique. Econ. Geol. 78, 527-529.

Lippmann, F. (1973) Sedimentary Carbonate Minerals, pp. 228. Springer-Verlag, Berlin.

Lonnee, J., Machel, H. G., 2006. Pervasive dolomitization with subsequent hydrothermal alteration in the Clarke Lake gas field, Middle Devonian Slave Point Formation, British Columbia, Canada. AAPG Bulletin 90(11), 1739-1761.

Marshall, D. J., 1988. Cathodoluminescence of Geological Materials, Boston, Unwin Hyman.

Machel, H. G., 2000. Application of cathodoluminescence to carbonate diagenesis. In Cathodoluminescence in geosciences (pp. 271-301). Springer Berlin Heidelberg.

Machel, H.G., Mountjoy, E.W., 1986. Chemistry and environments of dolomitization — a reappraisal. Earth Sci. Rev. 23, 175-222.

McCaffrey M. A., Lazar B., Holland H. D., 1987. The evaporation path of seawater and the coprecipitation of Br (super -) and K (super +) with halite. Journal of Sedimentary Research 57, 928–937.

McLennan, S.M., 1989. Rare earth elements in sedimentary rocks: influence of provenance and sedimentary processes. In: Lipin, B.R., McKay, G.A. (Eds.), Geochemistry and Mineralogy of Rare Earth Elements. Mineral. Soc. Am. Rev. Miner. 21, 169 - 200.

Mutti, M., 1994. Association of tepees and paleokarsts in the Ladinian Calcare Rosso (Southern Alps, Italy). Sedimentology, 41, 621 - 641.

Norman, D.I., Blamey, N.J.F., 2001. Quantitative analysis of fluid inclusion volatiles by a two mass spectrometer system, In: Noronha, F., Doria, A., Guedes, A. (Eds.), European Current Research on Fluid Inclusions, Porto 2001 (XVI ECROFI): Faculdidade de Ciencias do Porto, Departamento de Geologia, Memoria 7, 341 - 344.

Norman, D.I., Moore, J.N., 1997. Gaseous species in fluid inclusions: a fluid tracer and indicator of fluid processes [abs.]: European current research on fluid inclusions, No. XIV, Nancy, France, Abstracts, pp. 243-244.

Norman, D.I., Moore, J.N., 1999. Methane and excess N_2 and Ar in geothermal fluid inclusions. Proceedings: Twenty-fourth workshop of geothermal reservoir engineering, Stanford University, Stanford, California, January 22–24, pp. 233–240.

Nothdurft, L.D., Webb, G.E., Kamber, B.S., 2004. Rare earth element geochemistry of Late Devonian reefal carbonates, Canning Basin, Western Australia: confirmation of a seawater REE proxy in ancient limestones. Geochimica et Cosmochimica Acta 68, 263–283.

Obenholzner, J.H., 1991. Triassic volcanogenic sediments from the Southern Alps (Italy, Austria, Yugoslavia) - a contribution to the "Pietra verde" problem, In: R. Cas and C. Busby-Spera (Editors), Voleaniclastic Sedimentation. Sedimentary Geology 74: 157-171.

Olanipekun, B., Azmy, K., Brand, U., 2014. Dolomites of the Boat Harbour Formation in the Northern Peninsula, western Newfoundland, Canada: Implications for dolomitization history and porosity control. AAPG Bulletin 98, 765-791

Orberger, B., Friedrich, G., Woermann, E., 1990. The distribution of halogens and carbon in PGE-bearing ultramafics of the Acoje ophiolite block, Zambales, Philippines. Journal of Geochemical Exploration 37(1), 147-169.

Parry, W.T., Blamey, N.J.F., 2010. Faultfluid composition fromfluid inclusion measurements, Laramide age Uinta thrust fault, Utah. Chemical Geology 278, 105-119.

Pisa G., Castellarin A., Lucchini F., Rossi P. L., Simboli G., Bosellini A., Sommavilla E., 1979. "Middle Triassic magmatism in southern Alps. I: a review of general data in the Dolomites", Rivista italiana di paleontologia e stratigrafia 85(03-04), 1093-1110.

Rameil, N. 2008. Early diagenetic dolomitization and dedolomitization of Late Jurassic and earliest Cretaceous platform carbonates: a case study from the Jura Mountains (NW Switzerland, E France). Sedimentary Geology 212, 70-85.

Richter D.K., Gotte, T., Gotze, J, Neuser, R. D., 2003. Progress in application of cathodoluminescence (CL) in sedimentary petrology. Mineral Petrol 79: 127–166.

Ronchi, P., Jadoul, F., Ceriani, A., Di Giulio, A., Scotti, P., Ortenzi, A., Previde Massara, E., 2011. Multistage dolomitization and distribution of dolomitized bodies in Early Jurassic carbonate platforms (Southern Alps, Italy). Sedimentology, 58(2), 532-565.

Ronchi, P., Di Giulio, A., Ceriani, A., & Scotti, P., 2010. Contrasting fluid events giving rise to apparently similar diagenetic products; late-stage dolomite cements from the Southern Alps and central Apennines, Italy. Geological Society, London, Special Publications, 329(1), 397-413.

Scholle, P. A., Ulmer-Scholle, D. S., 2003. A Color Guide to the Petrography of Carbonate Rocks: Grains, textures, porosity, diagenesis, AAPG Memoir 77.

Shepherd, T.J., Rankin, A.H., Alderton, D.H.M., 1985. A Practical Guide to Fluid Inclusions. Blackie, London.

Shields, G.A., Carden, G.A.F., Veizer, J., Meidla, T., Rong, J., Li, R.Y., 2003. Sr, C, and O isotope geochemistry of Ordovician brachiopods: a major isotopic event around the Middle - Late Ordovician transition. Geochimica et Cosmochimica Acta 67, 2005 - 2025.

Sholkovitz, E., Landing, W.M., Lewis, B.L., 1994. Ocean particle chemistry: the fractionation of rare earth elements between suspended particles and seawater, Geochimica et Cosmochimica Acta 58, 1576-1580.

Sholkovitz, E., Shen, G.T., 1995. The incorporation of rare-earth elements in modern coral. Geochimica et Cosmochimica Acta 59, 2749-2756.

Sibson, R.H., 1977. Fault rocks and fault mechanisms. Geological Society of London 133, 191-213.

Sperber, C.M., Wilkinson, B.H., Peacor, D. R., 1984. Rock composition, dolomite stoichiometry, and rock/water reactions in dolomitic carbonate rocks. Journal of Geology 92(6), 609-622.

Tucker, M.E., and Wright, V.P. 1990. Carbonate Sedimentology. Blackwell Publishing, Oxford, UK.

Veizer, J., 1983. Chemical diagenesis of carbonates: theory and application of trace element technique. In: Arthur, M.A., Anderson, T.F., Kaplan, I.R., Veizer, J., Land, L.S. (Eds.), Stable Isotopes in Sedimentary Geology. Society of Economic Paleontologists and Mineralogists Short Course Notes, 10, pp. III-1–III-100.

Veizer, J., Ala, D., Azmy, K., Bruckschen, P., Bruhn, F., Buhl, D.,et al. 1999.$^{87}Sr/^{86}Sr$, $\delta^{18}O$ and $\delta^{13}C$ evolution of Phanerozoic seawater. Chemical Geology 161, 59-88.

Veizer, J., Compston, W., Clauer, N., Schidlowski, M., 1983.$^{87}Sr/^{86}Sr$ in Late Proterozoic carbonates: evidence for a "mantle" event at ~ 900 Ma ago. Geochimica et Cosmochimica Acta 47(2), 295-302.

Vola, G. and Jadoul, F., 2014. Applied stratigraphy and carbonate petrography of the Arabescato Orobico dimension stone from the Bergamasc Alps (Calcare Rosso, Italy). Italian Journal of Geoscience 133, 294-314.

Walter LM, Stueber A.M., Huston T. J., 1990. Br–Cl–Na systematics in Illinois basin fluids – constraints on fluid origin and evolution. Geology 18, 315–318.

Warren J., 2000. Dolomite: Occurrence, evolution and economically important associations, Earth-Science Reviews 52, 1-81.

Webb, G.E., Kamber, B.S., 2000. Rare earth elements in Holocene reefal microbialites: a new shallow seawater proxy. Geochimica et Cosmochimica Acta 64, 1557-1565.

Webb, G.E., Nothdurft, L.D., Kamber, B.S., Kloprogge, J.T., Zhao, J.-X. 2009. Rare earth element geochemistry of scleractinian coral skeleton during meteoric diagenesis: a before and after sequence through neomorphism of aragonite to calcite. Sedimentology 56, 1433-1463

Wilson, T. R. S., 1975. Salinity and the major elements of sea water. In Chemical oceanography, 2nd ed., vol. 1, ed., J. P. Riley and G. Skirrow, London, Academic Press, pp. 365-413.

Zhong, S., Mucci, A., 1995. Partitioning of rare earth elements (REEs) between calcite and seawater solutions at 25 C and 1 atm, and high dissolved REE concentrations. Geochimica et Cosmochimica Acta. 59(3), 443-453.

APPENDIX 1

SAMPLE, ELEMENTAL, ISOTOPIC GEOCHEMICAL AND REE GEOCHEMICAL COMPOSITIONS OF ESINO AND BRENO CARBONATES

Sample ID	Formation	Coordinate	$CaCO_3$%	$MgCO_3$%	Fe (ppm)	Mn (ppm)	Sr (ppm)	$\delta^{13}C$‰ (VPDB)	$\delta^{18}O$‰ (VPDB)
PE1-C1	Breno	45°53'1.29"N, 9°42'47.30"E	99.3	0.7	140.6	195.9	156.9	0.84	-8.85
PE1-C1	Breno	45°53'1.29"N, 9°42'47.30"E	99.1	0.9	176.5	192.6	159.7		
PE10-C1	Breno	45°53'5.60"N, 9°42'46.22"E	93.9	6.1	560.7	213.3	147.7	1.64	-6.22
PE10-C1	Breno	45°53'5.60"N, 9°42'46.22"E	92.9	7.1	702.6	213.6	152.6		
PE11-C1	Breno	45°53'5.60"N, 9°42'46.22"E	99.3	0.7	75.0	79.0	189.1	1.24	-8.19
PE11-C1	Breno	45°53'5.60"N, 9°42'46.22"E	99.1	0.9	125.7	94.4	232.9		
PE12-C1	Breno	45°53'5.60"N, 9°42'46.22"E	97.6	2.4	168.9	147.8	191.3	1.76	-8.08
PE12-C1	Breno	45°53'5.60"N, 9°42'46.22"E	97.1	2.9	227.0	157.8	198.3		
PE13-C1	Breno	45°53'5.41"N, 9°42'48.43"E	98.3	1.7	162.0	140.7	178.8	1.26	-8.48
PE13-C1	Breno	45°53'5.41"N, 9°42'48.43"E	97.9	2.1	255.4	162.9	205.7		
PE14-C1	Breno	45°53'5.41"N, 9°42'48.43"E	99.3	0.7	161.4	263.9	149.1	1.52	-8.60
PE14-C1	Breno	45°53'5.41"N, 9°42'48.43"E	99.1	0.9	222.5	281.6	160.7		
PE15-C1	Breno	45°53'5.41"N, 9°42'48.43"E	98.7	1.3	250.9	240.1	175.8	-0.05	-13.18
PE15-C1	Breno	45°53'5.41"N, 9°42'48.43"E	98.4	1.6	338.7	251.9	189.3		
PE16-C1	Breno	45°53'5.41"N, 9°42'48.43"E	99.2	0.8	93.8	98.3	145.6	1.75	-6.12
PE16-C1	Breno	45°53'5.41"N, 9°42'48.43"E	99.0	1.0	126.2	106.4	159.1		
PE17-C1	Breno	45°53'5.41"N, 9°42'48.43"E	99.1	0.9	72.9	69.8	193.1	1.73	-7.65
PE17-C1	Breno	45°53'5.41"N, 9°42'48.43"E	98.9	1.1	108.6	76.7	218.6		
PE4-C1	Breno	45°53'1.29"N, 9°42'47.30"E	99.0	1.0	116.8	113.6	173.3	1.44	-7.00
PE4-C1	Breno	45°53'1.29"N, 9°42'47.30"E	98.7	1.3	149.8	115.3	174.3		
PE5-C1	Breno	45°53'1.29"N, 9°42'47.30"E	99.2	0.8	55.6	55.8	196.3	1.73	-7.25
PE5-C1	Breno	45°53'1.29"N, 9°42'47.30"E	98.9	1.1	95.5	59.6	211.4		
PE7-C1	Breno	45°53'5.60"N, 9°42'46.22"E	95.9	4.1	232.2	173.2	156.0	1.75	-8.45
PE7-C1	Breno	45°53'5.60"N, 9°42'46.22"E	95.3	4.7	274.2	169.0	160.0		

Sample ID	Formation	Coordinate	$CaCO_3$%	$MgCO_3$%	Fe (ppm)	Mn (ppm)	Sr (ppm)	$\delta^{13}C$‰ (VPDB)	$\delta^{18}O$‰ (VPDB)
PE9-C1	Breno	45°53'5.60"N, 9°42'46.22"E	98.9	1.1	164.7	220.8	195.1	1.57	-7.59
PE9-C1	Breno	45°53'5.60"N, 9°42'46.22"E	98.4	1.6	232.5	233.2	206.5		
RE15-C1	Breno	45°54'2.40"N, 9°23'42.74"E	99.4	0.6	59.6	564.6	148.3	-0.13	-5.20
RE15-C1	Breno	45°54'2.40"N, 9°23'42.74"E	99.2	0.8	62.1	559.9	147.3		
AR4-C3	Breno	45°54'50.67"N, 9°47'44.37"E	99.1	0.9	1450.3	2299.1	93.3	1.58	-11.62
AR4-C3	Breno	45°54'50.67"N, 9°47'44.37"E	99.0	1.0	1999.2	2535.6	110.2		
BR-C3	Breno	45°52'40.27"N, 9°52'32.93"E	98.9	1.1	601.5	1117.9	116.1	1.19	-13.05
BR-C3	Breno	45°52'40.27"N, 9°52'32.93"E	98.9	1.1	766.8	1120.1	118.5		
BR2-C3	Breno	45°52'40.27"N, 9°52'32.93"E	94.7	5.3	3787.5	2792.0	47.5	1.08	-11.80
BR2-C3	Breno	45°52'40.27"N, 9°52'32.93"E	94.4	5.6	3239.7	2999.0	49.5		
PE3-C3	Breno	45°53'1.29"N, 9°42'47.30"E	98.5	1.5	181.0	1377.3	96.8	1.01	-7.56
PE3-C3	Breno	45°53'1.29"N, 9°42'47.30"E	98.3	1.7	194.8	1246.9	91.3		
PG1-C3	Breno	45°54'00.42"N, 9°41'10.45"E	99.4	0.6	74.0	273.0	648.9	0.99	-8.75
PG1-C3	Breno	45°54'00.42"N, 9°41'10.45"E	99.3	0.7	92.8	274.1	620.4		
RE15-C3	Breno	45°54'2.40"N, 9°23'42.74"E	95.8	4.2	260.5	440.1	67.3	0.25	-5.22
RE15-C3	Breno	45°54'2.40"N, 9°23'42.74"E	94.8	5.2	255.1	425.9	64.7		
AB1-D1	Breno	45°54'35.85"N, 9°19'53.11"E	58.1	41.9	3092.3	918.9	49.4	1.80	-6.08
AB1-D1	Breno	45°54'35.85"N, 9°19'53.11"E	52.7	47.3	2935.6	943.1	53.9		
AB2-D1	Breno	45°54'35.85"N, 9°19'53.11"E	56.5	43.5	1262.2	406.0	51.9	1.93	-6.15
AB2-D1	Breno	45°54'35.85"N, 9°19'53.11"E	50.7	49.3	1192.4	454.7	56.4		
AR5-D1	Breno	45°54'50.67"N, 9°47'44.37"E			11297.0	3032.2	70.0	2.38	-9.49
AR5-D1	Breno	45°54'50.67"N, 9°47'44.37"E			9028.9	3163.4	73.1	2.20	-9.60
AR5-D1	Breno	45°54'50.67"N, 9°47'44.37"E	56.2	43.8	10696.3	3248.8	47.8		
AR7-D1	Breno	45°54'50.67"N, 9°47'44.37"E			11887.4	3238.5	38.0	2.58	-10.24
AR7-D1	Breno	45°54'50.67"N, 9°47'44.37"E	58.5	41.5	9399.9	3251.1	38.2	2.36	-10.11
AR7-D1	Breno	45°54'50.67"N, 9°47'44.37"E	53.1	46.9	12619.4	4111.3	28.5		
PE10-D1	Breno	45°53'5.60"N, 9°42'46.22"E			3530.8	396.6	78.3	2.38	-6.93
PE10-D1	Breno	45°53'5.60"N, 9°42'46.22"E	64.6	35.4	1931.2	405.0	80.2		

Sample ID	Formation	Coordinate	$CaCO_3$%	$MgCO_3$%	Fe (ppm)	Mn (ppm)	Sr (ppm)	$\delta^{13}C$‰ (VPDB)	$\delta^{18}O$‰ (VPDB)
PE8-D1	Breno	45°53'5.60"N, 9°42'46.22"E			6267.1	292.2	95.2	1.37	-5.26
PE8-D1	Breno	45°53'5.60"N, 9°42'46.22"E	63.9	36.1	4518.5	287.0	88.7		
RE12-D1	Breno	45°54'2.40"N, 9°23'42.74"E	57.6	42.4	759.1	225.9	109.2	1.72	-0.76
RE12-D1	Breno	45°54'2.40"N, 9°23'42.74"E	48.7	51.3	803.2	241.6	114.6		
RE14-D1	Breno	45°54'2.40"N, 9°23'42.74"E	55.7	44.3	844.8	229.0	109.8	2.10	-0.78
RE14-D1	Breno	45°54'2.40"N, 9°23'42.74"E	50.9	49.1	926.1	248.7	102.3		
RE17-D1	Breno	45°54'2.40"N, 9°23'42.74"E	57.5	42.5	1028.3	440.9	103.5	1.87	-1.13
RE17-D1	Breno	45°54'2.40"N, 9°23'42.74"E	57.2	42.8	1023.8	438.4	112.3		
BR-D2	Breno	45°52'40.27"N, 9°52'32.93"E	61.0	39.0	963.9	283.3	25.5	1.83	-9.75
BR-D2	Breno	45°52'40.27"N, 9°52'32.93"E	50.3	49.7	2822.5	1047.4	72.6		
BR-D2	Breno	45°52'40.27"N, 9°52'32.93"E	46.1	53.9	922.4	232.2	18.5		
BR2-D2	Breno	45°52'40.27"N, 9°52'32.93"E			937.4	377.5	30.4	1.90	-9.44
BR2-D2	Breno	45°52'40.27"N, 9°52'32.93"E	60.3	39.7	689.9	366.2	30.0		
BR2-D2	Breno	45°52'40.27"N, 9°52'32.93"E	51.4	48.6	2049.8	582.9	25.3		
BR2-D2	Breno	45°52'40.27"N, 9°52'32.93"E	47.1	52.9	851.6	289.6	31.2		
BR3-D2	Breno	45°52'40.27"N, 9°52'32.93"E			3161.6	864.9	113.1	1.89	-9.34
BR3-D2	Breno	45°52'40.27"N, 9°52'32.93"E	62.9	37.1	2615.2	936.7	125.0		
BR3-D2	Breno	45°52'40.27"N, 9°52'32.93"E	55.1	44.9	2872.6	894.6	97.4		
PE10-D2	Breno	45°53'5.60"N, 9°42'46.22"E			2491.9	372.8	82.3	2.28	-7.05
PE10-D2	Breno	45°53'5.60"N, 9°42'46.22"E			1832.7	354.4	78.1		
PE11-D2	Breno	45°53'5.60"N, 9°42'46.22"E			1210.8	567.3	47.6	2.10	-8.79
PE11-D2	Breno	45°53'5.60"N, 9°42'46.22"E	59.9	40.1	990.0	609.4	52.5		
PE11-D2	Breno	45°53'5.60"N, 9°42'46.22"E	53.4	46.6	745.0	718.6	67.1		
PE12-D2	Breno	45°53'5.60"N, 9°42'46.22"E	60.7	39.3	967.5	1078.4	43.4	1.97	-7.90
PE12-D2	Breno	45°53'5.60"N, 9°42'46.22"E	44.7	55.3	939.1	885.7	33.6		
AB1-D3	Breno	45°54'35.85"N, 9°19'53.11"E	59.9	40.1	3852.0	982.9	60.4	1.60	-9.50
AB1-D3	Breno	45°54'35.85"N, 9°19'53.11"E	54.4	45.6	3467.5	1009.3	67.1		
AB2-D3	Breno	45°54'35.85"N, 9°19'53.11"E			2224.6	648.1	71.3	1.17	-10.40

Sample ID	Formation	Coordinate	$CaCO_3$%	$MgCO_3$%	Fe (ppm)	Mn (ppm)	Sr (ppm)	$\delta^{13}C$‰ (VPDB)	$\delta^{18}O$‰ (VPDB)
AB2-D3	Breno	45°54'35.85"N, 9°19'53.11"E			2176.6	733.1	81.8		
AR4-D3	Breno	45°54'50.67"N, 9°47'44.37"E	59.9	40.1	11749.6	3223.9	84.2	2.33	-6.37
AR4-D3	Breno	45°54'50.67"N, 9°47'44.37"E	51.1	48.9	16182.9	3601.8	98.6		
AR7-D3	Breno	45°54'50.67"N, 9°47'44.37"E	62.9	37.1	7249.7	2505.5	70.4	2.38	-8.77
AR7-D3	Breno	45°54'50.67"N, 9°47'44.37"E	54.3	45.7	8909.4	2494.1	72.1		
BR-D3	Breno	45°52'40.27"N, 9°52'32.93"E	59.9	40.1	1093.0	337.7	31.9	1.83	-9.88
BR-D3	Breno	45°52'40.27"N, 9°52'32.93"E	46.3	53.7	1234.0	320.9	31.0		
BR2-D3	Breno	45°52'40.27"N, 9°52'32.93"E	62.9	37.1	22371.0	6049.5	44.1	2.47	-10.09
BR2-D3	Breno	45°52'40.27"N, 9°52'32.93"E	53.9	46.1	24954.7	5592.2	42.8		
BR3-D3	Breno	45°52'40.27"N, 9°52'32.93"E	58.3	41.7	2052.4	1946.6	62.1	2.40	-9.31
BR3-D3	Breno	45°52'40.27"N, 9°52'32.93"E	48.2	51.8	2455.5	1641.3	61.3		
PE1-D3	Breno	45°53'1.29"N, 9°42'47.30"E	63.2	36.8	1592.0	830.4	60.2	2.34	-8.51
PE1-D3	Breno	45°53'1.29"N, 9°42'47.30"E	54.1	45.9	2753.6	914.1	68.7		
PE12-D3	Breno	45°53'5.60"N, 9°42'46.22"E	63.3	36.7	851.8	484.0	62.7	1.51	-8.29
PE12-D3	Breno	45°53'5.60"N, 9°42'46.22"E	54.6	45.4	1073.8	514.4	65.7		
PE13-D3	Breno	45°53'5.41"N, 9°42'48.43"E	64.9	35.1	714.0	266.4	63.6	2.04	-8.41
PE13-D3	Breno	45°53'5.41"N, 9°42'48.43"E	54.4	45.6	908.7	287.6	66.2		
PE14-D3	Breno	45°53'5.41"N, 9°42'48.43"E	57.8	42.2	3872.9	1601.7	35.6	2.14	-9.08
PE14-D3	Breno	45°53'5.41"N, 9°42'48.43"E	47.4	52.6	4442.6	1625.5	35.7		
PE15-D3	Breno	45°53'5.41"N, 9°42'48.43"E	57.9	42.1	3132.8	1195.6	42.8	2.35	-8.93
PE15-D3	Breno	45°53'5.41"N, 9°42'48.43"E	47.3	52.7	3266.8	1039.7	38.8		
PE16-D3	Breno	45°53'5.41"N, 9°42'48.43"E	59.8	40.2	2658.5	868.7	34.0	2.68	-9.28
PE16-D3	Breno	45°53'5.41"N, 9°42'48.43"E	47.2	52.8	2971.0	806.4	32.6		
PE17-D3	Breno	45°53'5.41"N, 9°42'48.43"E	59.6	40.4	948.0	441.0	50.0	2.34	-8.82
PE17-D3	Breno	45°53'5.41"N, 9°42'48.43"E	46.3	53.7	1068.6	405.1	46.5		
PE3-D3	Breno	45°53'1.29"N, 9°42'47.30"E	56.6	43.4	2042.0	709.0	40.1	2.88	-9.16
PE3-D3	Breno	45°53'1.29"N, 9°42'47.30"E	49.8	50.2	2409.8	664.4	41.4		
PE4-D3	Breno	45°53'1.29"N, 9°42'47.30"E	61.3	38.7	1752.3	1036.4	36.4	1.80	-8.35

Sample ID	Formation	Coordinate	$CaCO_3$%	$MgCO_3$%	Fe (ppm)	Mn (ppm)	Sr (ppm)	$\delta^{13}C$‰ (VPDB)	$\delta^{18}O$‰ (VPDB)
PE4-D3	Breno	45°53'1.29"N, 9°42'47.30"E	52.0	48.0	2143.3	982.6	37.5		
PE5-D3	Breno	45°53'1.29"N, 9°42'47.30"E	58.1	41.9	1461.9	717.2	31.7		
PE5-D3	Breno	45°53'1.29"N, 9°42'47.30"E	50.7	49.3	1740.0	651.3	30.7		
PE7-D3	Breno	45°53'5.60"N, 9°42'46.22"E	59.9	40.1	1102.0	620.5	54.5	1.53	-9.73
PE7-D3	Breno	45°53'5.60"N, 9°42'46.22"E	49.0	51.0	1150.5	535.7	49.4		
PE8-D3	Breno	45°53'5.60"N, 9°42'46.22"E	61.5	38.5	7415.9	419.7	150.8	0.86	-6.11
PE8-D3	Breno	45°53'5.60"N, 9°42'46.22"E	49.1	50.9	8617.7	406.4	146.7		
PE9-D3	Breno	45°53'5.60"N, 9°42'46.22"E	58.4	41.6	2138.1	1162.5	42.3	2.07	-8.12
PE9-D3	Breno	45°53'5.60"N, 9°42'46.22"E	45.5	54.5	2458.6	1093.4	40.2		
Vu-C1	Esino-Breno	45°52'40.27"N, 9°52'32.93"E	97.6	2.4	439.6	464.9	321.5	-0.43	-9.79
Vu-C1	Esino-Breno	45°52'40.27"N, 9°52'32.93"E	96.6	3.4	615.5	476.4	342.6		
Vu-C3	Esino-Breno	45°52'40.27"N, 9°52'32.93"E	99.1	0.9	76.6	2735.1	80.7	-0.01	-8.33
Vu-C3	Esino-Breno	45°52'40.27"N, 9°52'32.93"E	98.8	1.2	120.9	3654.7	98.3		
RE5-C1	Esino	45°54'1.40"N, 9°23'41.70"E	99.2	0.8	104.7	226.5	480.1	-1.06	-6.85
RE5-C1	Esino	45°54'1.40"N, 9°23'41.70"E	98.8	1.2	173.4	220.7	433.5		
RE6-C1	Esino	45°54'1.40"N, 9°23'41.70"E	98.7	1.3	263.9	83.3	393.9	1.20	-5.55
RE6-C1	Esino	45°54'1.40"N, 9°23'41.70"E	98.3	1.7	311.3	101.0	451.4		
RE7-C1	Esino	45°54'1.40"N, 9°23'41.70"E	99.2	0.8	192.2	209.3	534.4	0.64	-8.45
RE7-C1	Esino	45°54'1.40"N, 9°23'41.70"E	98.6	1.4	293.6	276.2	605.8		
RE11-C3	Esino	45°54'1.40"N, 9°23'41.70"E	98.4	1.6	243.3	185.9	72.4	0.41	-11.18
RE11-C3	Esino	45°54'1.40"N, 9°23'41.70"E	97.8	2.2	277.9	205.3	71.9		
RE6-C3	Esino	45°54'1.40"N, 9°23'41.70"E	95.9	4.1	399.1	102.0	366.9	0.07	-6.24
RE6-C3	Esino	45°54'1.40"N, 9°23'41.70"E	95.3	4.7	475.3	126.2	390.9		
ES-D1	Esino	45°52'40.27"N, 9°52'32.93"E			386.3	129.1	29.4	0.89	-7.87
ES-D1	Esino	45°52'40.27"N, 9°52'32.93"E	59.7	40.3	289.3	122.1	32.8		
ES-D1	Esino	45°52'40.27"N, 9°52'32.93"E	50.1	49.9	532.2	210.1	26.6		
ES1-D1	Esino	45°52'40.27"N, 9°52'32.93"E			11513.0	3354.5	48.0	1.93	-9.62
ES1-D1	Esino	45°52'40.27"N, 9°52'32.93"E	62.7	37.3	10311.2	3925.4	53.0	1.88	-9.55

Sample ID	Formation	Coordinate	$CaCO_3$%	$MgCO_3$%	Fe (ppm)	Mn (ppm)	Sr (ppm)	$\delta^{13}C$‰ (VPDB)	$\delta^{18}O$‰ (VPDB)
ES1-D1	Esino	45°52'40.27"N, 9°52'32.93"E	54.5	45.5	16734.8	4862.9	42.9		
RE1-D1	Esino	45°54'1.40"N, 9°23'41.70"E	56.1	43.9	2397.4	398.1	60.0	1.08	-5.55
RE1-D1	Esino	45°54'1.40"N, 9°23'41.70"E	53.1	46.9	2336.9	444.0	66.6		
RE11-D1	Esino	45°54'1.40"N, 9°23'41.70"E	53.9	46.1	1283.4	238.3	88.0	1.78	-1.55
RE11-D1	Esino	45°54'1.40"N, 9°23'41.70"E	52.9	47.1	1160.9	219.1	89.0		
RE13-D1	Esino	45°54'2.40"N, 9°23'42.74"E	58.9	41.1	8036.8	2592.8	48.2		
RE13-D1	Esino	45°54'2.40"N, 9°23'42.74"E	54.4	45.6	8969.2	2805.4	50.7		
RE2-D1	Esino	45°54'1.40"N, 9°23'41.70"E	58.4	41.6	1371.8	332.0	146.3	0.67	-3.64
RE2-D1	Esino	45°54'1.40"N, 9°23'41.70"E	57.2	42.8	1438.4	334.1	154.8		
RE3-D1	Esino	45°54'1.40"N, 9°23'41.70"E	58.7	41.3	2659.6	463.2	115.7	0.65	-3.05
RE3-D1	Esino	45°54'1.40"N, 9°23'41.70"E	57.1	42.9	3045.3	511.9	116.7		
RE6-D1	Esino	45°54'1.40"N, 9°23'41.70"E	62.6	37.4	3067.2	422.4	142.5	1.45	-3.78
RE6-D1	Esino	45°54'1.40"N, 9°23'41.70"E	59.2	40.8	3370.3	458.6	152.4		
RE8-D1	Esino	45°54'1.40"N, 9°23'41.70"E	55.5	44.5	1747.0	472.8	32.0	1.59	-6.17
RE8-D1	Esino	45°54'1.40"N, 9°23'41.70"E	54.4	45.6	1820.2	493.1	34.1		
ES-D2	Esino	45°52'40.27"N, 9°52'32.93"E	60.4	39.6	275.9	156.3	25.2	1.45	-8.49
ES-D2	Esino	45°52'40.27"N, 9°52'32.93"E	55.7	44.3	436.1	596.2	65.2		
ES-D2	Esino	45°52'40.27"N, 9°52'32.93"E	46.6	53.4	347.8	161.8	22.6		
RE3-D2	Esino	45°54'1.40"N, 9°23'41.70"E	57.0	43.0	2132.1	443.0	41.2	1.25	-6.58
RE3-D2	Esino	45°54'1.40"N, 9°23'41.70"E	56.6	43.4	1855.6	407.9	38.5		
ES1-D3	esino	45°52'40.27"N, 9°52'32.93"E	59.0	41.0	1524.9	580.4	33.1	1.79	-10.34
ES1-D3	esino	45°52'40.27"N, 9°52'32.93"E	45.1	54.9	2026.8	629.0	36.8		
RE1-D3	Esino	45°54'1.40"N, 9°23'41.70"E			5148.2	401.2	71.7	1.28	-9.18
RE1-D3	Esino	45°54'1.40"N, 9°23'41.70"E			4815.3	384.2	71.0		
RE1-D3	Esino	45°54'1.40"N, 9°23'41.70"E	48.5	51.5	6898.1	577.2	63.9		
RE11-D3	Esino	45°54'1.40"N, 9°23'41.70"E	58.4	41.6	2489.4	400.5	60.0	1.60	-9.50
RE11-D3	Esino	45°54'1.40"N, 9°23'41.70"E	55.7	44.3	2102.4	345.5	57.9		
RE2-D3	Esino	45°54'1.40"N, 9°23'41.70"E	56.9	43.1	5567.7	464.2	52.0	1.22	-9.38

Sample ID	Formation	Coordinate	$CaCO_3$%	$MgCO_3$%	Fe (ppm)	Mn (ppm)	Sr (ppm)	$\delta^{13}C$‰ (VPDB)	$\delta^{18}O$‰ (VPDB)
RE2-D3	Esino	45°54'1.40"N, 9°23'41.70"E	56.3	43.7	5600.8	490.7	56.3		
RE3-D3	Esino	45°54'1.40"N, 9°23'41.70"E	57.5	42.5	6149.6	510.1	58.6	1.22	-9.46
RE3-D3	Esino	45°54'1.40"N, 9°23'41.70"E	57.0	43.0	6388.1	493.6	53.9		
RE4-D3	Esino	45°54'1.40"N, 9°23'41.70"E	56.1	43.9	6737.4	597.7	57.8	1.39	-9.16
RE4-D3	Esino	45°54'1.40"N, 9°23'41.70"E	55.7	44.3	6391.7	558.3	50.4		

Sample ID	La (ppb)	Ce (ppb)	Pr (ppb)	Nd (ppb)	Sm (ppb)	Eu (ppb)	Gd (ppb)	Tb (ppb)	Dy (ppb)	Ho (ppb)	Er (ppb)	Tm (ppb)	Yb (ppb)	Lu (ppb)
PE1-C1	1467.8	3249.8	413.4	1602.3	247.8	58.2	228.2	28.4	137.1	23.0	73.0	10.6	72.8	12.2
PE10-C1	885.9	1556.9	173.9	680.0	181.9	18.3	169.6	27.7	184.5	35.4	111.5	14.2	81.3	13.2
PE11-C1	295.6	480.2	60.4	221.8	30.3	6.0	32.9	4.8	18.9	4.3	17.4	2.3	13.1	
PE12-C1	507.1	802.6	94.8	382.1	34.6	11.5	77.1	10.9	44.6	7.3	27.0	3.9	16.4	1.6
PE13-C1	1534.7	2664.6	296.6	1059.7	214.2	35.2	142.5	19.0	73.7	16.5	60.8	5.9	55.6	5.0
PE14-C1	444.7	723.4	82.2	292.9	48.0	20.9	58.1	5.3	28.6	4.5	15.2	3.5	8.7	
PE15-C1	438.4	722.1	86.4	330.3	33.3	11.3	41.0	6.2	24.2	3.1	17.8	1.9	21.2	1.2
PE16-C1	197.2	376.4	33.6	129.1	14.7	5.3	33.5	2.7	16.7	2.8	11.5	0.9	11.5	0.8
PE17-C1	198.2	331.5	36.6	125.8	36.4	8.8	31.4	0.4	17.4		10.4	0.6	11.9	
PE4-C1	422.4	735.1	82.4	328.5	68.8	6.6	58.9	8.2	47.9	9.0	21.4	2.5	21.8	0.4
PE5-C1	184.8	313.4	37.2	124.0	27.6	3.9	35.7	2.8	14.7	2.1	9.1	1.3	7.7	1.1
PE7-C1	501.0	944.3	119.0	434.4	79.6	18.5	84.4	11.4	43.5	10.1	30.3	5.0	31.0	1.1
PE9-C1	283.7	429.4	52.5	168.5	26.2	10.8	39.5	3.1	21.0	2.6	15.1	0.3	8.9	0.5
RE15-C1	1968.8	2915.1	364.8	1390.7	233.0	47.1	237.2	28.2	130.3	24.9	69.6	8.0	56.1	8.7
AR4-C3	2120.6	3980.3	528.5	1934.8	329.5	169.4	370.8	50.2	239.8	40.7	133.1	15.4	94.6	11.6
BR-C3	5075.8	10443.4	1663.3	6607.5	1524.1	308.7	1526.0	262.9	1366.5	277.8	760.6	113.7	751.0	115.1
BR2-C3	2305.2	3888.0	645.5	2638.4	510.6	126.0	498.8	78.0	423.2	89.1	267.2	46.7	314.2	48.6
PE3-C3	2133.2	5142.9	585.6	1984.0	243.5	41.5	242.1	25.6	85.7	9.7	34.2	6.8	20.7	1.6
PG1-C3	1686.8	3464.3	411.9	1584.1	292.9	71.3	286.5	49.2	214.0	39.8	118.9	14.3	85.7	14.7
RE15-C3	3419.4	5730.2	722.7	2780.6	453.6	85.6	444.6	58.4	280.2	57.0	155.4	22.8	142.9	20.0
AB1-D1	1935.3	4213.3	507.4	2005.3	369.6	83.0	352.6	51.7	275.1	51.2	156.5	20.9	139.3	16.3
AB2-D1	2036.4	5094.9	625.8	2439.5	471.2	92.9	452.9	66.7	347.8	68.2	205.6	27.2	179.8	25.6
AR5-D1	469.2	925.0	121.3	453.2	79.6	21.0	82.3	12.2	75.7	14.3	43.9	5.4	35.5	4.9
AR7-D1	316.4	657.6	79.9	318.4	61.4	11.1	64.2	10.4	52.2	11.8	34.3	4.3	35.3	4.7
PE10-D1	1192.7	2171.2	212.3	806.3	164.0	17.7	220.4	38.2	249.9	54.8	157.9	20.3	115.2	14.7
PE8-D1	7936.9	16176.5	1769.7	6764.6	1216.9	295.4	1181.9	148.4	612.7	112.6	304.6	38.3	228.3	32.5
RE12-D1	1055.8	2122.5	241.1	957.1	182.8	45.1	194.0	28.4	158.5	29.5	87.6	10.4	87.2	10.2
RE14-D1	971.8	2094.9	271.8	1078.0	222.2	47.9	206.5	28.7	159.8	24.8	81.2	14.0	70.7	9.1

Sample ID	La (ppb)	Ce (ppb)	Pr (ppb)	Nd (ppb)	Sm (ppb)	Eu (ppb)	Gd (ppb)	Tb (ppb)	Dy (ppb)	Ho (ppb)	Er (ppb)	Tm (ppb)	Yb (ppb)	Lu (ppb)
RE17-D1	4876.8	8654.1	1082.7	4314.8	787.5	219.1	784.4	112.7	567.0	104.8	311.1	38.1	249.6	34.8
BR-D2	584.4	857.9	103.9	412.7	90.0	15.9	120.3	24.0	145.9	33.4	91.6	13.1	78.8	12.2
BR-D2	907.8	1384.0	185.1	714.4	160.3	32.3	188.9	30.9	190.0	38.7	117.1	19.1	94.7	14.1
BR2-D2	610.5	953.7	120.3	477.4	102.6	19.1	133.4	24.1	154.6	34.5	96.5	13.8	87.8	12.1
BR2-D2	712.7	1075.9	136.2	542.9	105.1	21.1	136.3	28.0	168.7	37.3	110.5	17.6	89.2	14.1
BR3-D2	889.7	1353.3	175.6	717.4	143.3	37.3	197.7	31.7	183.9	38.9	104.9	13.6	82.5	11.7
PE10-D2	1298.1	2297.1	231.1	815.4	174.4	21.6	219.2	40.2	234.1	52.8	145.7	18.9	114.6	16.9
PE11-D2	518.8	750.3	88.8	329.4	59.8	13.6	68.9	10.4	59.3	13.0	34.4	2.9	18.1	2.2
PE11-D2	838.1	1362.9	165.8	623.7	106.6	23.1	123.8	17.1	82.1	17.5	52.2	6.8	23.2	2.3
PE12-D2	531.7	898.4	111.9	401.0	74.8	17.8	87.8	15.2	74.4	14.7	48.9	6.9	32.4	5.0
AB1-D3	2538.0	3451.5	352.3	1274.7	187.3	37.6	201.1	21.3	103.5	16.9	45.9	5.0	26.7	2.3
AB2-D3	5320.8	9057.5	997.3	3537.7	555.9	127.1	589.7	69.6	321.3	61.1	153.7	18.5	88.1	12.7
AR4-D3	599.9	1226.4	177.5	687.1	141.5	43.8	152.3	17.9	78.5	15.5	40.5	3.7	29.4	3.4
AR7-D3	514.4	890.0	118.3	439.2	81.4	20.5	70.5	10.2	50.7	7.2	31.2	3.2	26.1	2.4
BR-D3	774.7	1147.6	143.1	578.7	151.3	20.1	165.5	30.7	180.9	39.4	112.1	15.5	93.0	14.0
BR2-D3	654.4	1186.3	192.8	745.0	153.9	38.2	169.2	27.2	188.3	38.7	119.2	16.3	116.5	20.3
BR3-D3	747.7	1251.3	178.8	693.5	160.3	50.9	150.0	22.6	99.1	22.3	51.4	5.0	31.6	3.8
PE1-D3	516.1	947.8	128.2	488.1	126.8	26.3	90.3	12.5	57.1	9.8	36.6	5.1	24.3	3.6
PE12-D3	837.2	1354.5	162.7	589.1	108.1	24.4	124.8	19.5	92.2	18.1	53.3	6.3	32.7	3.7
PE13-D3	666.0	1252.3	159.7	591.7	131.7	27.9	123.7	22.3	106.0	24.3	61.9	9.8	45.1	6.7
PE14-D3	185.7	387.5	49.6	170.8	32.6	7.6	26.8	4.9	25.0	4.4	10.9	2.0	11.2	1.9
PE15-D3	269.8	497.9	60.6	228.4	61.4	13.5	58.2	6.4	44.0	6.7	24.1	3.0	14.5	0.6
PE16-D3	337.3	525.9	52.5	197.5	55.0	5.7	49.0	6.4	34.5	9.1	25.6	3.4	12.4	1.3
PE17-D3	331.2	459.8	49.9	188.4	33.7	9.7	43.4	4.0	24.9	5.7	12.0	0.4	12.1	2.1
PE3-D3	898.8	2434.2	206.3	660.5	93.9	17.7	86.0	9.8	42.3	7.4	16.3	2.4	17.7	2.9
PE4-D3	348.0	548.0	55.4	216.5	27.3		54.1	8.7	39.4	6.4	19.9	4.2	15.4	1.1
PE5-D3	190.7	283.8	36.8	137.6	34.0	7.9	28.2	2.2	32.1	5.2	14.0	3.1	10.7	
PE7-D3	1000.3	1601.7	202.4	760.0	146.6	39.8	162.5	24.3	117.4	23.8	60.0	7.2	31.1	5.2

Sample ID	La (ppb)	Ce (ppb)	Pr (ppb)	Nd (ppb)	Sm (ppb)	Eu (ppb)	Gd (ppb)	Tb (ppb)	Dy (ppb)	Ho (ppb)	Er (ppb)	Tm (ppb)	Yb (ppb)	Lu (ppb)
PE8-D3	5594.1	10261.7	1100.1	4128.6	657.0	225.4	715.7	74.4	282.0	43.7	114.2	9.4	53.1	8.2
PE9-D3	386.6	646.2	72.6	256.9	53.4	9.3	70.8	9.6	61.1	14.0	38.2	4.4	27.0	2.4
Vu-C1	2676.0	4729.6	656.9	2755.4	597.5	193.1	727.4	119.2	756.7	172.4	531.2	79.4	494.3	79.3
Vu-C3	7369.6	18335.9	1593.0	6152.3	1282.5	483.5	1546.1	258.7	1494.4	343.8	1086.4	157.1	1126.7	186.3
RE5-C1	635.9	1393.1	153.4	611.0	108.6	25.8	101.9	12.5	72.2	12.8	40.9	6.0	44.0	5.3
RE6-C1	874.6	1904.5	225.9	873.9	147.9	39.2	148.7	21.2	122.7	19.3	58.1	7.9	54.8	9.3
RE7-C1	5640.3	11963.7	1518.0	5909.9	999.6	187.9	838.3	94.9	380.6	62.0	175.2	17.5	137.1	19.5
RE11-C3	3081.5	6269.6	758.8	3002.3	574.8	116.4	536.9	64.5	289.8	51.4	133.1	15.6	102.5	15.6
RE6-C3	1237.6	2792.7	311.1	1172.6	219.1	65.1	243.7	41.8	252.2	42.7	150.9	25.5	163.9	22.3
ES-D1	516.6	707.5	107.9	482.6	101.0	27.4	146.3	25.4	173.8	37.4	124.8	17.2	111.8	15.7
ES1-D1	334.2	477.9	74.3	308.0	57.4	20.0	75.0	11.2	75.1	18.8	50.1	8.9	47.4	7.1
RE1-D1	2425.4	5588.8	688.6	2898.7	548.0	115.2	554.6	87.6	462.1	85.7	231.2	28.6	162.6	17.2
RE11-D1	1192.3	2737.0	302.1	1191.3	237.1	54.3	242.4	35.7	194.7	34.7	99.1	14.9	85.0	10.4
RE13-D1	1395.6	2868.9	370.5	1500.3	305.9	66.9	308.1	44.0	271.1	55.3	153.1	18.7	124.8	19.7
RE2-D1	2536.4	6727.3	1058.8	4547.5	874.3	160.5	737.2	95.9	472.9	86.3	235.6	27.2	184.8	21.4
RE3-D1	2115.1	4573.2	554.6	2165.5	398.6	95.3	465.3	66.4	334.0	57.4	155.4	19.8	106.1	14.5
RE3-D1	3042.4	6360.4	984.3	4098.5	808.0	170.2	741.7	109.6	552.6	97.8	264.3	32.4	221.5	30.7
RE6-D1	2037.8	4535.0	629.5	2608.1	507.5	119.9	494.0	68.8	345.4	67.8	176.4	22.9	151.6	21.0
RE8-D1	784.4	2094.9	257.6	1092.8	249.7	57.1	254.7	39.2	209.2	41.4	110.5	13.9	79.4	9.5
ES-D2	353.0	480.8	74.5	289.8	52.5	15.2	93.5	14.9	104.2	24.9	84.5	12.3	74.0	12.4
ES-D2	472.2	744.9	120.6	481.9	102.3	24.1	117.0	19.6	113.9	25.3	77.0	11.5	61.0	6.3
ES1-D3	279.9	292.8	65.7	265.8	47.5	10.8	61.6	8.1	61.6	15.5	48.6	4.2	31.8	6.2
RE1-D3	3393.8	6190.0	825.9	3242.6	529.1	97.3	630.2	75.2	356.0	61.0	166.0	16.5	85.9	8.9
RE11-D3	1953.8	3219.0	408.2	1502.6	280.0	64.7	295.4	38.3	201.5	36.9	93.6	10.8	66.2	8.1
RE2-D3	2142.5	4279.3	525.8	2045.3	349.0	85.9	432.4	60.7	320.3	56.4	145.9	15.4	88.6	10.2
RE3-D3	3238.5	6359.2	751.3	2819.3	478.1	92.6	545.8	62.8	290.9	48.7	120.0	13.0	61.3	7.3
RE4-D3	6943.3	18094.8	2267.0	8657.7	1569.4	297.5	1609.6	221.3	1060.3	182.3	485.6	54.8	336.8	40.4

APPENDIX 2

FLUID-INCLUSION MICROTHERMOMETRIC MEASUREMENTS OF ESINO AND BRENO CARBONATES

Sample ID	Host Mineral	Occurrence	Degree of fill	Th	Ti	Tm	Eq. wt% NaCl (Bodnar, 2003)
AR7-C3	C3	Cluster	0.95	128.6	-20.5	-7.8	11.5
AR7-C3	C3	Cluster	0.95	116.2	-28.1	-18.4	21.3
AR7-C3	C3	Cluster	0.95	114.8	-30.3	-13.1	17.0
AR7-C3	C3	Cluster	0.95	139.5	-33.8	-22.7	24.1
AR7-C3	C3	Cluster	0.95	124.9	-36.3	-23.1	24.4
AR7-C3	C3	Cluster	0.95	118.4	-43.0	-28.4	27.7
AR7-C3	C3	Cluster	0.95	113.1	-36.7	-22.6	24.1
AR7-C3	C3	Cluster	0.95	105.5	-48.7	-30.1	28.7
AR7-C3	C3	Cluster	0.95	112.3	-50.0	-20.1	22.4
AR7-C3	C3	Cluster	0.95	109.2	-43.8	-15.1	18.7
AR7-C3	C3	Cluster	0.95	104.8	-46.7	-20.0	22.4
AR7-C3	C3	Cluster	0.95	114.5	-49.9	-17.7	20.7
AR7-C3	C3	Cluster	0.95	114.6	-44.7	-16.9	20.1
AR7-C3	C3	Cluster	0.95	111.5	-40.1	-18.6	21.4
AR7-C3	C3	Cluster	0.95	109.9	-40.5	-11.7	15.7
AR7-C3	C3	Cluster	0.95	97.7	-41.3	-21.5	23.4
AR7-C3	C3	Cluster	0.95	98.2	-25.2	-12.9	16.8
AR7-C3	C3	Cluster	0.95	116.4	-31.6	-12.7	16.6
AR7-C3	C3	Cluster	0.95	99.3	-42.5	-25.2	25.7
AR7-C3	C3	Cluster	0.95	102.4	-26.2	-10.0	13.9
AR7-C3	C3	Cluster	0.95	121.6	-45.7	-22.7	24.1
AR7-C3	C3	Cluster	0.95	117.9	-35.8	-18.4	21.3
AR7-C3	C3	Cluster	0.95	105.5	-33.1	-13.1	17.0
AR7-C3	C3	Cluster	0.95	122.3	-30.7	-7.8	11.5
AR7-C3	C3	Cluster	0.95	126.1	-28.4		
BR-C3	C3	Cluster	0.95	113.0	-48.1	-24.6	25.3
BR-C3	C3	Cluster	0.95	110.0	-49.2	-19.8	22.2
BR-C3	C3	Cluster	0.95	104.8	-44.5	-22.0	23.7
BR-C3	C3	Cluster	0.95	123.3	-47.3	-26.4	26.4
BR-C3	C3	Cluster	0.95	102.1	-38.1	-14.5	18.2
BR-C3	C3	Cluster	0.95	105.4	-42.8	-8.6	12.4
BR-C3	C3	Cluster	0.95	103.3	-43.0	-14.3	18.0
BR-C3	C3	Cluster	0.95	119.7	-39.4	-22.6	24.1
BR-C3	C3	Cluster	0.95	129.1	-42.2	-24.3	25.1
BR-C3	C3	Cluster	0.95	124.5	-49.0	-20.9	23.0

Sample I-D	Host Mineral	Occurrence	Degree of fill	Th	Ti	Tm	Eq. wt% NaCl (Bodnar, 2003)
BR-C3	C3	Cluster	0.95	122.5	-51.8	-21.5	23.4
BR-C3	C3	Cluster	0.95	90.9	-40.8	-16.0	19.4
BR-C3	C3	Cluster	0.95	103.1	-46.9	-14.6	18.3
BR-C3	C3	Cluster	0.95	102.0	-50.3	-29.0	28.0
BR-C3	C3	Cluster	0.95	109.4	-43.0	-22.4	24.0
BR-C3	C3	Cluster	0.95	112.0		-16.3	19.7
BR-C3	C3	Cluster	0.95	112.2		-23.0	24.3
BR-C3	C3	Cluster	0.95	106.3		-15.7	19.2
BR-C3	C3	Cluster	0.95	103.4		-13.6	17.4
BR-C3	C3	Cluster	0.95	124.5	-36.1		
BR-C3	C3	Cluster	0.95	117.0	-46.3		
BR-C3	C3	Cluster	0.95	114.0	-51.2		
BR-C3	C3	Cluster	0.95	117.0			
BR-C3	C3	Cluster	0.95	115.0			
BR-C3	C3	Cluster	0.95	118.2			
BR-C3	C3	Cluster	0.95	120.0			
BR-C3	C3	Cluster	0.95	98.0			
BR-C3	C3	Cluster	0.95	118.0			
BR-C3	C3	Cluster	0.95	103.0			
BR-C3	C3	Cluster	0.95	102.0			
BR-C3	C3	Cluster	0.95	99.0			
PG1-C3	C3	Cluster	0.95	120.9	-45.5	-29.4	28.3
PG1-C3	C3	Cluster	0.95	106.1	-38.5	-12.5	16.4
PG1-C3	C3	Cluster	0.95	107.8	-40.2	-16.9	20.1
PG1-C3	C3	Cluster	0.95	109.3	-41.1	-21.8	23.6
PG1-C3	C3	Cluster	0.95	101.6	-41.9	-24.5	25.3
PG1-C3	C3	Cluster	0.95	108.9	-41.0	-28.5	27.7
PG1-C3	C3	Cluster	0.95	109.3	-42.4	-26.2	26.3
PG1-C3	C3	Cluster	0.95	106.9	-45.0	-28.5	27.7
PG1-C3	C3	Cluster	0.95	110.1	-36.2	-15.9	19.4
PG1-C3	C3	Cluster	0.95	108.9	-32.3	-13.7	17.5
PG1-C3	C3	Cluster	0.95	105.4	-45.5	-19.9	22.3
PG1-C3	C3	Cluster	0.95	119.8	-38.1	-11.1	15.1
PG1-C3	C3	Cluster	0.95	104.8	-29.3	-16.3	19.7
PG1-C3	C3	Cluster	0.95	100.1	-30.1	-17.8	20.8
PG1-C3	C3	Cluster	0.95	106.2	-37.3	-18.5	21.3
PG1-C3	C3	Cluster	0.95	106.4	-46.5	-30.1	28.7
PG1-C3	C3	Cluster	0.95	99.1	-41.8	-28.4	27.7
PG1-C3	C3	Cluster	0.95	102.0	-40.0	-23.1	24.4

Sample I-D	Host Mineral	Occurrence	Degree of fill	Th	Ti	Tm	Eq. wt% NaCl (Bodnar, 2003)
PG1-C3	C3	Isolated	0.95	115.2	-43.1	-30.7	29.1
PG1-C3	C3	Cluster	0.95	117.5	-43.6	-25.8	26.1
PG1-C3	C3	Cluster	0.95	119.5	-45.7		
PG1-C3	C3	Isolated	0.95	120.1	-39.1		
PG1-C3	C3	Cluster	0.95	109.6	-42.4		
PG1-C3	C3	Cluster	0.95	113.1			
BR-D2	D2	Cluster	0.95	107.9	-43.0	-26.8	26.7
BR-D2	D2	Cluster	0.95	108.7		-18.6	21.4
BR-D2	D2	Cluster	0.95	106.6		-20.1	22.4
BR-D2	D2	Cluster	0.95	116.2		-19.1	21.8
BR-D2	D2	Cluster	0.95	106.7		-20.2	22.5
BR-D2	D2	Cluster	0.95	97.8		-18.8	21.5
BR-D2	D2	Cluster	0.95	98.4		-17.3	20.4
BR-D2	D2	Cluster	0.95	100.0		-20.8	22.9
BR-D2	D2	Cluster	0.95	103.2		-24.4	25.2
BR-D2	D2	Cluster	0.95	108.1		-21.7	23.5
BR-D2	D2	Cluster	0.95	106.1		-24.1	25.0
BR-D2	D2	Cluster	0.95	111.4		-20.3	22.6
BR-D2	D2	Cluster	0.95	99.8		-18.5	21.3
BR-D2	D2	Cluster	0.95	104.3		-20.2	22.5
BR-D2	D2	Cluster	0.95	103.0		-14.9	18.6
BR-D2	D2	Cluster	0.95	96.7		-17.8	20.8
BR-D2	D2	Cluster	0.95	102.8		-21.8	23.6
BR-D2	D2	Cluster	0.95	111.2		-20.2	22.5
BR-D2	D2	Cluster	0.95	118.3		-18.9	21.6
BR-D2	D2	Cluster	0.95	124.2		-19.3	21.9
BR-D2	D2	Cluster	0.95	119.4		-17.9	20.9
BR-D2	D2	Cluster	0.95	115.3		-18.4	21.3
BR-D2	D2	Cluster	0.95	106.3		-22.5	24.0
BR-D2	D2	Cluster	0.95	97.2		-21.2	23.2
BR-D2	D2	Cluster	0.95	124.1		-21.7	23.5
BR-D2	D2	Cluster	0.95	114.6		-22.6	24.1
BR-D2	D2	Cluster	0.95	117.8		-20.7	22.8
BR-D2	D2	Cluster	0.95	113.4		-23.1	24.4
BR-D2	D2	Cluster	0.95	100.4		-18.3	21.2
BR-D2	D2	Cluster	0.95	112.6		-21.9	23.6
BR-D2	D2	Cluster	0.95	95.8		-17.1	20.3
BR-D2	D2	Cluster	0.95	116.2		-18.6	21.4
BR-D2	D2	Cluster	0.95	106.3		-25.6	25.9

Sample I-D	Host Mineral	Occurrence	Degree of fill	Th	Ti	Tm	Eq. wt% NaCl (Bodnar, 2003)
BR-D2	D2	Cluster	0.95	107.7		-18.8	21.5
BR-D2	D2	Cluster	0.95	94.2		-24.3	25.1
BR-D2	D2	Cluster	0.95	113.3		-16.1	19.5
BR-D2	D2	Cluster	0.95	97.1		-23.2	24.5
BR-D2	D2	Cluster	0.95	104.8		-18.8	21.5
BR-D2	D2	Cluster	0.95	103.2		-20.3	22.6
BR-D2	D2	Cluster	0.95	98.3		-23.4	24.6
BR-D2	D2	Cluster	0.95	100.0		-24.5	25.3
BR-D2	D2	Cluster	0.95	101.5		-19.5	22.0
BR-D2	D2	Cluster	0.95	116.4		-21.2	23.2
BR-D2	D2	Cluster	0.95	104.3		-21.9	23.6
BR-D2	D2	Cluster	0.95	100.1			
BR-D2	D2	Cluster	0.95	105.1			
BR-D2	D2	Cluster	0.95	116.4			
BR-D2	D2	Cluster	0.95	117.8			
BR-D2	D2	Cluster	0.95	109.6			
BR-D2	D2	Cluster	0.95	117.2			
BR-D2	D2	Cluster	0.95	102.5			
BR-D2	D2	Cluster	0.95	94.9			
BR-D2	D2	Cluster	0.95	110.3			
BR-D2	D2	Cluster	0.95	107.5			
BR-D2	D2	Cluster	0.95	94.4			
BR-D2	D2	Cluster	0.95	128.2			
BR-D2	D2	Cluster	0.95	126.3			
BR-D2	D2	Cluster	0.95	98.1			
BR-D3	D3	Cluster	0.95	95.6	-23.5	-10.9	14.9
BR-D3	D3	Cluster	0.95	117.6	-51.0	-26.3	26.4
BR-D3	D3	Cluster	0.95	101.3	-21.5	-11.1	15.1
BR-D3	D3	Cluster	0.95	100.4	-23.5	-12.4	16.3
BR-D3	D3	Cluster	0.95	105.0	-31.3	-12.9	16.8
BR-D3	D3	Cluster	0.95	109.3	-30.0	-10.4	14.4
BR-D3	D3	Cluster	0.95	113.3	-35.4	-12.0	16.0
BR-D3	D3	Cluster	0.95	114.8	-28.2	-15.1	18.7
BR-D3	D3	Cluster	0.95	120.8	-29.1	-15.0	18.6
BR-D3	D3	Cluster	0.95	134.7	-33.7	-22.8	24.2
BR-D3	D3	Cluster	0.95	144.1	-27.2	-12.3	16.2
BR-D3	D3	Cluster	0.95	139.6	-24.0	-11.4	15.4
BR-D3	D3	Cluster	0.95	129.3	-25.4	-16.0	19.4
BR-D3	D3	Cluster	0.95	117.5	-27.2	-16.0	19.4

Sample I-D	Host Mineral	Occurrence	Degree of fill	Th	Ti	Tm	Eq. wt% NaCl (Bodnar, 2003)
BR-D3	D3	Cluster	0.95	142.1	-26.5	-16.0	19.4
BR-D3	D3	Cluster	0.95	128.3	-17.9	-7.8	11.5
BR-D3	D3	Cluster	0.95	132.7	-22.1	-13.4	17.3
BR-D3	D3	Cluster	0.95	120.1	-20.7	-11.7	15.7
BR-D3	D3	Cluster	0.95	113.7	-36.3	-20.9	23.0
BR-D3	D3	Cluster	0.95	98.9	-44.3	-30.7	29.1
BR-D3	D3	Cluster	0.95	107.3	-38.7	-28.5	27.7
BR-D3	D3	Cluster	0.95	114.2	-39.7	-27.6	27.2
BR-D3	D3	Cluster	0.95	139.2	-35.1	-14.9	18.6
BR-D3	D3	Cluster	0.95	128.6	-34.3	-19.0	21.7
BR-D3	D3	Cluster	0.95	128.6	-33.6	-15.6	19.1
BR-D3	D3	Cluster	0.95	111.8	-48.5	-29.5	28.3
BR-D3	D3	Cluster	0.95	123.5	-36.3	-20.6	22.8
BR-D3	D3	Cluster	0.95	117.8	-40.2	-22.1	23.8
BR-D3	D3	Cluster	0.95	104.6	-28.3	-16.7	20.0
BR-D3	D3	Cluster	0.95	116.4	-27.9	-17.3	20.4
BR-D3	D3	Cluster	0.95	109.8	-34.8	-21.2	23.2
BR-D3	D3	Cluster	0.95	103.2	-32.2	-18.5	21.3
BR-D3	D3	Cluster	0.95	104.6	-36.2	-19.3	21.9
BR-D3	D3	Cluster	0.95	111.5	-31.7	-19.1	21.8
BR-D3	D3	Cluster	0.95	113.8	-41.4	-24.6	25.3
BR-D3	D3	Cluster	0.95	144.4	-20.0		
BR-D3	D3	Cluster	0.95	129.2	-20.0		
BR-D3	D3	Cluster	0.95	113.8	-20.0		
BR-D3	D3	Cluster	0.95	114.9	-30.7		
BR-D3	D3	Cluster	0.95	141.8			
BR-D3	D3	Cluster	0.95	131.8			
ES1-D3	D3	Cluster	0.95	112.8	-35.4	-17.8	20.8
ES1-D3	D3	Cluster	0.95	110.8	-33.8	-22.6	24.1
ES1-D3	D3	Cluster	0.95	114.2	-32.4	-18.1	21.0
ES1-D3	D3	Cluster	0.95	90.5	-33.1	-18.1	21.0
ES1-D3	D3	Cluster	0.95	88.9	-36.2	-23.1	24.4
ES1-D3	D3	Cluster	0.95	120.3	-26.9	-7.9	11.6
ES1-D3	D3	Cluster	0.95	122.5	-28.8	-8.8	12.6
ES1-D3	D3	Cluster	0.95	124.6	-30.0	-10.0	13.9
ES1-D3	D3	Cluster	0.95	127.2	-34.3	-10.6	14.6
ES1-D3	D3	Cluster	0.95	112.9	-39.6	-10.9	14.9
ES1-D3	D3	Cluster	0.95	116.1	-45.5	-31.5	29.6
ES1-D3	D3	Cluster	0.95	107.6		-27.4	27.0

Sample I-D	Host Mineral	Occurrence	Degree of fill	Th	Ti	Tm	Eq. wt% NaCl (Bodnar, 2003)
ES1-D3	D3	Cluster	0.95	91.4		-21.0	23.0
ES1-D3	D3	Cluster	0.95	115.4		-20.1	22.4
ES1-D3	D3	Cluster	0.95	92.1		-16.9	20.1
ES1-D3	D3	Cluster	0.95	92.7		-12.2	16.1
ES1-D3	D3	Cluster	0.95	106.7		-8.3	12.0
ES1-D3	D3	Cluster	0.95	117.8		-20.0	22.4
ES1-D3	D3	Cluster	0.95	126.3		-18.6	21.4
ES1-D3	D3	Cluster	0.95	120.7		-15.1	18.7
ES1-D3	D3	Cluster	0.95	115.0		-21.0	23.0
ES1-D3	D3	Cluster	0.95	114.0		-16.0	19.4
ES1-D3	D3	Cluster	0.95	110.0		-13.0	16.9
ES1-D3	D3	Cluster	0.95	99.7		-14.7	18.4
ES1-D3	D3	Cluster	0.95	99.7		-14.7	18.4
ES1-D3	D3	Cluster	0.95	99.7		-14.7	18.4
ES1-D3	D3	Cluster	0.95	98.3		-15.2	18.8
ES1-D3	D3	Cluster	0.95	107.2		-17.3	20.4
ES1-D3	D3	Cluster	0.95	107.2		-17.3	20.4
ES1-D3	D3	Cluster	0.95	108.5		-16.5	19.8
ES1-D3	D3	Cluster	0.95	108.5		-16.5	19.8
ES1-D3	D3	Cluster	0.95	109.7		-18.6	21.4
ES1-D3	D3	Cluster	0.95	109.7		-18.6	21.4
ES1-D3	D3	Cluster	0.95	110.3		-23.8	24.8
ES1-D3	D3	Cluster	0.95	110.3		-23.8	24.8
ES1-D3	D3	Cluster	0.95	112.1		-20.9	23.0
ES1-D3	D3	Cluster	0.95	113.9		-24.9	25.5
ES1-D3	D3	Cluster	0.95	90.5	-39.3		
ES1-D3	D3	Cluster	0.95			-14.2	18.0
ES1-D3	D3	Cluster	0.95			-13.2	17.1
ES1-D3	D3	Cluster	0.95			-16.1	19.5
PE5-D3	D3	Cluster	0.95	95.3	-36.3	-25.4	25.8
PE5-D3	D3	Cluster	0.95	88.9	-48.3	-31.8	29.8
PE5-D3	D3	Cluster	0.95	93.7	-47.8	-29.9	28.6
PE5-D3	D3	Cluster	0.95	91.5	-41.9	-27.1	26.9
PE5-D3	D3	Cluster	0.95	117.0	-35.3	-15.1	18.7
PE5-D3	D3	Cluster	0.95	113.3	-33.4	-20.0	22.4
PE5-D3	D3	Cluster	0.95	96.6	-28.7	-17.8	20.8
PE5-D3	D3	Cluster	0.95	113.4	-28.7	-19.3	21.9
PE5-D3	D3	Cluster	0.95	90.1	-24.1	-14.6	18.3
PE5-D3	D3	Cluster	0.95	91.0	-25.1	-16.8	20.1

Sample I-D	Host Mineral	Occurrence	Degree of fill	Th	Ti	Tm	Eq. wt% NaCl (Bodnar, 2003)
PE5-D3	D3	Cluster	0.95	92.3	-22.9	-15.7	19.2
PE5-D3	D3	Cluster	0.95	121.1	-43.1	-26.4	26.4
PE5-D3	D3	Cluster	0.95	85.6	-23.4	-12.7	16.6
PE5-D3	D3	Cluster	0.95	86.5	-20.6	-9.9	13.8
PE5-D3	D3	Cluster	0.95	94.0	-28.3	-15.9	19.4
PE5-D3	D3	Cluster	0.95	98.1	-29.2	-16.6	19.9
PE5-D3	D3	Cluster	0.95	104.5	-23.4	-10.1	14.0
PE5-D3	D3	Cluster	0.95	102.3	-24.5	-13.6	17.4
PE5-D3	D3	Cluster	0.95	113.2	-29.3	-19.0	21.7
PE5-D3	D3	Cluster	0.95	121.8	-27.2	-12.7	16.6
PE5-D3	D3	Cluster	0.95	98.5	-40.3	-18.5	21.3
PE5-D3	D3	Cluster	0.95	114.6		-19.3	21.9
PE5-D3	D3	Cluster	0.95	109.8		-16.6	19.9
PE5-D3	D3	Cluster	0.95	107.9		-15.7	19.2
PE5-D3	D3	Cluster	0.95	104.6		-22.4	24.0
PE5-D3	D3	Cluster	0.95	95.6		-20.7	22.8
PE5-D3	D3	Cluster	0.95	103.3	-37.6		
PE5-D3	D3	Cluster	0.95	99.3	-27.5		
PE5-D3	D3	Cluster	0.95	97.2			
PE5-D3	D3	Cluster	0.95		-32.3	-17.0	20.2
PE5-D3	D3	Cluster	0.95		-35.6	-24.0	25.0
PE5-D3	D3	Cluster	0.95		-29.8	-17.6	20.7

APPENDIX 3

FLUID-INCLUSION GAS DATA OF ESINO AND BRENO CARBONATES

Sample	Crush#	H_2	He	CH_4	H_2O	N_2	H_2S	Ar	CO_2
AR5-C1	9116a	0.018	0.002	1.132	84.851	1.732	0.005	0.029	12.207
	9116b	0.058	0.003	1.483	84.463	1.498	0.003	0.018	12.452
	9116c	0.086	0.006	2.880	80.147	2.798	0.004	0.046	14.001
	9116d	0.058	0.004	1.884	85.246	1.784	0.004	0.025	10.969
	9116e	0.146	0.007	2.566	80.073	2.669	0.004	0.036	14.459
Weighted Mean		0.080	0.005	2.110	82.955	2.141	0.004	0.031	12.645
AR5-C1	9101a	0.062	0.004	2.044	85.935	1.168	0.001	0.017	10.751
	9101b	0.014	0.002	1.434	86.465	1.154	0.004	0.023	10.880
	9101c	0.033	0.002	1.686	88.952	1.013	0.003	0.013	8.284
	9101d	0.051	0.005	5.133	79.386	1.856	0.004	0.024	13.520
	9101e	0.052	0.007	3.833	76.547	2.353	0.003	0.017	17.158
	9101f	0.295	0.006	4.497	72.652	2.066	0.000	0.023	20.427
	9101g	1.342	0.005	4.803	75.204	2.179	0.003	0.029	16.353
Weighted Mean		0.180	0.004	2.752	83.900	1.433	0.003	0.018	11.686
PE4-C1	9258a	0.000	0.000	0.015	92.544	2.518	0.003	0.034	4.885
	9258b	0.010	0.000	0.053	91.677	3.196	0.001	0.033	5.030
	9258c	0.011	0.000	0.050	90.421	3.680	0.001	0.039	5.798
	9258d	0.000	0.000	0.042	91.998	2.679	0.001	0.028	5.252
	9258e	0.001	0.000	0.023	95.726	1.287	0.002	0.013	2.948
	9258f	0.012	0.000	0.034	95.167	1.366	0.001	0.015	3.404
Weighted Mean		0.006	0.000	0.035	93.425	2.209	0.001	0.024	4.300
PE5-C1	9260a	0.000	0.000	0.037	98.684	0.086	0.025	0.001	1.167
	9260b	0.000	0.000	0.041	99.111	0.042	0.019	0.000	0.787
	9260c	0.000	0.000	0.051	99.261	0.039	0.016	0.000	0.633
	9260d	0.001	0.000	0.059	99.155	0.042	0.028	0.000	0.715
	9260e	0.004	0.000	0.073	99.217	0.054	0.023	0.000	0.628
	9260f	0.000	0.000	0.081	98.990	0.108	0.031	0.001	0.789
Weighted Mean		0.001	0.000	0.059	99.091	0.061	0.024	0.001	0.764
PE5-C1	9079c	0.000	0.000	0.065	98.957	0.147	0.049	0.002	0.774
	9079d	0.000	0.000	0.104	98.700	0.071	0.052	0.001	1.067
	9079e	0.000	0.000	0.065	99.114	0.163	0.030	0.002	0.622
	9079f	0.000	0.000	0.067	99.221	0.056	0.034	0.001	0.614
	9079g	0.000	0.000	0.073	98.895	0.340	0.034	0.003	0.647
	9079h	0.000	0.000	0.078	99.073	0.054	0.044	0.001	0.739
	9079j	0.000	0.000	0.057	98.773	0.323	0.042	0.004	0.794
	9079k	0.000	0.000	0.071	98.990	0.102	0.037	0.001	0.785

Sample	Crush#	H_2	He	CH_4	H_2O	N_2	H_2S	Ar	CO_2
Weighted Mean		0.000	0.000	0.071	99.003	0.149	0.039	0.002	0.728
Ar5-D1	9248a	0.000	0.004	2.203	74.673	2.322	0.000	0.042	20.756
	9248b	0.023	0.003	1.250	79.123	1.389	0.000	0.028	18.184
	9248c	0.009	0.001	0.973	87.158	1.103	0.000	0.018	10.738
	9248d	0.016	0.002	1.711	83.139	1.413	0.000	0.023	13.696
	9248e	0.027	0.002	1.589	81.706	1.207	0.000	0.025	15.444
	9248f	0.056	0.003	1.746	81.610	1.202	0.000	0.023	15.359
	9248g	0.080	0.004	2.598	79.123	1.209	0.000	0.026	16.960
	9248h	0.084	0.004	2.873	80.237	1.313	0.000	0.030	15.459
Weighted Mean		0.052	0.003	2.054	81.387	1.259	0.000	0.025	15.220
AR7-D1	9250a	0.024	0.002	0.829	83.045	1.043	0.000	0.016	15.041
	9250b	0.072	0.002	0.894	86.170	1.133	0.000	0.020	11.709
	9250c	0.025	0.002	1.002	85.817	0.925	0.000	0.018	12.212
	9250d	0.038	0.002	0.984	88.567	0.868	0.000	0.012	9.528
	9250e	0.020	0.001	0.672	93.256	0.398	0.000	0.007	5.647
	9250f	0.056	0.003	1.264	83.522	1.204	0.000	0.022	13.931
Weighted Mean		0.038	0.002	0.950	87.863	0.855	0.000	0.014	10.277
ES1-D1	9251a	0.190	0.003	0.314	82.084	0.441	0.000	0.004	16.965
	9251b	0.000	0.002	0.148	89.930	0.409	0.000	0.003	9.506
	9251c	0.001	0.003	0.156	87.277	0.335	0.000	0.003	12.225
	9251d	0.126	0.002	0.203	87.438	0.380	0.000	0.004	11.846
	9251e	0.686	0.003	0.561	87.587	0.509	0.000	0.005	10.648
Weighted Mean		0.201	0.003	0.271	87.392	0.411	0.000	0.004	11.718
BR-D2	9121a	0.005	0.004	1.064	95.528	0.277	0.006	0.003	3.110
	9121b	0.004	0.001	0.361	97.901	0.096	0.006	0.002	1.626
	9121c	0.000	0.002	0.539	97.706	0.215	0.004	0.003	1.529
	9121d	0.001	0.001	0.699	97.339	0.200	0.004	0.003	1.751
	9121e	0.000	0.002	0.811	96.851	0.189	0.013	0.003	2.129
	9121f	0.000	0.002	0.753	97.347	0.139	0.009	0.003	1.746
	9121g	0.000	0.002	0.852	97.217	0.169	0.007	0.003	1.748
	9121h	0.000	0.002	0.641	98.166	0.122	0.002	0.002	1.061
Weighted Mean		0.001	0.002	0.622	97.744	0.142	0.005	0.002	1.478
BR2-D2	9247a	0.000	0.001	0.448	97.830	0.397	0.000	0.004	1.320
	9247b	0.000	0.001	0.285	98.570	0.169	0.001	0.002	0.973
	9247c	0.000	0.002	0.545	97.966	0.413	0.002	0.006	1.067
	9247d	0.000	0.005	1.711	94.313	0.544	0.007	0.007	3.413
	9247e	0.000	0.003	1.199	96.845	0.100	0.004	0.001	1.848
Weighted Mean		0.000	0.003	1.118	96.403	0.339	0.004	0.004	2.128
BR3-D2	9246a	0.000	0.003	0.627	90.004	5.925	0.011	0.101	3.329

Sample	Crush#	H_2	He	CH_4	H_2O	N_2	H_2S	Ar	CO_2
	9246b	0.000	0.001	0.209	96.717	1.858	0.007	0.027	1.181
	9246c	0.000	0.002	0.398	96.300	1.334	0.007	0.020	1.940
	9246d	0.000	0.003	0.473	95.427	1.525	0.004	0.023	2.545
	9246e	0.000	0.002	0.478	95.066	1.183	0.009	0.018	3.244
	9246f	0.000	0.004	0.701	93.804	1.353	0.006	0.023	4.109
	9246g	0.000	0.001	0.358	95.629	1.253	0.008	0.017	2.733
	9246h	0.000	0.002	0.363	96.785	0.772	0.005	0.013	2.061
	9246j	0.000	0.002	0.562	93.975	1.358	0.007	0.019	4.077
	9246k	0.000	0.002	0.460	95.609	0.947	0.005	0.013	2.964
Weighted Mean		0.000	0.002	0.438	95.424	1.376	0.006	0.021	2.733
ES1-D3	9102a	0.000	0.003	0.067	95.999	0.235	0.015	0.003	3.642
	9102b	0.000	0.002	0.028	98.194	0.087	0.003	0.001	1.683
	9102c	0.000	0.002	0.038	97.883	0.134	0.006	0.001	1.933
	9102d	0.000	0.001	0.023	98.511	0.081	0.006	0.000	1.374
	9102f	0.000	0.001	0.035	97.696	0.079	0.003	0.001	2.183
	9102g	0.000	0.002	0.023	98.503	0.081	0.002	0.001	1.385
	9102h	0.000	0.002	0.028	97.988	0.075	0.004	0.001	1.900
	9117a	0.000	0.002	0.034	98.288	0.130	0.001	0.001	1.541
	9117b	0.000	0.002	0.036	97.696	0.132	0.001	0.001	2.130
	9117c	0.000	0.002	0.040	98.092	0.111	0.001	0.001	1.752
	9117d	0.000	0.003	0.063	97.403	0.199	0.002	0.001	2.318
Weighted Mean		0.000	0.002	0.052	97.208	0.173	0.007	0.002	2.539
ES1-D3	9261a	0.000	0.010	0.297	75.309	1.436	0.001	0.015	22.932
	9261b	0.000	0.005	0.084	93.227	0.355	0.001	0.003	6.326
	9261c	0.006	0.008	0.161	87.667	0.466	0.001	0.004	11.687
Weighted Mean		0.002	0.007	0.137	89.032	0.530	0.001	0.005	10.286
PE1-D3	9249a	0.000	0.002	0.141	93.058	3.104	0.007	0.031	3.657
	9249b	0.000	0.001	0.053	97.353	1.448	0.001	0.012	1.132
	9249c	0.000	0.001	0.051	97.093	1.686	0.001	0.014	1.153
	9249d	0.000	0.001	0.068	97.584	1.129	0.000	0.009	1.209
	9249e	0.000	0.001	0.078	96.563	1.394	0.002	0.011	1.950
Weighted Mean		0.000	0.001	0.088	95.877	1.918	0.003	0.017	2.096
PE14-D3	9252a	0.008	0.010	0.898	90.037	1.601	0.000	0.017	7.429
	9252b	0.003	0.005	0.443	93.677	0.603	0.000	0.006	5.263
Weighted Mean		0.005	0.007	0.607	92.360	0.964	0.000	0.010	6.047
PE3-D3	9122a	0.000	0.000	0.174	97.314	0.069	0.092	0.001	2.347
	9122b	0.000	0.000	0.092	96.591	0.051	0.127	0.001	3.135
	9122c	0.000	0.000	0.087	96.704	0.050	0.135	0.000	3.020
	9122d	0.000	0.000	0.085	95.999	0.084	0.147	0.001	3.680

Sample	Crush#	H_2	He	CH_4	H_2O	N_2	H_2S	Ar	CO_2
	9122e	0.000	0.000	0.040	96.582	0.058	0.173	0.001	3.141
	9122f	0.000	0.000	0.122	94.237	0.131	0.213	0.001	5.273
	9122g	0.000	0.000	0.125	95.972	0.085	0.217	0.001	3.592
	9122h	0.000	0.000	0.125	95.933	0.081	0.221	0.001	3.631
	9122j	0.000	0.000	0.138	95.454	0.095	0.290	0.001	4.013
Weighted Mean		0.000	0.000	0.116	95.576	0.093	0.208	0.001	3.993
PE3-D3	9262a	0.000	0.002	0.149	97.465	0.346	0.004	0.004	2.028
	9262b	0.000	0.002	0.177	98.194	0.327	0.005	0.003	1.292
	9262c	0.000	0.002	0.128	98.687	0.201	0.002	0.002	0.978
	9262d	0.000	0.003	0.164	98.448	0.206	0.002	0.002	1.175
	9262e	0.000	0.002	0.140	98.304	0.217	0.006	0.002	1.330
	9262f	0.000	0.004	0.300	97.080	0.353	0.005	0.003	2.255
Weighted Mean		0.000	0.002	0.176	98.089	0.261	0.004	0.003	1.465
PE4-D3	9259a	0.000	0.001	0.038	98.961	0.210	0.001	0.003	0.787
	9259b	0.000	0.001	0.050	98.303	0.250	0.001	0.004	1.391
	9259c	0.000	0.001	0.080	98.714	0.234	0.000	0.003	0.968
	9259d	0.000	0.001	0.075	98.471	0.176	0.001	0.002	1.274
	9259e	0.000	0.001	0.090	98.500	0.230	0.001	0.003	1.175
	9259f	0.000	0.001	0.085	98.247	0.244	0.001	0.003	1.420
	9259g	0.000	0.001	0.066	98.295	0.238	0.001	0.003	1.396
	9259h	0.000	0.001	0.082	98.072	0.214	0.001	0.003	1.629
Weighted Mean		0.000	0.001	0.075	98.379	0.226	0.001	0.003	1.316
PE5-D3	9263b	0.003	0.001	0.093	98.601	0.107	0.001	0.001	1.193
	9263c	0.000	0.001	0.121	98.687	0.115	0.001	0.001	1.075
	9263d	0.000	0.001	0.100	98.723	0.112	0.001	0.001	1.063
	9263e	0.000	0.001	0.093	98.531	0.225	0.001	0.002	1.148
	9263f	0.000	0.001	0.150	96.902	0.175	0.003	0.002	2.768
	9263g	0.000	0.001	0.181	97.314	0.212	0.002	0.002	2.288
Weighted Mean		0.000	0.001	0.138	97.747	0.172	0.002	0.002	1.939
PE5-D3	9245a	0.000	0.001	0.079	98.347	0.357	0.000	0.004	1.211
	9245b	0.000	0.001	0.073	98.572	0.355	0.000	0.003	0.995
	9245c	0.000	0.001	0.069	98.385	0.343	0.000	0.004	1.199
	9245d	0.000	0.001	0.066	98.276	0.558	0.000	0.006	1.093
	9245e	0.000	0.001	0.072	98.298	0.426	0.000	0.004	1.199
	9245f	0.000	0.001	0.086	97.918	0.409	0.000	0.004	1.581
	9245g	0.000	0.001	0.070	98.344	0.258	0.000	0.003	1.324
Weighted Mean		0.000	0.001	0.074	98.252	0.399	0.000	0.004	1.270
PE13-D3	9243a	0.000	0.001	0.088	97.886	0.225	0.000	0.003	1.797
	9243b	0.000	0.001	0.057	98.808	0.107	0.001	0.001	1.025

Sample	Crush#	H_2	He	CH_4	H_2O	N_2	H_2S	Ar	CO_2
	9243c	0.000	0.001	0.070	98.778	0.098	0.001	0.001	1.050
	9243d	0.000	0.001	0.098	98.524	0.083	0.001	0.001	1.292
	9243e	0.000	0.002	0.133	97.954	0.128	0.002	0.001	1.780
Weighted Mean		0.000	0.001	0.099	98.377	0.113	0.001	0.001	1.408
PE15-D3	9244a	0.000	0.001	0.153	97.679	0.088	0.000	0.001	2.077
	9244b	0.000	0.001	0.236	97.888	0.121	0.005	0.001	1.748
	9244c	0.000	0.001	0.113	98.652	0.077	0.000	0.001	1.156
	9244d	0.000	0.001	0.156	98.141	0.090	0.000	0.000	1.611
	9244e	0.000	0.001	0.139	98.028	0.067	0.000	0.001	1.764
	9244f	0.000	0.002	0.238	97.325	0.101	0.000	0.000	2.334
Weighted Mean		0.000	0.001	0.163	97.998	0.085	0.000	0.001	1.752